

TOPOLOGICAL INVESTIGATIONS IN PHYSICS

A. TOZZI
J.F. PETERS

S^{n-3}

S^{n-2}

S^{n-1}

S^n

TOPOLOGICAL INVESTIGATIONS IN PHYSICS

An assembly of our published and unpublished papers

Arturo Tozzi

Center for Nonlinear Science, University of North Texas
1155 Union Circle, #311427
Denton, TX 76203-5017, USA, and
Computational Intelligence Laboratory, University of Manitoba, Winnipeg, Canada
Winnipeg R3T 5V6 Manitoba
ASL NA2 Nord
tozziarturo@libero.it

James F. Peters

Department of Electrical and Computer Engineering, University of Manitoba
75A Chancellor's Circle, Winnipeg, MB R3T 5V6, Canada and
Department of Mathematics, Adiyaman University, 02040 Adiyaman, Turkey,
Department of Mathematics, Faculty of Arts and Sciences, Adiyaman University
02040 Adiyaman, Turkey and Computational Intelligence Laboratory, University of
Manitoba, WPG, MB, R3T 5V6, Canada
james.peters3@umanitoba.ca

This manuscript encompasses our published and unpublished topological results in physics. Topology, the mathematical branch that assesses objects and their properties preserved through deformations, stretching and twisting, allows the investigation of the most general physical systems features. In particular, the Borsuk-Ulam Theorem (BUT) states that, if a single point projects to a higher spatial dimension, it gives rise to two antipodal points with matching description. Physical counterparts of BUT and its variants allow an inquiry of physical problems. The opportunity to treat systems as topological structures makes BUT a universal principle underlying natural phenomena.

CONTENT

Borsuk-Ulam theorem

- 1) Tozzi A, Peters JF. 2016. The Borsuk-Ulam Theorem: an Universal Principle for Physical Systems. viXra:1610.0221
- 2) Tozzi A. 2016. Borsuk-Ulam Theorem Extended to Hyperbolic Spaces. In Computational Proximity. Excursions in the Topology of Digital Images, edited by J F Peters, 169–171. doi:10.1007/978-3-319-30262-1.

Relativity

- 3) Tozzi A, Peters JF, Chafin C, De Falco D. 2016. Time as a Gauge Field. ViXra, 1608.0434v1.

Quantum mechanics

- 4) Peters JF, Tozzi A. 2016. Quantum Entanglement on a Hypersphere. Int J Theoret Phys, 1–8. doi:10.1007/s10773-016-2998-7.

Cosmology

- 5) Tozzi A, Peters JF, Ramanna S. 2016. Computational Geometry Provides Indirect Evidence of Dark Matter Location in Cosmic Structures. viXra:1610.0071.

Strings and branes

- 6) Tozzi A, Peters JF. 2016. Topological Framework for Brane Cosmology. viXra:1608.0397.

Pre-big bang scenarios

- 7) Tozzi A, Peters JF. 2016. Towards a Monster Group Encompassing the Universe. viXra:1609.0027.
- 8) Tozzi A, Peters JF, Chafin C, De Falco D. 2016. Time Symmetry Breaking in Pre-Big Bang Vacuum State. viXra:1609.0352.

Nonlinear systems

- 9) Tozzi A, Peters JF. 2016. A Theorem from Topology Unveils the Mystery of Fractals and Power Laws. viXra:1610.0223
- 10) Tozzi A, Peters JF. 2016. The Borsuk-Ulam Theorem Elucidates Chaotic Systems. viXra:1610.0222

Note concerning the published papers: the versions reported here are just sketches of the finally published manuscripts

THE BORSUK-ULAM THEOREM: AN UNIVERSAL PRINCIPLE FOR PHYSICAL SYSTEMS

The Borsuk-Ulam Theorem (BUT) states that a single point, if embedded in one spatial dimension higher, gives rise to two antipodal points with matching descriptions and similar features. Novel BUT variants allow the assessment of countless physical systems, from entropies to quantum entanglement. We argue that BUT, cast in a quantitative fashion which has the potential of being operationalized, is a universal principle underlying a number of natural phenomena.

Topology, which assesses the properties that are preserved through deformations, stretchings and twistings of objects (Manetti; Krantz), is a underrated methodological approach with countless possible applications. In particular, we show that novel incarnations of the “classical” Borsuk-Ulam theorem (BUT) lead to a better comprehension and assessment of several physical phenomena. BUT and its variants provide indeed a topological methodology for the evaluation of the most general features of systems activity, cast in an empirical fashion that has the potential to be operationalized.

The “standard” version of the Borsuk-Ulam theorem (BUT). The notation S^n denotes an n -sphere, which is a generalization of the circle (Weeks). A n -sphere is a n -dimensional structure of constant, positive curvature, embedded in a $n+1$ space (Marsaglia; Henderson). For example, a 1-sphere (S^1) is the one-dimensional circumference surrounding a 2-dimensional disk, while a 2-sphere (S^2) is the 2-dimensional surface of a 3-dimensional ball (a beach ball is a good example). A 3-sphere is a 3-dimensional manifold which is enclosed in a Euclidean 4-dimensional space called a 4-ball. A 3-sphere is thus the surface of a 4-dimensional ball, while a 4-dimensional ball is the interior of a 3-sphere, in the same way as a bottle of water is made of a glass surface and a liquid content. The Borsuk-Ulam Theorem (Borsuk 1933; Dodson) states that, if a sphere S^n is mapped continuously into a n -dimensional Euclidean space R^n , there is at least one pair of antipodal points on S^n which map onto the same point of R^n (Beyer) (**Figure A**). Points on S^n are *antipodal*, provided they are diametrically opposite. Examples of antipodal points are the opposite points along the circumference of a circle, or the poles of a sphere (Matousek). The **SUPPLEMENTARY INFORMATION 1** provides a mathematical treatment for technical readers.

Matching signals (Signal-BUT). The concept of antipodal points can be generalized to countless types of systems’ signals (Borsuk 1958-59; Borsuk 1969). They can be used not just for the description of simple topological points, but also of more complicated structures, such as shapes of space (spatial patterns), of shapes of time (temporal patterns), vectors or tensors, functions, signals, thermodynamical parameters, movements, trajectories and general symmetries (Peters 2016) (**SUPPLEMENTARY INFORMATION 2**). If we simply evaluate systems activity instead of “signals”, BUT leads naturally to the possibility of a region-based, not simply point-based, geometry, with many applications. A region can have indeed features such as area, diameter, average signal value, and so on. We are thus allowed to describe systems features as antipodal points on a n -sphere. If we map the two points on a $n-1$ –sphere, we obtain a single point. This means that signal shapes can be compared (Weeks; Peters 2016): the two antipodal points standing for systems features are assessed at one level of observation, while the single point at a lower level (Tozzi 2016a).

BUT for non-antipodal points (Re-BUT). The BUT can be generalized not just for the evaluation of antipodal, but also of non-antipodal points on an n -sphere (**Figure B**). We can consider regions on an n -sphere that are either adjacent or far apart (Tozzi 2016a). And ReBUT applies, provided there are a pair of regions on n -sphere with the same feature value. Therefore, the two points (or regions) do not need necessarily to be antipodal, in order to be described together (Peters 2016). This makes it possible to evaluate matching signals, even if they are not “opposite”, but “near” each other: the antipodal points restriction from the “standard” BUT is no longer needed.

Generalization of BUT to antipodal points occurring on hyperbolic manifolds (Hyper-BUT). The original formulation of BUT describes antipodal points on spatial manifolds in every dimension, provided the n -sphere is a convex structure with positive curvature (i.e, a ball). However, many natural phenomena occur on manifolds endowed with other types of geometry. BUT can be generalized also to symmetries occurring either on flat manifolds, or on Riemannian hyperbolic n -manifolds of constant sectional curvature -1 and concave shape (i.e, a saddle) (Mitroi-Symeonidis). In other words, whether the systems function displays a concave, convex or flat structure, it does not matter: we may always find the points with matching description predicted by BUT. For further details, see Tozzi (2016a).

Changes in the n value of S^n spheres (S^n -BUT). Although BUT was originally described just in case of n being a natural number which expresses a structure embedded in a spatial dimension, nevertheless the value of n can stand for other types of numbers. The n value of S^n can be also cast as an integer, a rational or an irrational number (Tozzi 2016). The n value could express completely different parameters: for example, we might regard functions or shapes as embedded in a sphere in which n does not stand for a spatial dimension, but for the time or a fractal dimension. This makes it possible to use the n parameter as a versatile tool for the description of systems features.

Systems' symmetry breaking (Sym-BUT). Symmetries are widespread invariances underlining countless physical systems (Weyl). A symmetry break occurs when the symmetry is present at one level of observation, but "hidden" at another level (Roldàn). BUT tells us that symmetries can be found when evaluating the system in a proper dimension, while they disappear (are hidden or broken) when we evaluate the same system in just one dimension lower. The symmetries are widespread at every level of organization and may be regarded as the most general feature of systems, perhaps more general than free-energy and entropy constraints too (Tozzi 2016). Thus, giving insights into symmetries provides a very general approach to every kind of systems function.

BUT without euclidean spaces (No-R-BUT). A S^n manifold can also not map to a R^{n-1} Euclidean space, but straight to a S^{n-1} manifold. In other words, in this BUT formulation the Euclidean space is not mentioned. In many applications (for example, in fractal systems), we do not need the Euclidean manifold (the ball) at all: by an intrinsic, "internal" point of view, a manifold may exist in - and on - itself, and does not need to lie in any dimensional space (Weeks). Therefore, we do not need a S^n manifold curving into a dimensional space R^n : we may think that the manifold just does exist by itself. Without the BUT limitation of the Euclidean space, we are allowed to modify the S^n exponent such that it can be not just a natural number, but also other kinds of numbers, as already described above for the S^n -BUT. Another important consequence is that a n -sphere may map on itself: the projection of two antipodal points to a single point into a dimension lower can be internal to the same n -sphere.

BUT's four versatile ingredients (summarized in the **Table**) can be modified in different guises, in order to achieve a wide range of uses. To make an example, when we just consider quantum systems just one dimension higher, we are able to assess entanglement from an unusual perspective. A quantum entanglement's composite system does not display separable states and a single constituent cannot be fully described without considering the other states. If we introduce quantum entanglement on a hypersphere -, derived from signals originating on the surface of an ordinary 3D sphere - a separable state can be achieved for each of the entangled particles, just by embedding them in a higher dimensional space. When the particles are entangled at the 3D level and un-entangled at the 4D hypersphere level, we accomplish a composite system in which each local constituent is equipped with a pure state. Other examples of BUT applications are provided in **Figures C-E**. For additional applications in nonlinear chaotic dynamics (evaluation of S^n spheres equipped with a n = Feigenbaum constant), see Tozzi (2016a and 2016b).

A shift in conceptualizations is evident in the BUT approach: the opportunity to treat physical systems as topological structures gives us the invaluable chance to evaluate them through correspondences from topological spaces to algebraic groups (Matoušek; Yang; Dol'nikov). Embracing systems in the framework of algebraic topology (Willard; Dodson) means that transformations (the antipodal points) can be described as paths or trajectories on "abstract" structures: the BUT perspective allows a system's property located in the real space (the physical milieu's geometric space) to be translated to an abstract space (called topological configuration space manifolds) and *vice-versa*, enabling us to achieve maps from one level to another. It makes it possible for us to study systems interactions in terms of affine connections and "proximity" among signals, in order to explain, for example, how network communities integrate or segregate information (**SUPPLEMENTARY INFORMATION 2**).

INGREDIENTS	GENERAL FEATURES	SPECIFIC FEATURES
1) CONTINUOUS FUNCTION	LANDSCAPE	Observation
2) TWO ANTIPODAL POINTS (BUT) or REGIONS (ReBUT)	SPATIAL PATTERNS	Points
		Regions
		Diameters
		Areas
		Shapes
		Concave manifolds
	TEMPORAL PATTERNS	Movements
		Trajectories
	FUNCTIONS	Symmetries
		Proximities
Affine connections		
Vectors		
Regions		
Homologies		
SIGNALS	i.e., average signal value	
3) N-VALUES	NUMBER	Natural
		Fractional
		Irrational
	DIMENSION	Spatial
		Temporal
		Thermodynamical parameters
		Index dimension
Absence of Euclidean space		
4) MAPPING FROM A HIGHER TO A LOWER DIMENSION (and vice versa)	FIXED	Description
	IN MOTION	Real-Time Description
	SYMMETRIES	Increased in a n-dimension; decreased in a n-1 dimension

Table. Different features of each one of the four ingredients of BUT and its variants.

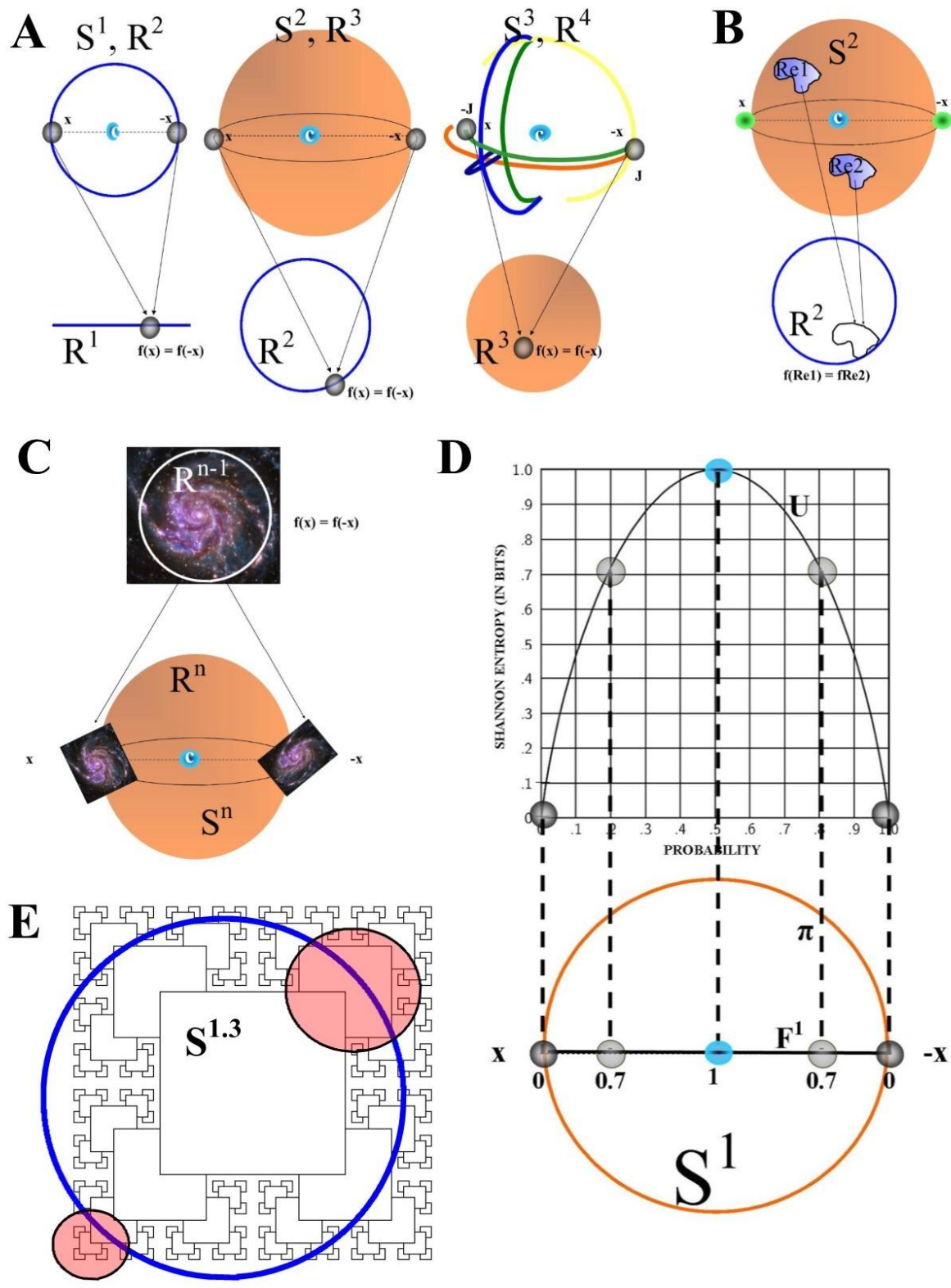


Figure. Many phenomena can be described by BUT and its variants. **A:** the “standard” BUT for different values of S^n (a circle, a sphere and a hypersphere). **B:** A simplified sketch of Re-BUT. **C:** ReBUT allows the evaluation of gravitational lenses. **D:** Shannon (ergodic) entropy values projected to a S^1 sphere: i.e. when entropy = 0.7, two antipodal points are displayed on a S^1 's diameter. Also “non-ergodic” entropies (i.e. not following the Shannon’s curve) could be

evaluated on other diameters of S^1 : the use of BUT variants wipes away this long-standing limit of Shannon entropy. **E**: on a self-similar structure, two antipodal points (corresponding to the distinctive scale-free's higher and lower magnifications) are embedded in a n-sphere equipped with $n =$ rational number (the fractal dimension: in this example, 1.3).

REFERENCES

- 1) Beyer WA, Zardecki A. The early history of the ham sandwich theorem. American Mathematical Monthly, 111, n. 1, 2004, 58-61
- 2) Borsuk, M. Dreisatz über die n-dimensionale euklidische sphäre, Fundamenta Mathematicae XX (1933), 177–190.
- 3) Borsuk, K. Concerning the classification of topological spaces from the standpoint of the theory of retracts, Fund. Math., XLVI, 321-330 (1958-1959), MR0104216.
- 4) Borsuk, K. Fundamental retracts and extensions of fundamental sequences, Fund. Math. 64(1), 55–85 (1969), MR0243520.
- 5) Dodson, C.T.J. and P.E. Parker, A user's guide to algebraic topology, Kluwer, Dordrecht, Netherlands, 1997, xii+405 pp. ISBN: 0-7923-4292-5, MR1430097.
- 6) Dol'nikov V. L. A generalization of the ham sandwich theorem. Math. Notes, 52:771–779, 1992. (refs: pp. 29, 51, 64)
- 7) Krantz, S.G. A guide to topology, The Mathematical Association of America, Washington, D.C., 2009, ix + 107pp.
- 8) Manetti, M. Topology, Springer, Heidelberg, 2015, xii+309 pp., DOI 10.1007/978-3-319-16958-3.
- 9) Marsaglia, G. (1972). "Choosing a Point from the Surface of a Sphere". Annals of Mathematical Statistics 43 (2): 645–646. doi:10.1214/aoms/1177692644
- 10) Matoušek, J. Using the Borsuk–Ulam Theorem. Lectures on Topological Methods in Combinatorics and Geometry. Springer-Verlag Berlin Heidelberg, 2003
- 11) Mitroi-Symeonidis F-C. Convexity and sandwich theorems. European Journal of Research in Applied Sciences, vol. 1 (2015), pp. 9-11
- 12) Henderson, D.W. (1996). Experiencing geometry on plane and sphere. Prentice Hall. ISBN 978-0-13-373770-7.
- 13) Peters JF (2016) Computational Proximity. Excursions in the Topology of Digital Images. Intelligent Systems Reference Library, Springer, Berlin, *in press*.
- 14) Roldán E, Martínez IA, Parrondo JMR, Petrov D. Universal features in the energetics of symmetry breaking. Nature Physics 10, 457–461 (2014) doi:10.1038/nphys2940
- 15) Tozzi A., Peters JF. (2016a) A topological approach unveils system invariances and broken symmetries in the brain. Journal of Neuroscience Research, *in press*.
- 16) Tozzi A., Peters JF. (2016b). Towards a fourth spatial dimension of brain activity. Cognitive Neurodynamics, *in press*. DOI: 10.1007/s11571-016-9379-z
- 17) Yang C.T. On theorems of Borsuk–Ulam, Kakutani–Yamabe–Yujob^o and Dynson, I. Annals of Math., 60:262–282, 1954.
- 18) Weeks JR. The shape of space, IInd edition. Marcel Dekker, inc. New York-Basel. 2002
- 19) Weyl, H (1982). Symmetry. Princeton: Princeton University Press. ISBN 0-691-02374-3.
- 20) Willard, S. General topology, Dover Pub., Inc., Mineola, NY, 1970, xii +369pp, ISBN: 0-486-43479-6 54-02, MR0264581.

SUPPLEMENTARY INFORMATION 1

The “standard” version of the Borsuk-Ulam theorem (BUT). The Borsuk-Ulam Theorem (BUT) is a remarkable finding by K. Borsuk (Borsuk 1933) about Euclidean n-spheres and antipodal points. It states that (Dodson 1997):

Every continuous map $f : S^n \rightarrow R^n$ must identify a pair of antipodal points (on S^n). (Figure 1).

An n-sphere is formed by points which are constant distance from the origin in $(n+1)$ -dimensions (Marsaglia). For example, a 3-sphere (also called *glome* or *hypersphere*) of radius r (where r may be any positive real number) is defined as the set of points in 4D Euclidean space at distance r from some fixed center point \mathbf{c} (which may be any point in the 4D space) (Henderson). From a geometer's perspective, we have the following n-spheres, starting with the perimeter of a circle (S^1) and advancing to S^3 , which is the smallest hypersphere (Figure 1), embedded in a 4-ball:

1-sphere $S^1 : x_1^2 + x_2^2$ (circle perimeter),

2-sphere $S^2 : x_1^2 + x_2^2 + x_3^2$ (surface of the common sphere, i.e., a beach ball),

3-sphere $S^3 : x_1^2 + x_2^2 + x_3^2 + x_4^2$ (hypersphere surface), ...,

n-sphere $S^n : x_1^2 + x_2^2 + x_3^2 + \dots + x_n^2$

SUPPLEMENTARY INFORMATION 2

Re-BUT variant for non-antipodal signals. Let a pair of systems modules (for sake of simplicity, we will talk about a pair of cortical or subcortical neural modules), represented by A^n, B^n , be n -spheres that interact and then separate. This is an example of the situation described by Schrödinger (1935). Let $p_1, -p_1$ be a pair of antipodal points on A^n and let $q_1, -q_1$ be a pair of antipodal points on B^n . Also let f, g be continuous functions and, using BUT, assume that:

$f : A^n \rightarrow \mathbb{R}^n$, such that $f(p_1) = f(-p_1)$, and

$g : B^n \rightarrow \mathbb{R}^n$, such that $g(q_1) = g(-q_1)$.

From BUT, the signal value $f(p_1)$ from A^n can be used to make observations about B^n , provided $f(p_1) = g(-q_1)$. This situation is analogous to the one described by Schrödinger in his paper on separated systems (Schrödinger 1935). That is, we look for an affine connexion (affinity) between modules represented by their feature vectors and by a sameness described by continuous functions on the modules. Using BUT, if antipodal points on A^n, B^n emit a common a signal value, then an affine connexion between the physical entities is established. However, this situation is less than satisfactory, since it is not apparent how to make the connexion between the n -spheres A^n, B^n based on the fact that both n -spheres have pairs of antipodal points that map to the same vector in \mathbb{R}^n .

Schrödinger was dissatisfied with attempting to find a connexion between vectors using a principle from Euclidean geometry, namely, two vectors are equal when their components are equal. He thought that it is more satisfactory to establish a connexion between physical entities using the notion of continuous transfer (of energy) between points on a curve finitely apart from each other (Schrödinger 1944). But this alternative is still not satisfactory, because curvature is described using rather complicated tensors such as the Riemann-Christoffel curvature tensor, which has 96 components, and the Weyl's metrical tensor, which has 40 components. An alternative to Schrödinger's approaches to establishing affinities between physical entities (neural modules) is obtainable by introducing a region-based form of BUT (denoted by ReBUT). To use our knowledge of one n -sphere to gain knowledge about another d -sphere with $d \leq n$, we consider separated regions instead of antipodal points on an n -sphere.

The terminology we use is explained, next. **Region.** A "region" (denoted by Re) on an n -sphere (i.e, a neural module) is a set containing one or more points. A singleton region is the same as point. Each region is a set of modules. Each module has only feature, namely, its location identified by a vector. By contrast, such a region Re (into a module) not only has location represented by its centroid (center of mass) but also region features such as diameter, area, entropy, shape, porous (shape with holes, i.e., some of the points in Re have gaps between them), average signal value and so on. **Family of regions 2^{S^n} .** The collection (family) of all subsets on the n -sphere S^n is denoted by 2^{S^n} . **Regions $Re_1, Re_2 \in 2^{S^n}$.** Regions Re_1, Re_2 are members in 2^{S^n} . **Feature value probe $\phi : Re \rightarrow \mathbb{R}$.** A feature value probe is a real-valued function that extracts a feature value from a region. **Region feature k-vector.** Let $\phi_1, \phi_2, \dots, \phi_k$ be k region feature value probes. A feature value vector for a region on an n -sphere has the following form: $(\phi_1(Re), \phi_2(Re), \dots, \phi_k(Re))$, called region feature vector.

Theorem 1. ReBUT. Assume that the regions on an n -sphere have n features. If $f : 2^{S^n} \rightarrow \mathbb{R}^n$ is a continuous function, then $f(Re_1) = f(Re_2)$ for at least one pair of regions $Re_1, Re_2 \in 2^{S^n}$ (Peters 2016). (**Figure B**).

Proof. The function $f(Re_1)$ is a feature vector in \mathbb{R}^n for region $Re_1 \in 2^{S^n}$. Given region $Re_1 \in 2^{S^n}$ on an n sphere, we know, from the symmetry of the latter, that there are many possible regions Re_2 with feature vectors that match the feature vector of Re_1 . Hence, $f(Re_1) = f(Re_2)$ for some $Re_2 \in 2^{S^n}$.

For example, let each each region on a 2-sphere (a brain module) have two features, namely, area and diameter. Since there are many regions on a 2-sphere with the same area and diameter, from ReBUT, we know that $f(Re_1) = f(Re_2)$ for at least one pair of regions $Re_1, Re_2 \in S^2$. This means that the antipodal points restriction of the "classical" BUT is no longer needed, when we consider regions on an n -sphere. In fact, we can now consider neural regions that are either adjacent or separated (far apart). And ReBUT applies, provided the feature vector for a region on an n -sphere (a nervous module) has n feature values.

Observations Via ReBUT for symmetrical physical entities (two separated cortical modules). In touch with Schrödinger's Programme of Observations, we want to use our knowledge on physical entity A (a cortical module) to gain knowledge about another physical entity B (another cortical module) that is separated from A. We do this using ReBUT. Let S_1^n, S_2^n be a pair of n -spheres that represent a pair of separated cortical modules. The regions on the surface of an n -sphere are comparable to mailboxes, each one containing information about some part of a module. All that we know about an n -sphere is summarized by the collection of feature vectors that describe the regions on an n -sphere.

Apply ReBUT to the pair of n -spheres S_1^n, S_2^n . Let $f : S_1^n \rightarrow \mathbb{R}^n$ be a continuous function on S_1^n and let $g : S_2^n \rightarrow \mathbb{R}^n$

be a continuous function on S_2^n . Let Re_1^1, Re_1^2 be a pair of regions on S_1^n and let Re_2^1, Re_2^2 be a pair of regions on S_2^n that

satisfy ReBUT. That is, from ReBUT, we obtain $f(Re_1^1) = f(Re_1^2)$ and $f(Re_2^1) = f(Re_2^2)$ on the separated n-spheres. Then the pair of n-spheres S_1^n, S_2^n resemble each other (similarity between the physical entities is established, provided $f(Re_1^1) = f(Re_2^1)$).

Observations Via ReBUT for asymmetrical physical entities (a cortical and a subcortical module). Let $S^n, S^d, d \leq n$ be n-sphere and d-sphere, respectively, that represent a pair of physical entities (in this case, a cortical and subcortical nervous module). Assume that each region on S^n is described by a feature vector with n-components and assume that each region on S^d is described by a feature vector with d-components with $n \neq d$. All that we know about the n-sphere (the cortical module) is summarized by the collection of feature vectors (each with n-components) that describe the regions on an n-sphere. By contrast, all that we know about the d-sphere (the subcortical module) is summarized by the collection of feature vectors (each with d-components) that describe the regions on an d-sphere.

Let $Re1, Re2$ on S^n that satisfy ReBUT and let $Re3, Re4$ on S^d that satisfy ReBUT. This means that $f(Re1) = f(Re2)$ on R^n and $g(Re3) = g(Re4)$ on R^d . Hence, the feature vectors $f(Re1), g(Re3)$ are not comparable, since each has a different number of components. Even so, we can compare $f(Re1), g(Re3)$ componentwise. Let $\varphi_1, \varphi_2, \dots, \varphi_n$ be n region feature value probes. A feature value vector for a region on the n-sphere S^n has the following form:

$\Phi(Re1) = (\varphi_1(Re1), \varphi_2(Re1), \dots, \varphi_n(Re1))$, i.e, a S^n region Re1 feature vector.

Further, let $\varphi_1, \varphi_2, \dots, \varphi_d$ be d region feature value probes, $n \neq d$. A feature value vector for a region on the n-sphere S^n has the following form:

$\Phi(Re3) = (\varphi_1(Re3), \varphi_2(Re3), \dots, \varphi_d(Re3))$, i.e a S^d region Re3 feature vector.

The continuation of the Schrödinger's Programme of Observations via ReBUT for asymmetrical physical entities (i.e., cortical and subcortical modules represented by hyperspheres with different dimensions), is made possible by the fact that d region features are the same for both the modules. The pair of hyperspheres' feature vectors $f(Re1), g(Re3)$ are descriptions of similar regions, provided S^n, S^d each contains at least one region $Re1$ on S^n and at least one region on S^d with feature vectors $\Phi(Re1), \Phi(Re3)$ with up to $n-d$ matching components. In other words, separated neural modules, represented by hyperspheres with different dimensions, have feature vectors that are componentwise comparable. The separated modules are similar, provided there is a feature vector $f(Re1)$ for a region $Re1$ on a hypersphere S^n which has d components with values that match the values of the corresponding components in the feature vector $f(Re1)$ for a region $Re3$ on a hypersphere S^d . For example, we may evaluate the case of similarity between neural regions on hyperspheres with different dimensions (a brain surface and a thalamus surface). Let $\varphi_1, \varphi_2, \varphi_3$ be three region feature value probes for region features diameter, area, shape, respectively, on a 3-sphere (a cortical module). And let φ_1, φ_2 be two region feature value probes for region features diameter, area, respectively, on a 2-sphere (for example, a thalamic module). Let $Re1, Re2$ be regions on a hypersphere S^2 that satisfy ReBUT and let $Re3, Re4$ be regions on a hypersphere S^1 that satisfy ReBUT. If $\Phi(R1) = (\varphi_1(R3), \varphi_1(R2) = \varphi_1(R4)$ (matching components), then the hypersphere S^2 is similar to S^1 . This tells us that there are similarities between the separated nervous structures represented by the hyperspheres S^2 and S^1 .

REFERENCES SUPPLEMENTARY INFORMATION

- 1) Schrödinger E, Discussion of probability relations between separated systems, Math. Proceedings of the Cambridge Philos. Soc. 31 (1935), no. 04, 555–563, MR1479992.
- 2) Schrödinger E. The affine connection in physical field theories, Nature 153 (1944), 572-575, MR0010800.

GENERALIZATION OF BORSUK-ULAM THEOREM TO HYPERBOLIC IMAGES

We stated that it is necessary to correlate images geometric regions with semantic features, such as oblong, concave, perpendicular, circular and so on. The Borsuk-Ulam theorem describes the presence of antipodal points on convex manifolds in every dimension. However, many images display figures equipped with another type of geometry: the hyperbolic one, characterized by sectional curvature -1 . i.e., a concave shape. Now the question is whether the antipodal points predicted by BUT can be detected not also on positive-curvature images as stated by Borsuk, but also on images equipped with negative curvature. In other words, is possible to transport such antipodal points onto riemannian manifolds with NEGATIVE curvature? The answer is positive, if we perform a parallel transport of the two antipodal points of S^n onto the hyperbolic manifold. Although parallel-transport requires the solution of a second-order differential equation, however analysis shows us that we are allowed to use the first order approximation of the parallel transport – that we pursue in terms of solving geodesic equations for the sufficient statistics (Hairer 2004). There are different routes one can take to achieve the goal: one needs to resort to one of the following generic transport procedures.

- 1) Ehresmann connection (see **Figure**) (Ehresmann, 1950).
- 2) Levi-Civita connection (Boothby 1986).
- 3) We can formulate the Hessian operator on the Riemannian manifold in terms of the Laplace-Beltrami operator (Jost 2002).
- 4) We can retain a first-order approximation and formulate descent directions that are orthogonal to the previous descent ones, through numerical analysis with the conjugate gradient-descent algorithm (Snyman 2005). Routinely used in optimization, conjugate gradient descent methods have been used for gradient descent on manifolds traced out by energy functions such as the variational free-energy (Sengupta 2014).

In summary, the BUT can be generalized also to concave figures, in order to look for antipodal points also in images equipped with a negative curvature.

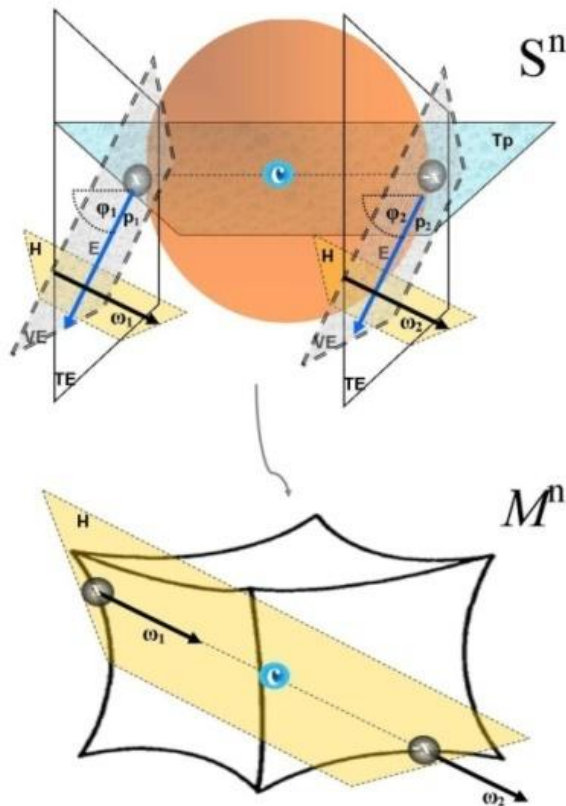


Figure. Parallel transport on Riemannian manifolds of two antipodal points p (corresponding to x and $-x$ of the BUT), from the convex S^n manifold to the concave one M^n . After an Ehresmann connection has been performed and the vectors

ω on S^n are achieved, the standard projection method (Hairer 2004) allows us to use the Riemann exponential map $\exp(\omega)$ to map the vector from $S^n \rightarrow M^n$, and the logarithmic map $\log(\omega)$ for the opposite mapping $M^n \rightarrow S^n$. Let H be the plane on the convex Riemannian manifold M^n where the vectors ω_1 and ω_2 (representing the antipodal points x or $-x$) lie. Once achieved the center of the hyperbolic manifold M^n through the ham-sandwich theorem, we are allowed to map the two antipodal points from S^n to M^n .

REFERENCES

- 1) Boothby WM. An introduction to differentiable manifolds and Riemannian geometry. (1986) Academic Press. ISBN 0-12-116052-1.
- 2) Ehresmann, C. (1950). Les connexions infinitésimales dans un espace fibré différentiable. *Colloque de Topologie*, Bruxelles, pp. 29–55.
- 3) Hairer E, Lubich C, Wanner G. Geometric Numerical Integration: Structure Preserving Algorithms for Ordinary Differential Equations. 2004. Springer.
- 4) Jost J. Riemannian Geometry and Geometric Analysis. (2002). Berlin: Springer-Verlag, ISBN 3-540-42627-2.
- 5) Sengupta B, Friston KJ, Penny WD. Efficient gradient computation for dynamical models. *Neuroimage*. 2014 Sep;98:521-7. doi: 10.1016/j.neuroimage.2014.04.040. Epub 2014 Apr 23.
- 6) Snyman JA. Practical Mathematical Optimization: An Introduction to Basic Optimization Theory and Classical and New Gradient-Based Algorithms. (2005) Springer Publishing. ISBN 0-387-24348-8

TIME AS A GAUGE FIELD

The concepts of “constraints” and “virtual displacement” from analytical mechanics shed new light on the role of time and timescales in physical systems such as the Universe. We propose a covariant version of a gauge theory, in which the required global symmetry stands for the real constrained trajectories, i.e. the energetic gradient flows dictated by the second law of thermodynamics. The virtual displacements, occurring while time is held constant, stand for the local transformations acting on the system and able to “break” the symmetry. The time stands for the gauge field able to keep the Lagrangian invariant. We also provide a theoretical framework in which a topological approach to gravitational lenses is able to elucidate aspects of our theory of “time as a gauge field”. Thus, time is no longer one of the four phase space coordinates of a 4-D Riemannian Universe: it is just a gauge field superimposed to a 3-D system.

INTRODUCTION

Many current theories emphasize the foremost role of the “time” and “timescales” in different physical and biological fields, from cosmology – the 4-D Riemannian Universe –, to cellular function¹ and neural activity^{2,3}. Is such a tenet true? Although stochastic variables and random fluctuations regulated by the Langevin and the Fokker-Planck equations frequently occur⁴, physical and biological activities are only partially Brownian, since they are “constrained”. For example, the protein-folding final conformation is dictated by the minimum frustration principle on long evolutionary timescales, which states that proteins’ energy decreases more than expected, as they assume conformations progressively more like the native state^{5,6}. A strong bias in the protein’s surface energy landscape towards the native basin occurs, overcoming the asperities of the rugged landscape^{7,8}. In other words, proteins were enriched by evolution for sequences with the propensity to fold into the lowest energetic structures. Constraints also occur in countless other systems, from the nonlinear chaotic paths governed by strange attractors, to the structure of biological entities, ruled by their specific genetic pools. Despite the large number of different scenarios, the processes governing constraints on physical and biological systems may be generalized, taking into account a universal principle: the second law of thermodynamics, which states that “*every process occurring in nature proceeds in the sense in which the sum of the entropies of all bodies taking part in the process is increased*” (Planck’s formulation). In such a framework, the concepts of “virtual displacement” - from the far-flung branch of analytical mechanics - come into play^{9,10,11,12}. In this paper we will indeed elucidate, via a gauge theory, that close relationships occur among virtual displacements, probabilities and time.

In order to assess our theory, we also use the concept of gravitational lens. The latter is a distribution of matter (such as a cluster of galaxies) between a distant source and a terrestrial observer, capable of bending the light from the source, as it travels towards the observer. The amount of bending is one of the predictions of Einstein’s general theory of relativity. For example, the light from a distant galaxy is deviated due to the gravitational effects of a foreground celestial body, which acts like a lens and makes the distant source appear either distorted and magnified. In this paper, we argue that the mechanism of gravitational lenses can be explained in the algebraic topological terms of the Borsuk-Ulam theorem. Such a finding makes it possible to hypothesize a theory of time as a gauge field.

The manuscript contains four sections. The first section describes the virtual and real constraints in the framework of a “frozen” time. The second section, taking into account probabilistic arguments, shows how is possible to insert virtual constraints on the Shannon entropy’s plot, in order to correlate informational entropy with the arrow of time. The third section illustrates the procedure to sketch gauge theory based on the three above mentioned ingredients: constraints, probabilities and time. In the fourth section, a topological approach to gravitational lenses comes into play and shows how the methodology can be applied in order to clarify a theory of “time as a gauge field”.

VIRTUAL CONSTRAINTS

The key concept of virtual constraints is a dynamically imposed outer feedback control, so that the trajectory of a particle or an agent in the system’s phase space can be “forced” towards the desired orbits and outputs¹³. The virtual constraints reduce the degrees of freedom, coordinating the evolution of the various links throughout a single variable. A closed-loop mechanism is achieved, wherein dynamic behaviour is fully determined by the evolution of simplest lower-dimension system¹⁴. The resulting system is called a “virtual limit system”.

In mathematical terms, we define a set of $n - 1$ outputs (or constraints):

$$y = \varphi(p, q) = \bar{q} - h(\theta, p) = \bar{q} - h(\theta, p(t)),$$

where y and $\varphi(p, q)$ are the outputs or constraints, $\vec{q} \in R^{n-l}$ is a vector describing the actuated coordinates and velocities, p is the set of the design parameters, $\theta \in R$ is the unactuated variable, $\theta(q)$ is a function of the generalized coordinates of q . The latter equation describes the most general condition.

An inner-feedback loop is used to perform output feedback linearization in a local domain, where the matrix is invertible:

$$\psi(q)u = k(q; \dot{q}) + v,$$

where v is the outer feedback loop. Note that the equation includes a term \dot{q} which depends on time, where the upper

dot stands for the partial time derivative, i.e., $\dot{q} = \frac{\partial q}{\partial t}$ (de Wit *et al.* 2003)²⁶.

If an outer feedback loop v is designed to zeroing the output y , we get a partially linearized system in the form:

$$\ddot{y} = v.$$

Then the full system dynamic is captured by the solutions of:

$$\alpha(\theta)\ddot{\theta} + \beta(\theta)\dot{\theta}^2 + \gamma(\theta) = 0,$$

together with the imposed constraint for mean q -value:

$$\bar{q} = h(\theta, p),$$

where $\theta(q)$, $\alpha(\theta)$, $\beta(\theta)$ and $\gamma(\theta)$ are scalar functions depending on the inner feedback loop.

In conclusion, the virtual constraints are forces external to the system's phase space, able to modify an internal trajectory towards the required one. This process allows one to deal with high-dimensional systems with underactuated degree one, by only analyzing this second-order nonlinear equation.

In analytical mechanics the researchers cope with under-actuated Lagrangian systems of the form:

$$\frac{d}{dt} \left(\frac{\partial L}{\partial \dot{q}} \right) - \frac{\partial L}{\partial q} = B(q)u,$$

where q and \dot{q} are vectors of generalized coordinates and velocities, $L(q; \dot{q})$ is a Lagrangian of the system, $B(q)$ is a matrix function of an appropriate dimension, with rank equal to the number of inputs and u is a vector of independent control inputs. The under-actuation means that $\dim u < \dim q$, i.e., the number of actuators is less than the number of its degrees of freedom.

A virtual displacement is an assumed change of system coordinates occurring while time is held constant. It is called "virtual" rather than "real", since no actual displacement takes place without the passage of time. Computerized simulations may be performed to see what happens to physical and biological paths when time is kept fixed, *e.g.*, during the movements of animals in an environment, or during cytoplasmatic enzymatic reactions. For further details about the methodology, see **Figure 1**.

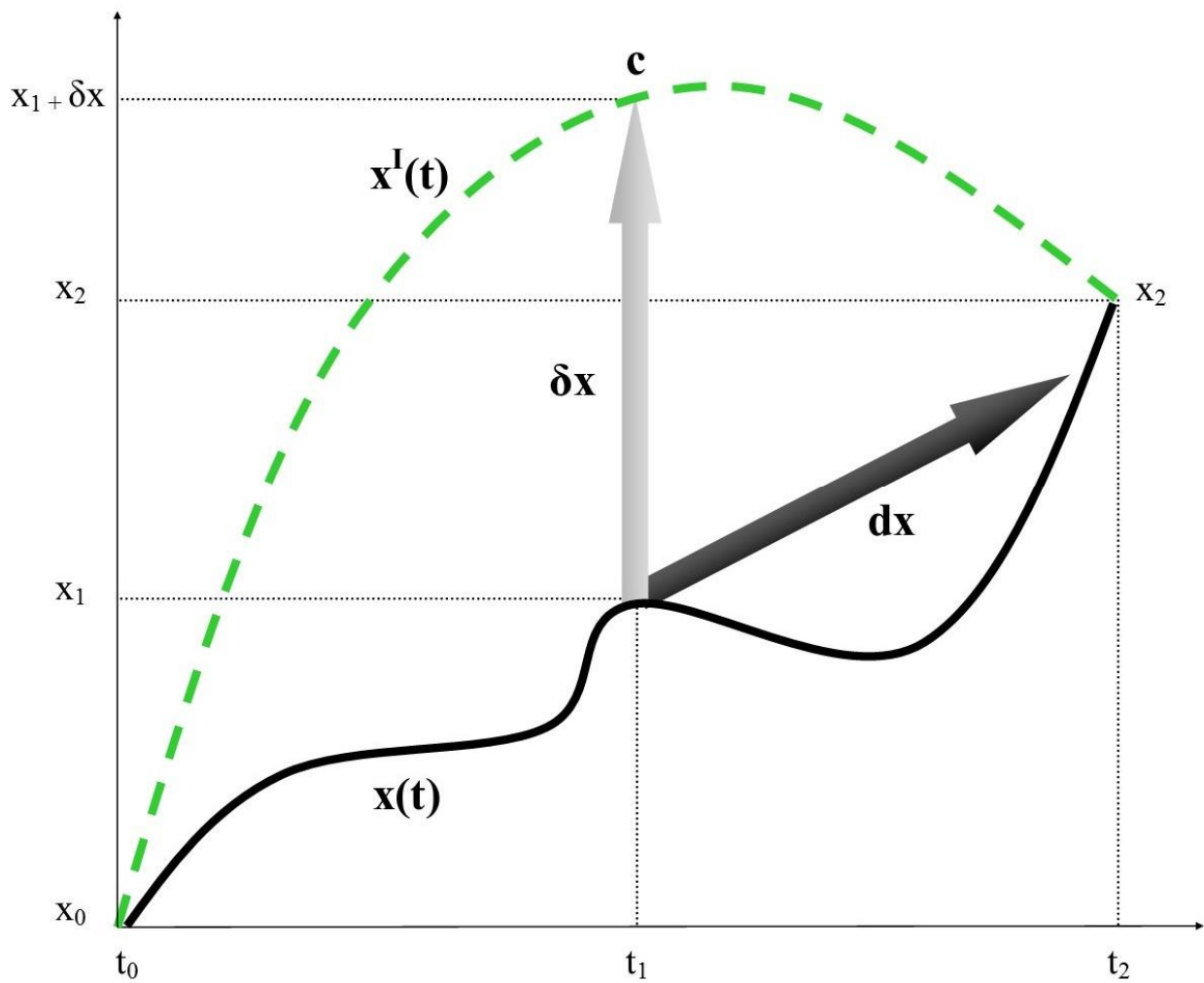


Figure 1. A graph plotting time t on the X-axis and the space x on the Y-axis. We evaluated two trajectories which both display a starting position at x_0 and an ending position at x_2 . The black solid curve $x(t)$ is the particle trajectory, while the dotted black curve $x^I(t)$ is the virtual trajectory. At position x_1 and time t_1 , the virtual displacement δx - from x_1 to the point c - is shown (grey arrow). The regular displacement dx is a vector pointing in the direction of the motion (black arrow), which arises from differentiating with respect to time parameter along the path of the motion. In contrast, the virtual displacement δx is a tangent vector to the constraining manifold at a fixed time, because it arises from the differentiation with respect to the enumerating paths of the motion, varied in a manner consistent with the constraints.

INFORMATIONAL ENTROPY AND TIME

The real displacements are governed by the second law of thermodynamics. In every system, either physical or biological, the thermodynamical entropy relentlessly increases from time T_0 to $T_2 = \infty$, until its maximum value. In our case, it is however preferable to use the informational entropy, instead of the thermodynamical one. Indeed, the two entropies are linked through the formula:

$$S = k H$$

in which S is the thermodynamical entropy, k is the Boltzmann constant and H is the Shannon informational entropy. The informational entropy, apart from the invaluable advantage of quantifying the macroscopic states without a perfect knowledge of the microscopic ones, is not directly linked with time, allowing us to remove such parameter from our system. However, we need to introduce the arrow of time on the "classic" Shannon's curve: we did it by adding a third

dimension to its 2-D plot (**Figure 2**). The vector of time ζ lies in a plane forming an angle A with the 2-D plane of Shannon entropy. Note that the timescales expressed by the vector ζ in the graphic may vary, depending on which system we are evaluating. As an example, if we take into account the system Universe, T_0 stands for the state of minimum entropy – the initial Big Bang -, while $T_2 = \infty$ stands for the state of maximum entropy, *i.e.*, the hypothetical final state of the Universe. Starting from the probability of a virtual constraint c , we may calculate the corresponding point T_1 on the arrow of time, in order to know how much time is still required to reach $T_2 = \infty$ (which stands for the system’s “real” final state at the energetic equilibrium). There is however a still unknown parameter left: the value of the angle A , which is not implied to be constant, but could change in different examined systems. The next section answers the question: how can we find the value of the angle A ?

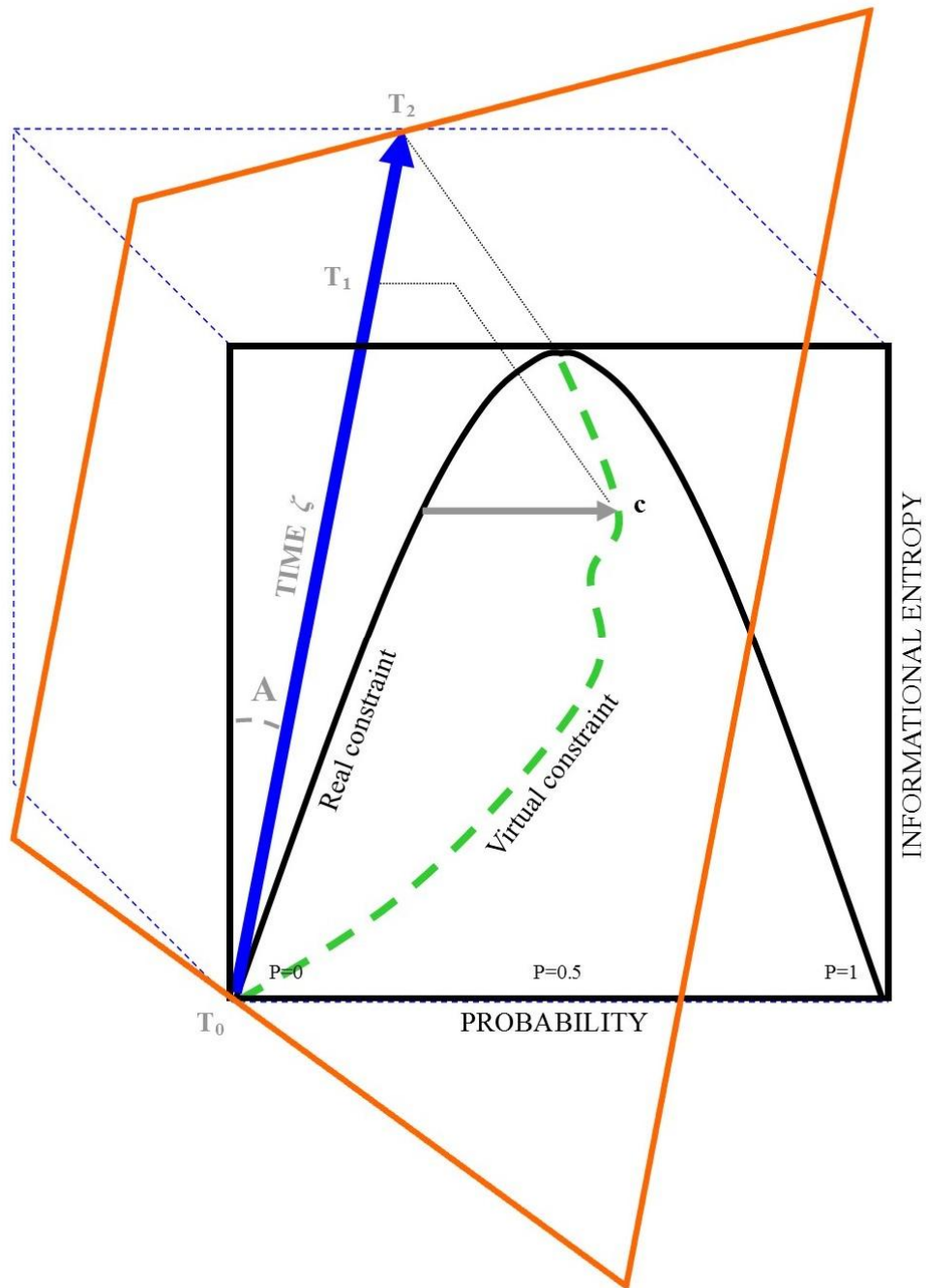


Figure 2. The informational entropy is plotted as a function of the random variable p , in the case of two possibilities with probabilities p and $(1-p)$. The solid line black stands for the Shannon entropy (under ergodic conditions). The values

$p=0$ and $p=1$ stand for the minimum entropy, $p=0.5$ for the maximum entropy. The arrow of time ζ (grey solid line) lies on a third coordinate of the phase space and is equipped with the angle A . Due to the energetic gradient flows dictated by the second law of thermodynamics, the time, in its route from T_0 to $T_2 = \infty$, is correlated with an increase in informational entropy. Given a virtual displacement c on the virtual trajectory (dotted black line), the corresponding value of T_1 on the arrow of time can be calculated, provided the value of A is known.

TIME IS A GAUGE FIELD: BUILDING A GAUGE THEORY

Here we examine the possibility to sketch a on differential geometry-based theory of the real and virtual trajectories' phase space. We need to build a system where the real displacement - the real trajectory of particles or events - stands for the continuous, global symmetry. Such a symmetry consists in the energetic constraints that the second law of thermodynamics enforces on the system. However, the energetic gradient flow occurs just in long timescales. In turn, in the very instant in which T is "frozen", fixed and equals to zero, the virtual displacement occurs, standing for a continuous group of local transformations able to "break" the symmetry. The local loss of symmetry (a disturbance of the gradient flow) needs however to be ripristinated, by introducing a continuous field – the time - able to restore the gradient flow. The time, in such a framework, stands for a field acting on the system, which is continuous at nonrelativistic timescales. There are many possible ways to deal with a theory of the virtual displacements in a differential geometric sense, for example by analyzing them in terms of sections of fibre bundles, jet manifolds and Ehresmann connections^{15,16,17}. We went through a system characterized by a global invariant symmetry. In order to quantitatively assess the required forces, we followed the procedure shown in the oversimplified **Figure 3**. In **Figure 3A**, as an example, we choose four random areas in a 3D system and equipped them with transformations belonging to the $SO(2)$ Lie group, isomorphic to the rotation group of the circle. The Lie group stands for the measure of probability density in each of the four areas. The manifold is unfolded and flattened into a two-dimensional reconstruction¹⁸ (**Figure 3B**), allowing the entire system surface to be transferred to an atlas M of C^∞ (smooth), finite dimensional manifolds, each corresponding to one of the four single areas at a fixed time= 0 (**Figure 3B**). The set of virtual displacements describing area-specific probabilities stands for a continuous group of local transformations acting on sections of M . M is thus equipped with a constant matrix G belonging to the $SO(2)$ Lie group.

M is a principal G -bundle P characterized by a trivial, smooth and differentiable fibre bundle, by vector bundles E and by a tangent bundle TE (**Figure 3B**). Virtual displacements are described by a field of vectors and angles, representing the action G on the chosen local section E of P . **Figure 3B** depicts the four forces G as four vector bundles E arising from four points p in the tangent space T_p . They are equipped with four n -dimensional rotation angles φ ($\varphi_1, \varphi_2, \dots, \varphi_n$)^T representing the (local) virtual displacement (expressed in terms of probability state) of every area. Rotations through tiny angles link nearby transformations of angles φ arising from points p : as a result, the linear approximation of the function G at p (and its angle φ) in each dimension can be described by introducing a partial derivative. Changes in degree of φ in selected areas match with virtual displacements' different probabilities and hence with different trajectory configurations.

The geometric "link" between L and φ can be defined in terms of a connection form, the Ehresmann connection¹⁹. If we identify the horizontal space H , perpendicular to the vertical space VE , we can extrapolate the Ehresmann connection ω , which is a vector on TE (**Figure 3B**). The Lagrangian density L is indeed a function of TE and H . It is possible to formulate all rates of change of ω and φ in terms of a covariant derivative - a linear differential operator in each associated TE - which allows different points (and their angles) to be compared. By mapping every vector ω of P into the bijective, diffeomorphic P^l space, a curvature form is constructed (**Figure 3C**). When the vectors ω^l intersect the unique horizontal lift corresponding to the invariant L , the angles σ are achieved. The behaviour of the vectors ω^l and the angles σ can be described compactly by point-wise vector addition of the partial derivatives of the function G at each point. As a result, we get a single vector: $\vec{\Omega} = \vec{\omega}_1 + \vec{\omega}_2 + \dots + \vec{\omega}_n$. The angle Σ is introduced (**Figure 3D**), standing for the interaction Lagrangian L_{int} and expressing the values of vector addition.

If the lines L and Ω are parallel, Σ equals zero, L_{int} equals L and the symmetry of the system is preserved. Otherwise, if L and Ω are not parallel (as in nearly all physical and biological systems at $T=0$), Σ is different from zero, L_{int} is different from L and the system displays a "broken" symmetry. In this case – to ensure the invariance of L and to restore the symmetry – we need to define a covariant derivative such that the derivative of Σ will again transform identically with Σ . According to the covariant version of gauge theories²⁰, the correction terms are reinterpreted as couplings to an additional divergent counter term, the gauge field, by allowing the symmetry parameter to vary from place to place in the local coordinate system. **Figure 3E** shows the procedure in a very abridged form. If we do not take L into account and examine

the sole vector \mathcal{Q} and its angle Σ , we observe nothing else than a single force. If instead we regard L as a vector that results from the scalar components of its vector space v , then \mathcal{Q} (and its angle Σ) turns out to be just one of the covariant components of L . To ensure that L is invariant, we need to add another component: we introduce the vector ζ , equipped with the angle Π . The latter stands for the gauge field Lagrangian L_{gf} and expresses the global value of the required gauge field. We are thus able to make accurate predictions of the forces: we can extrapolate from Π the values of the gauge field required to render the trajectories invariant under different virtual displacements.

Our scheme resembles a gauge theory^{21,22}, but with some distinctions. The physical gauge theories are based on three tenets^{23,24}:

- a) The system is equipped with a continuous, preserved “global” symmetry (and a corresponding Lagrangian).
- b) The system displays a continuous group of “local” transformations, equipped with a Lie group.
- c) The Lagrangian is kept invariant under such local transformations by a “gauge field”, i.e. a continuous force acting on the system.

The Lagrangian, through its connections with Noether’s theorem, throws a bridge between symmetries and energetic requirements. Note that the concept of the Lagrangian is slightly different in our model: instead of referring to the principle of least action and the “preservation” of a physical quantity as usual in gauge theories, it refers to the “dissipation” of a physical quantity through a gradient flow.

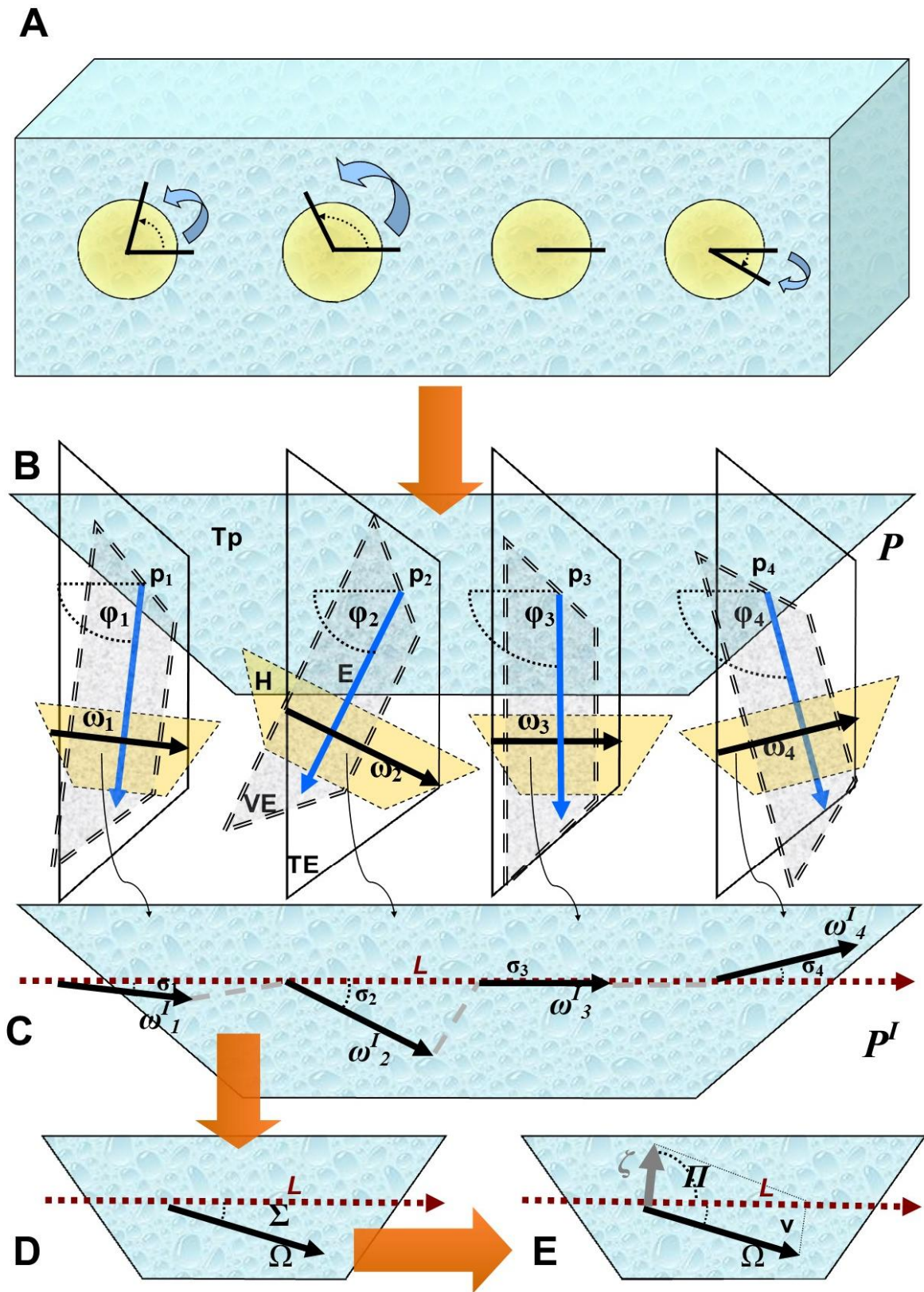


Figure 3. Oversimplified analysis of virtual displacements in a system equipped with a global, invariant symmetry (the real constraints). Four virtual displacements - expressed as measures of probability states in four areas of a 3D system, at time kept fixed at zero - are equipped with a Lie group (Figure 3A) and mapped on a 2-D manifold (Figure 3B). An

Ehresmann connection is performed (**Figure 3C**) and the required gauge field (the vector ζ , equipped with the angle Π) can be calculated (**Figures 4D-E**). See the main text for further details.

TIME AS A GAUGE FIELD: CLUES FROM A TOPOLOGICAL APPROACH TO GRAVITATIONAL LENSES

In this section we argue that the mechanism of gravitational lenses can be explained in the algebraic topological terms of the Borsuk-Ulam theorem (BUT). Indeed, gravitational lensing in the framework of BUT provides us the mathematical apparatus to build the theory of time as gauge field, which is otherwise too theoretical and untestable.

At first, we need to discuss the “standard” version of the Borsuk-Ulam theorem (BUT), which states states that (Borsuk)^{29,30}:

Every continuous map $f : S^n \rightarrow R^n$ must identify a pair of antipodal points (on S^n).

This means that the n -sphere S^n maps to the space R^n , which is an n -dimensional Euclidean space. Another less technical definition is: if a sphere is mapped continuously into a plane set, there is at least one pair of antipodal points having the same image; that is, they are mapped to the same point of the plane (Dodson)³¹. The notation S^n denotes an n -sphere, which is a generalization of the circle. A n -sphere is a n -dimensional structure embedded in a $n+1$ space. For example, a 1-sphere (S^1) is the one-dimensional circumference surrounding a 2-dimensional disk, while a 2-sphere (S^2) is the 2-dimensional surface of a 3-dimensional ball (a beach ball is a good example). An n -sphere is formed by points which are constant distance from the origin in $(n+1)$ -dimensions. For example, a 3-sphere (also called *glome* or *hypersphere*) of radius r (where r may be any positive real number) is defined as the set of points in 4D Euclidean space at distance r from some fixed center point c (which may be any point in the 4D space). A 3-sphere is a simply connected 3-dimensional manifold of constant, positive curvature, which is enclosed in a Euclidean 4-dimensional space called a 4-ball. A 3-sphere is thus the surface or boundary of a 4-dimensional ball, while a 4-dimensional ball is the interior of a 3-sphere, in the same way as a bottle of water is made of a glass surface and a liquid content.

Points on S^n are *antipodal*, provided they are diametrically opposite. Examples of antipodal points are the endpoints of a line segment, or the opposite points along the circumference of a circle. Further, every continuous function from a n -sphere S^n into Euclidean n -space R^n maps some pair of antipodal points of S^n to the same point of R^n . For example, if we use the mapping $f: S^3 \rightarrow R^3$, then $f(x)$ in R^3 is just a signal value (a real number associated with x in S^3) and $f(x) = f(-x)$ in R^3 . When $g: S^2 \rightarrow R^2$, the continuous function $g(x)$ in R^2 is a vector in R^2 that describes the x embedded in S^2 . In other words, a point embedded in a R^n manifold is projected to two opposite points on a S^{n+1} -sphere, and vice versa.

It is noteworthy that the concept of antipodal points can be generalized to countless types of system signals. The two opposite points can be used not just for the description of simple topological points, but also for more complicated structures, such as shapes of space (spatial patterns), shapes of time (temporal patterns), vectors or tensors, functions, signals, thermodynamical parameters, movements, trajectories, and general symmetries too (Peters)²⁸. If we simply evaluate systems activity instead of “signals”, BUT leads naturally to the possibility of a region-based geometry (called ReBUT), instead of point-based one, with many applications. Indeed, a region can have features such as area, diameter, average signal value, and so on. The concept of reBUT and generalized antipodal points may be also applied to the mechanism of gravitational lenses (**Figure 4**). We are allowed to describe gravitational lenses’ regional features (i.e., average gradient direction, average intensity, feature vectors with many components, such as, for example, diameter, surface area, and gradient direction) as antipodal points on a n -sphere: the antipodal points, even if they are distorted, display indeed matching descriptions. A cosmic body emitting a light stands for the single point embedded in R^{n-1} , which projects to two antipodal points onto a n -sphere embedded in a dimension higher, i.e., R^n . In other words, if we map the two opposite points on an $n-1$ sphere, we obtain a single point, and vice versa. The two antipodal points standing for systems features are assessed at one level of observation, while the single point is assessed at a lower level. The BUT scenario provides, in this way, a vehicle for characterizing and modelling gravitational lenses.

It can be argued that the antipodal points on a gravitational lens are not exactly “opposite” each other. However, the applications of BUT can be generalized not just for the evaluation of brain symmetries as antipodal points, but also for non-antipodal points on an n -sphere (Peters)²⁸. We can also consider homotopic regions on an n -sphere that are either adjacent or far apart. And BUT applies, provided there are a pair of regions on an n -sphere with the same feature values. We are thus allowed to say that the two points (or regions) do not need necessarily to be antipodal, in order to be described together (Peters)²⁸. This makes it possible to evaluate matching signals, even if they are not “opposite”, but “near” one each other: the antipodal points restriction from the “classical” BUT is no longer needed.

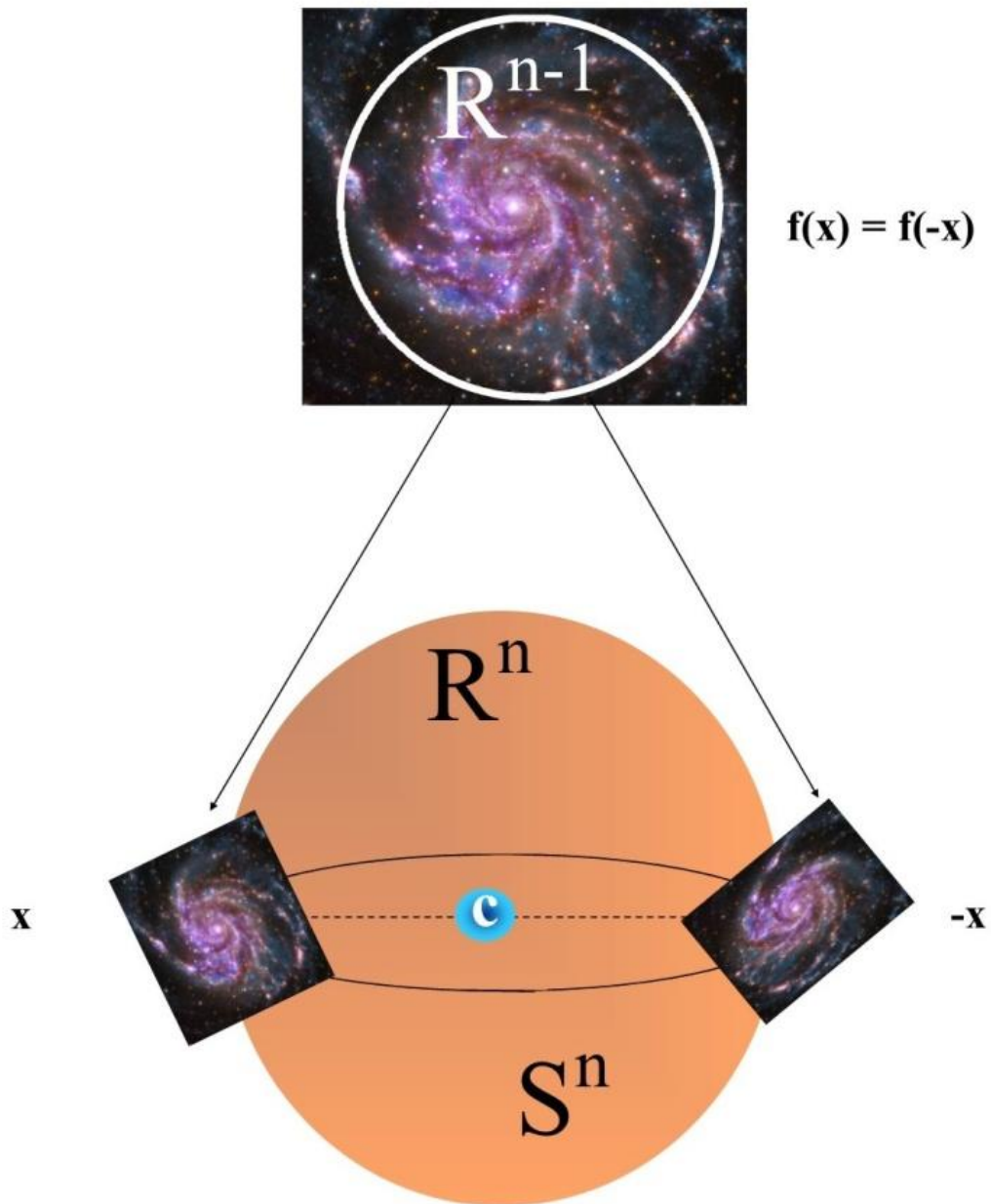


Figure 4. A simplified scheme of the application of the Borsuk-Ulam theorem to a gravitational lens. Two antipodal points in S^n project to a single point in R^n , and vice versa. Remind that every S^n is embedded in a $n+1$ -ball, so that every S^n is one-dimension higher than the corresponding R^n manifold. See the main text for further details.

A 3D Universe... plus time. By applying the equations of general relativity, the measure of the curvature of gravitational lens makes it possible to calculate the mass of the hidden cosmic object. Indeed, according to general relativity, when light passes around a massive object, it is distorted and bent towards an observer's eye, because of the curvature of the 4D spacetime. Since light moves at a constant speed, lensing changes the direction of the velocity of the light, but not the magnitude. The angle of deflection is:

$$\theta = \frac{4GM}{rc^2},$$

Where M is the mass at a distance r from the affected radiation, G is the universal constant of gravitation and c is the speed of light in a vacuum: the more the mass, the more the light angle deflection. In such a way, we are able to achieve the total quantity of matter which causes the gravitational lens effect: by measuring the distortion geometry, the mass of the intervening cluster causing the phenomena can be obtained. In the case of the Universe, according to the Einstein's dictates, the 4D dimension (the spacetime) occurs when the mechanism of gravitational lensing takes place. It means that the fourth dimension "appears" just when the light is projected, through gravitational lensing, in a dimension higher, while the hidden galaxy is equipped with just three dimensions. Therefore, according to BUT and Einstein claims, the gravitational lensing lies in a R^n space, i.e., a 4D riemannian manifold (the spacetime), while the "hidden" celestial body, which generates the light producing the gravitational lens, needs to lie in a R^{n-1} space, i.e, the three "classical" Euclidean dimensions. This means that we achieve a dimensionality reduction: a Universe equipped with just three dimensions, plus the time. The latter is the fourth dimension, provided that we consider it as superimposed to a 3D Universe. Thus, we are allowed to argue that the angle reflection is caused by a further dimension, displayed by the n -sphere generated by the gravitational lens. Without such a higher dimension, the angle reflection does not exist and the mass cannot be measured.

Gauge fields and time in the framework of BUT. According to BUT, we achieved a system with three dimensions plus the time. In such a vein, what is the role of the time? We need to invoke once again BUT, and its close relationships with the symmetries. Symmetries are widespread invariances underlining countless physical and biological systems (Weyl)³². A symmetry break occurs when the symmetry is present at one level of observation, but "hidden" at another level (Roldán)³³. BUT tells us that we can find, on an n -dimensional sphere, a pair of opposite points that have same encoding on an $n-1$ sphere. This means that symmetries can be found when evaluating the system in a proper dimension, while they disappear (are hidden or broken) when we evaluate the same system in just one dimension lower. We emphasize that the symmetries are widespread at every level of organization and may be regarded as the most general feature of systems, perhaps more general than free-energy and entropy constraints too. Indeed, recent data suggest that thermodynamic requirements have close relationships with symmetries. The recent, interesting observation that entropy production is strictly correlated with symmetry breaking in quasistatic processes paves the way to use system invariances for the estimation of the free energy of metastable states and the energy requirements of computations and information processing (Roldán)³³. Thus, giving insights into symmetries provides a very general approach to every kind of systems function. In such a vein, BUT provides a topological methodology for the evaluation of the most general features of systems activity, i.e., the symmetries, cast in a physical fashion that has the potential to be operationalized. The symmetries, in turn, are closely linked with gauge theories, and in particular with gauge fields. The n -sphere displaying the antipodal points (the symmetries) is equipped with a dimension more than the euclidean space where the the single point (symmetry break) occurs. This extra-dimension where BUT occurs might stand for a gauge field which, superimposed to the system, gives rise to the invariance of the symmetry, by "restoring" it with the simple add of a unity to the n member of BUT (from R^n to R^{n+1}). Although BUT was originally limited to the case of n being a natural number which expresses a structure embedded in a spatial dimension, nevertheless the value of n in the brain S^n can also stand for other types of numbers (Tozzi)²⁷. The n exponent does not need necessarily either to be a natural number or embedded in a spatial dimension. The n value of S^n can be casted as an integer, a rational or an irrational number. The BUT can be used not just for the description of "spatial" dimensions equipped with natural numbers, but also of antipodal points on spheres equipped with other kinds of n 's dimensions, for example a fractal dimension d . It allows us to use the n parameter as a versatile tool for the description of systems symmetries.

CONCLUSION

We showed that the vector of time is able to represent the energetic gradient of the system, locally "broken" by timeless perturbations. We also provided a topological approach to gravitational lensing which strengthens our hypothesis. It allows us to draw some conclusions.

In analytical mechanics, the concept of virtual displacement - related to virtual work - is meaningful only when discussing a system subject to constraints on its motion. As stated above, this is the case of physical and biological activity. Virtual displacements occur exclusively in space and the underrated role of the sole "spatial" modifications needs to be emphasized when bearing in mind physical and biological activities. While virtual displacements take place, time is fixed and $\delta t = 0$. Thus, changes in physical/biological functions can be independent of the passage of time. When time equals $\neq 0$, the real trajectory does not exist: it is the passing of time that gives rise to the real displacement. It has been recently suggested that time is an emergent phenomenon arising from the quantistic entanglement and it exists just for observers inside the universe²⁵: any god-like observer outside sees a static, unchanging universe, just as the Wheeler-DeWitt equations predict (note that time plays a role neither in such equations, nor in the formulation of the entangled states). If time stands for a continuous gauge field acting on the system's Universe, the theory of a 4D Riemannian Universe needs

to be revised: time is not anymore one of the four coordinates of the phase space of the system Universe, but becomes just a field, a vector superimposed to an otherwise “simple” 3D Universe. It may also be hypothesized that the virtual constraints in the Universe stand for singularities and timeless perturbations, which could be regarded as places in which life occurs.

REFERENCES

1. Kravchick, D.O. & Jordan, B.A. Presynapses go nuclear! *EMBO J.* **34**, 984-986 (2015).
2. Linkenkaer-Hansen, K., Nikouline, V.V., Palva, J.M., & Ilmoniemi R.J. Long-range temporal correlations and scaling behavior in human brain oscillations. *J. Neurosci.* **21**, 1370-1377 (2001).
3. Papo, D. How can we study reasoning in the brain? *Front Hum Neurosci.* **9**, 222 (2015).
4. Ribault, C., Sekimoto, K. & Triller, A. From the stochasticity of molecular processes to the variability of synaptic transmission. *Nat. Rev. Neurosci.* **12**, 375–387 (2011).
5. Bryngelson, J.D. & Wolynes, P.G. Spin glasses and the statistical mechanics of protein folding. *Proc. Natl. Acad. Sci. U S A.* **84**, 7524-7528 (1987).
6. Ferreiro, D.U, Hegler, J.A., Komives E.A. & Wolynes, P.G. On the role of frustration in the energy landscapes of allosteric proteins. *Proc Natl Acad Sci U S A.* **108**, 3499-503 (2011).
7. Onuchic, J.N., Luthey-Schulten, Z. & Wolynes, P.G. Theory of protein folding: the energy landscape perspective. *Annu. Rev. Phys Chem.* **48**, 545-600 (1997).
8. Sutto, L., Lätzer, J., Hegler, J.A., Ferreiro, D.U., & Wolynes, P.G. Consequences of localized frustration for the folding mechanism of the IM7 protein. *Proc. Natl. Acad. Sci. U S A.* 2007 **104**, 19825-19830 (2007).
9. Torby, B. *Energy Methods. Advanced Dynamics for Engineers.* HRW Series in Mechanical Engineering (CBS College Publishing, United States of America, 1984).
10. Goldstein, H. *Classical Mechanics* (Addison-Wesley Publishing Co., Reading, Massachusetts, 1980).
11. Sommerfeld, A. *Mechanics, Lectures on Theoretical Physics, vol. I* (Academic Press, New York, 1952).
12. Landau, L.L. & Lifshitz, M. *Mechanics* (Pergamon Press, Oxford, 1976).
13. Canudas-de-Wit, C. On the concept of virtual constraints as a tool for walking robot control and balancing. *Annual Reviews in Control* **28**, 157–166 (2004).
14. Stepp, C.E., Hillman, R.E. & Heaton, J.T. A virtual trajectory model predicts differences in vocal fold kinematics in individuals with vocal hyperfunction. *J Acoust Soc Am.* **127**, 3166-3176 (2010).
15. Kolar, I. & Michor, P. W. *Natural operations in differential geometry* (Springer-Verlag, Berlin, 1993).
16. Abraham, R.H. & Marsden, J. E. *Foundations of mechanics*, (Benjamin-Cummings, London, 1978).
17. Lang, S. *Differential and Riemannian manifolds* (Springer-Verlag, Berlin, New York, 1995).
18. Van Essen, D.C. A Population-Average, Landmark- and Surface-based (PALS) atlas of human cerebral cortex. *Neuroimage* **28**, 635–666 (2005).
19. Ehresmann, C. Les connexions infinitésimales dans un espace fibrée différentiable. *Colloque de Topologie, Bruxelles*, pp. 29–55 (1950).
20. DeWitt, B.S. Quantum Theory of Gravity II. The Manifestly Covariant Theory. *Phys. Rev.* **160**, 1195-1239 (1967).
21. Higgs, P.W. Broken Symmetries and the Masses of Gauge Bosons. *Phys. Rev. Lett.* **13**, 508 (1964).
22. 't Hooft, G. Renormalizable Lagrangians for massive Yang-Mills fields. *Nuclear Physics B* **35**, 167–188 (1971).
23. Zeidler, E. *Quantum Field Theory III: Gauge Theory.* Springer-Verlag, Berlin, Heideberg (2011).
24. Helland, I. S. Statistical inference under symmetry. *International Statistical Review* **72**, 409-422 (2004).
25. Moreva, E.V., Brida, G., Gramegna, M., Giovannetti, V., Maccone, L. & Genovese, M. Time from quantum entanglement: An experimental illustration. *Physical Review A* **89**, 052122 (2013).
26. De Wit, C.C., P. Tsiotras, E. Velenis, M. Basset, G. Gissinger, Dynamic tire friction models for vehicle traction/braking control, *Vehicle System Dynamics* 39(3),189-226 (2003).
27. Tozzi A., Peters J.F. A topological approach unveils system invariances and broken symmetries in the brain. *Journal of Neuroscience Research*, 2016, in press.
28. Peters, J.F. *Computational Proximity. Excursions in the Topology of Digital Images*, Springer, 2016, in press.
29. Borsuk, K. Drie satze uber die n-dimensional euklidische sphere, *Fund. Math.* XX, 177-190 (1933).
30. Borsuk, K. Concerning the classification of topological spaces from the standpoint of the theory of retracts, *Fund. Math.*, XLVI, 321-330 (1959), MR0104216.
31. Dodson, C.T.J., Parker, P.E. *A user’s guide to algebraic topology*, Kluwer, 1997, xii+405 pp., MR1430097.
32. Weyl, H (1982). *Symmetry*. Princeton: Princeton University Press. ISBN 0-691-02374-3.
33. Roldán E, Martínez IA, Parrondo JMR, Petrov D. Universal features in the energetics of symmetry breaking. *Nature Physics* 10, 457–461 (2014) doi:10.1038/nphys2940

QUANTUM ENTANGLEMENT ON A HYPERSPHERE

A quantum entanglement's composite system does not display separable states and a single constituent cannot be fully described without considering the other states. We introduce quantum entanglement on a hypersphere - which is a 4D space undetectable by observers living in a 3D world -, derived from signals originating on the surface of an ordinary 3D sphere. From the far-flung branch of algebraic topology, the Borsuk-Ulam theorem states that, when a pair of opposite (antipodal) points on a hypersphere are projected onto the surface of 3D sphere, the projections have matching description. In touch with this theorem, we show that a separable state can be achieved for each of the entangled particles, just by embedding them in a higher dimensional space. We view quantum entanglement as the simultaneous activation of signals in a 3D space mapped into a hypersphere. By showing that the particles are entangled at the 3D level and un-entangled at the 4D hypersphere level, we achieved a composite system in which each local constituent is equipped with a pure state. We anticipate this new view of quantum entanglement leading to what are known as qubit information systems.

1. INTRODUCTION

Quantum entanglement is a widely accepted, experimentally verified physical phenomenon occurring when a system of particles interact as a whole, in a way such that the quantum state of each particle cannot be described independently and their physical properties - such as position or spin - are instantly correlated (1). When a composite system is entangled, it is impossible to separate its components and attribute to each one a definite pure state. Quantum state cannot be factored as a product of states of its local constituents (e.g. individual particles) and one constituent cannot be fully described without considering the other(s) (2-4). It gives rise to a paradoxical effect: it seems that one particle of an entangled pair "knows" what measurement has been randomly performed on the other, even though such information cannot be communicated between them. While a composite system is always expressible as a sum of products of states of local constituents, when the system is entangled the sum necessarily has more than one term. This means that we cannot recognize cause/effect relationships. In such a framework, the Borsuk-Ulam theorem (BUT) from topology comes into play, leading to a game-changing result: the hypersphere quantum information theorem. The BUT states that every continuous map from a n -sphere (denoted S^n) to a n -Euclidean space must identify on S^n a pair of antipodal points directly opposite each other (5) (Figure 1). To make an example, the case $n=1$ says that there always exist a pair of opposite points on the earth's equator with the same temperature. An 3-sphere (called a hypersphere) is a generalization of the circle: mathematically, it is a simply connected manifold of constant, positive curvature that maps to a 3-dimensional Euclidean space (6). When we examine a system equipped with quantum entanglement, we usually do not take into account a noteworthy feature: our measurements are on a S^2 manifold, which is a 3D world.

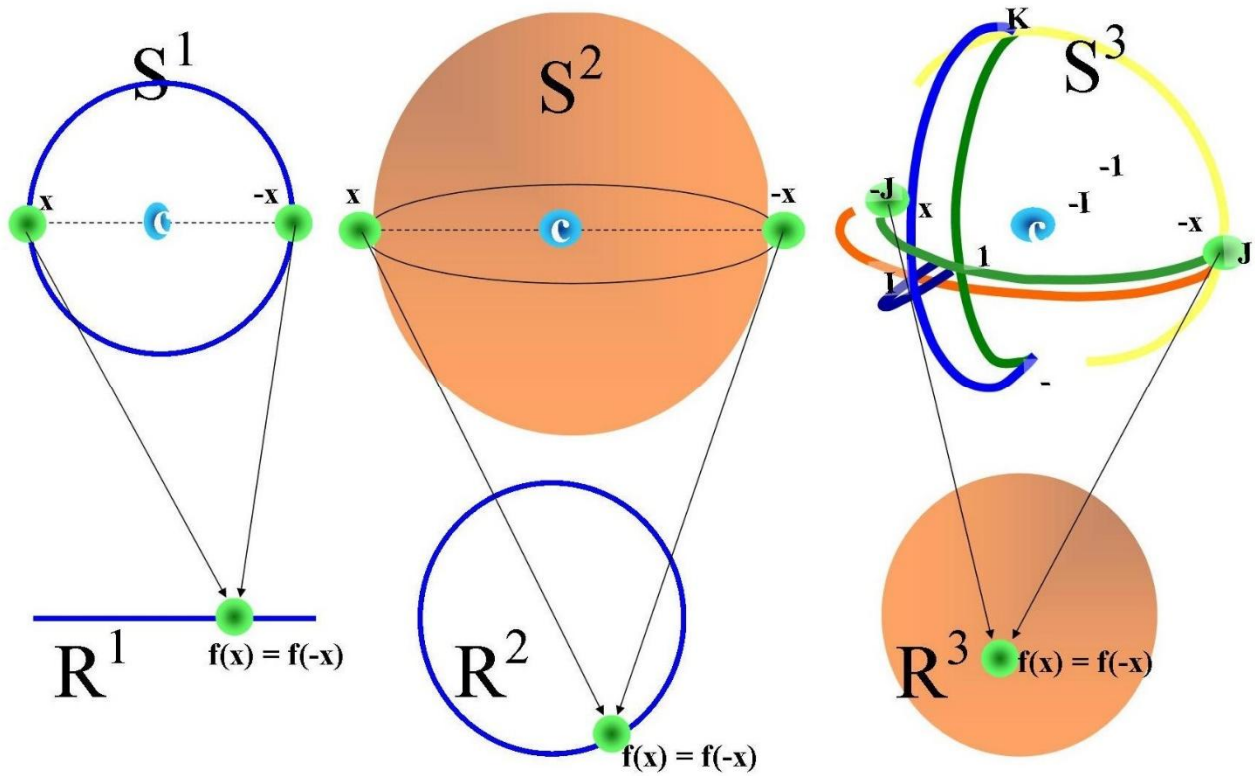


Figure 1. The Borsuk-Ulam theorem for different values of S^n . Two antipodal points in S^n project to a single point in R^n , and vice versa. Remind that every S^n is embedded in a $n+1$ -ball, and thus every S^n is one-dimension higher than the corresponding R^n .

2. THEORY

Our basic approach is to map entangled system signals in S^2 to S^3 . Notice that our S^2 measurements illustrate just the “hints” of such an S^3 activity analogous to way one recognizes an object from its shadow projected on a screen. The spheres equipped with $n > 2$ are not detectable in the usual spatial 3-dimensions and are thus challenging to assess. If we look just at mappings on the surface of S^3 system, we find the puzzling picture of quantum entanglement, apparently incompatible with our perceptions. BUT also states that every continuous function maps each pair of antipodal n -sphere surface points into surface vectors on a Euclidean n -space. This means that entanglement (*i.e.*, a system not formed by two product states) can be seen as just 3D space surface points that have a corresponding pair of S^3 antipodal points (pure states!). We demonstrate that each of the two entangled particles may have a pure state, provided they are embedded in a dimension higher: the system is entangled at the S^2 level, but un-entangled at the S^3 hypersphere level. We thus obtain a 4D composite system, factored as a product of states of its local constituents.

In keeping with recent work on quantum computation, quantum distillation and quantum information science (1,2), we propose an approach to entanglement which provides a new source of quantum information, by mapping entangled quanta on a 3D surface to unentangled quanta on the surface of a hypersphere. The old adage that opposites are attracted to each other, applies here. This analogy, applied to the problem of extracting information from entangled quanta, gets it impetus from BUT, a discovery made by Borsuk (5) in 1933. If we start with entangled quanta with antipodal locations on the surface of a sphere, then a continuous mapping of surface particles to a higher level quanta on the surface of a hypersphere results in matching quantum information derived from the entangled quanta. This information is reversible for invertible continuous mappings of antipodal surface quanta into the surface of a hypersphere. Schrödinger (7)¹⁷ observed that we must gather information about the entangled quanta to achieve *disentanglement*. His work provides yet another solution to the disentanglement problem. In this instance, our proposed continuous mapping of surface quanta to hypersphere surface quanta is analogous to what Schrödinger calls a *programme of observations* as a means of finding representatives

of entangled quanta. In our case, the quantum-mapping images are representatives of entangled quanta, with the added bonus that the images provide matching signatures of the entangled surface quanta.

3. MATHEMATICAL MODEL AND EQUATIONS

The basic approach is to think in terms of a homotopic mapping of a 3D shape produced by one continuous function that can be deformed into another shape by a second continuous function. To do this, we first consider the BUT theorem. An n -dimensional Euclidean vector space is denoted by R^n . Thus, for example, a feature vector $x \in R^n$ models the description of a surface signal. BUT states that every continuous map $f : S^n \rightarrow R^n$ must identify a pair of antipodal points – diametrically opposite points on an n -sphere (8-11). Points are antipodal, provided they are diametrically opposite (9). Examples of antipodal points are the endpoints of a line segment, or opposite points along the circumference of a circle, or poles of a sphere.

We will follow the terminology displayed in **BOX**. The notation S^n designates an n -sphere. We have the following n -spheres, starting with the perimeter of a circle (this is S^1) and advancing to S^3 , which is the smallest hypersphere:

1-sphere $S^1 : x_1^2 + x_2^2 \rightarrow R^2$ (circle perimeter),

2-sphere $S^2 : x_1^2 + x_2^2 + x_3^2 \rightarrow R^3$ (surface),

3-sphere $S^3 : x_1^2 + x_2^2 + x_3^2 + x_4^2 \rightarrow R^4$ (smallest hypersphere surface), ...,

n -sphere $S^n : x_1^2 + x_2^2 + x_3^2 + \dots + x_n^2 \rightarrow R^n$

If we view the phase space of quantum entanglement as a n -sphere and the feature space for signals as a finite-dimensional Euclidean topological space, then BUT tells us that for each description $f(x)$ of a signal x , we can expect to find an antipodal feature vector $f(-x)$ that describes a signal on the opposite (antipodal) to x with a matching description (**Figure 2**).

Let X denote a nonempty set of points on the surface of a 3D system. We assume that that is a topological space, which means that the unions and intersections of the subsets of x belong to X . Let X, Y be topological spaces. Recall that a function or map $f : X \rightarrow Y$ on a set X to a set Y is a subset $X \times Y$, so that for each $x \in X$ there is a unique $y \in Y$ such that $(x, y) \in f$ (usually written $y = f(x)$). The mapping f is defined by a rule that tells us how to find $f(x)$. A mapping $f : X \rightarrow Y$ is continuous, provided $A \subset Y$ is open, then the inverse $f^{-1}(A) \subset X$ is also open (8,11,12) ^{14,19,22}. In this view of continuous mappings from a signals topological space X on the surface of a 3-sphere to the signal feature space R^n , we can consider not just one signal feature vector $x \in R^n$, but also mappings from X to a set of signal feature vectors $f(X)$. This expanded view of signals has interest, since every connected set of feature vectors $f(X)$ has a shape, which has direct bearing on the study of the shapes of space (13). This means that signal shapes (in our case, mappings of sets of entangled particles) can be compared.

A consideration of $f(X)$ (set of region signal descriptions entangled on a n -sphere) instead of $f(x)$ (description of a single signal x) leads to a region-based view of signals, which arises naturally in terms of a comparison of shapes produced by different mappings from X (object space) to the feature space R^n .

Let $f, g : X \rightarrow Y$ be continuous mappings from X to Y . The continuous map $H : X \times [0,1] \rightarrow Y$ is defined by $H(x,0) = f(x)$, $H(x,1) = g(x)$, for every $x \in X$.

The mapping H is a homotopy (6,14,15), if there is a continuous transformation (called a deformation) from f to g . The continuous maps f, g are called homotopic maps, provided $f(X)$ continuously deforms into $g(X)$ (denoted by $f(X) \rightarrow g(X)$). The sets of points $f(X), g(X)$ are called shapes (8,13).

The mapping $H : X \times [0,1] \rightarrow R^n$, where $H(X,0)$ and $H(X,1)$ are homotopic, provided $f(X)$ and $g(X)$ have the same shape. That is, $f(X)$ and $g(X)$ are homotopic, if:

$$\|f(X) - g(X)\| < \|f(X)\|, \text{ for all } x \in X.$$

BOX

The following notation and terminology is used in this paper:

Qubit stands for quantum information.

Qubit system stands for a system that can be in one of an infinite number of states.

A space X is pathwise-connected, provided, for every two points $A, B \in X$, there is a path connecting them (22). This means that each pair of points A, B are connected by a curve lying wholly within X .

1-sphere: S^1 stands for a 1-sphere (i.e, a collection of circles). Each $x \in S^1$ is a vector (x_1, x_2) on the perimeter of a S^1 circle. $A \in S^1$, is a vector (x_1, x_2) on the circumference of a 1-sphere.

2-sphere: S^2 is a 2-sphere (for example, a common beach ball). Each $x \in S^2$ is a vector (x_1, x_2, x_3) .

$(A, q(A))$ is a vector on the surface of a 2-sphere, in which $q(A) \in R$ is a real number that is a signal value.

$|q(A)\rangle_{q(A)}$ stands for a singlet state vector written as a ket $|q(A)\rangle_{q(A)}$ of the signal $q(A)$ on a 2-sphere.

3-sphere: S^3 stands for a 3-sphere (the smallest hypersphere). Each $x \in S^3$ is a vector (x_1, x_2, x_3, x_4) .

$f(q(A)) \in S^3$ is a vector $(A, q(A), f(q(A)))$ on the surface of a hypersphere S^3 , while $f(q(-A)) \in S^3$ is a vector $((-A, q(-A), f(q(-A)))$. Observe that $f(q(A)) = f(q(-A))$ is predicted by BUT.

$|f(q(A))\rangle_{q(A)}$ is a singlet state vector written as a ket $|f(q(A))\rangle$ of the description of $q(A)$ on the 3-sphere.

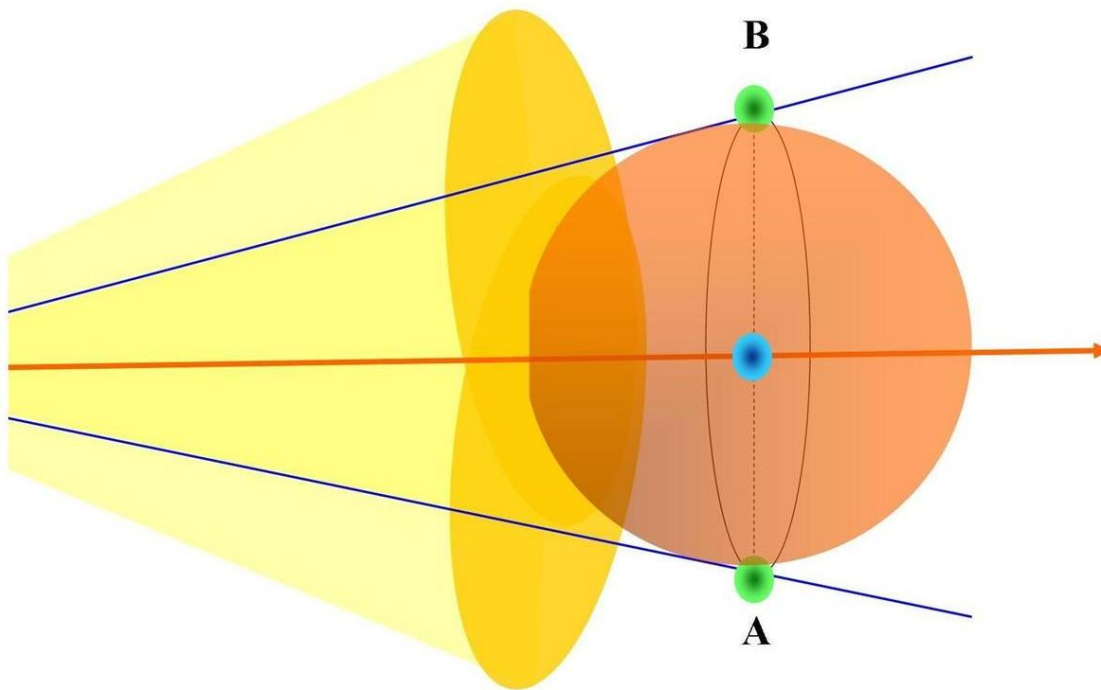
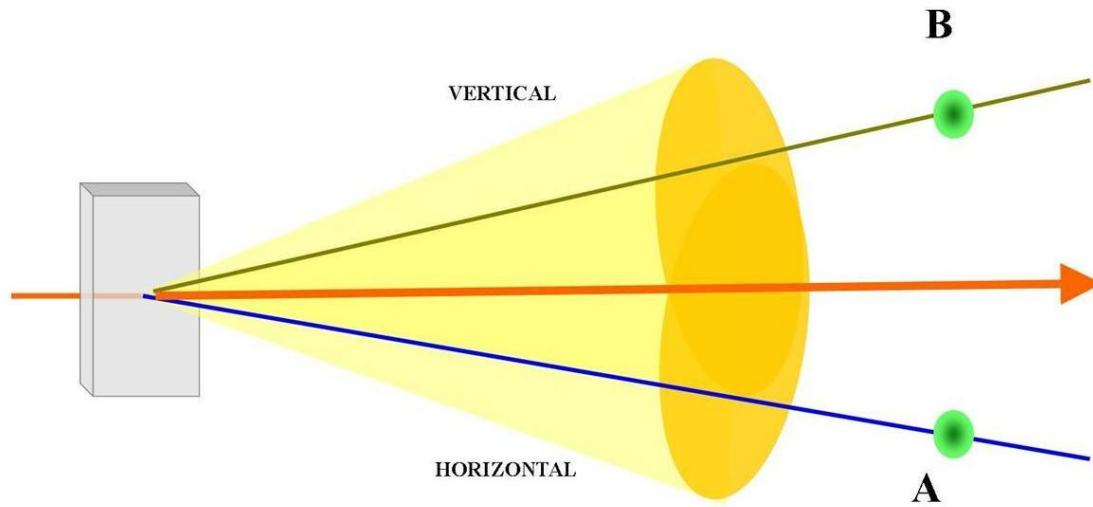


Figure 2A. Spontaneous parametric down-conversion, the commonest method used to create quantum entanglement, may generate a pair of photons entangled in polarisation (23,24). When a strong laser beam is conveyed through a nonlinear crystal, the most of photons continue straight through the crystal, while a small amount are splitted into photon pairs. The two photons may share the same polarization (type I correlation), or may be equipped with mutually perpendicular polarizations (type II correlation). In the latter case, displayed in Figure, we are in front of a pair of horizontally- and vertically- polarized entangled photons (A and B). These type II photons display trajectories, constrained within the two cones, which may exist simultaneously in the lines where the cones intersect.

Figure 2B. The two cones represent sources of pairs of photons that become entangled. We embedded the two points A and B (visually represented by blobs with dark centers), corresponding to the entangled particles of **Figure 1A**, in a

circumference centred in the laser beam. Such a circumference is one of the circles surrounding the sphere S^n . For the Borsuk-Ulam theorem, the two antipodal points A and B are described by the same function, provided they are embedded in S^n . The function stands for the physical properties corresponding to the quantum entanglement of the two particles A and B : in this framework, it becomes clear that the two points are strictly correlated. Note that the figure is just an oversimplification: the S^n sphere, which is actually a 3-sphere, is depicted as a simple 2-sphere, to make it easier to recognize.

4. RESULTS AND DISCUSSION

Once achieved an association between the geometric notion of shape and homotopies, we introduce the following theorem:

Hypersphere Quantum Information Theorem. Let $\{|f(q(-A))\rangle\}$ be a set of pathwise-connected qubit vectors on the surface of a hypersphere S^4 in a normed linear space. The shape $\{|f(q(-A))\rangle\}$ induced by the set of path-connected qubit state vectors can be deformed onto the shape $\{|f(q(A))\rangle\}$ on a 4-sphere.

Proof: The proof is an immediate consequence of the Borsuk-Ulam Theorem. From BUT, each $|f(q(A))\rangle = |f(q(-A))\rangle$. Hence the shape $\{|f(q(-A))\rangle\}$ deforms into the shape $\{|f(q(A))\rangle\}$.

Next, we investigate quantum entanglement on an n -Sphere embedded in a normed linear space X . Let $E(A,B)$ denote the entanglement of vectors A,B on a normed linear space. Conventional entanglement is represented by:

$$E(A,B) = 1/\sqrt{2} (|0\rangle_A \otimes |1\rangle_B - |1\rangle_A \otimes |0\rangle_B).$$

Let $S^1 \in X$ be the circumference (perimeter) of a 1-sphere circle, $A, -A \in X$ the quanta (vectors) on X and, finally, let $A, -A$ be antipodal quanta on X . Let $q : X \rightarrow \mathbb{R}$ be a mapping from a quantum A on X into the reals \mathbb{R} and $q(A), q(B) \in \mathbb{R}$ be real-valued antipodal entangled signals. In addition, let Q be a set of signal values originating from points A, B on the perimeter X of a 1-sphere circle.

Remark 1. For A in S^n , the point A (also called a state) and the signal $q(A)$ defines a vector $(A, q(A))$ on the surface of a 2-sphere. That is, $Sq(A)A \in S^2$. Signals on an S^2 surface are then mapped to feature vectors $f(q(A)) \in S^3$ that describe the signals $q(A)$. From this, we can rewrite the quantum entanglement model in the following way. Let $E(A,-A)$ denote the quantum entanglement of states $A,-A$, defined by:

$$E(A,-A) = 1/\sqrt{2} (|q(A)\rangle_A \otimes |q(B)\rangle_{-A} - |q(-A)\rangle_{-A} \otimes |q(A)\rangle_A).$$

Let Q be a set of signals on the surface of a 2-sphere, Y be a set of feature vectors S^3 on the surface of a 4-dimensional hypersphere and $f : Q \rightarrow Y$ be a continuous mapping on the set of signals Q into Y . Let $q,-q \in Q$ be antipodal quantum signals.

Remark 2. $f(q(A))$ defines a feature vector $(A, q(A), f(q(A)))$ on the surface of a hypersphere S^3 . That is, $|f(q(A))\rangle q(A) \in S^3$. Each qubit provides information about a signal $q(A)$. In addition, the Borsuk-Ulam Theorem predicts the presence of antipodal qubits $f(q(A)), f(q(-A))$, such that the information provided by $f(q(-A))$ matches the information provided by $f(q(A))$. From this, we obtain a new form of entanglement, at the information level on a hypersphere. Let $E(q(A), q(-A))$ denote the quantum entanglement of states $q(A), q(-A)$, defined by:

$$E(q(A), q(-A)) = 1/\sqrt{2} (|f(q(A))\rangle_{q(A)} \otimes |f(q(-A))\rangle_{q(-A)} - |f(q(-A))\rangle_{q(-A)} \otimes |f(q(A))\rangle_{q(A)}).$$

Let the qubit system $Y = \{Sf(q(A))\}$ be a set of pathwise-connected qubit vectors on the surface of a hypersphere S^3 in a Hilbert space, which defines a quantum information system. That is, the set of descriptions Y of signals provides a model for a process about a collection of signals. From the Hypersphere Quantum Information Theorem, we know that the shape $\{|f(q(-A))\rangle\}$ can be deformed into the shape Y . In addition, from the Borsuk-Ulam Theorem, we also know that:

$$|f(q(A))\rangle = |f(q(-A))\rangle.$$

This means that a definite pure state can be attributed to $|f(q(A))\rangle$. The system is thus entangled at the S^2 level, while is un-entangled at the S^3 hypersphere level.

The geometrical aspects of entanglement have been already investigated by offering a numerical approach, iteratively refining an estimated separable state towards the target state to be tested, and checking if the target state can indeed be reached (16)¹⁶. We gave instead a different geometrical account of quantum entanglement, by exploring the possibility of a correlation between it and the Borsuk-Ulam Theorem. We showed that there are striking analogies between the antipodal points evoked by BUT and the entangled particles evoked by quantistics, such that the phenomenon of quantum

entanglement can be investigated in guise of an n-sphere embedded in a Hilbert Space. This leads naturally to the possibility of a region-based, instead of a point-based, geometry in which we view collections of signals as surface shapes, where one shape maps to another antipodal one (17-21). We have developed a mathematical model of antipodal points and regions cast in a physically-informed fashion, resulting in a framework that has the potential to be operationalized and assessed empirically. The notion that information about particles resides on a hypersphere is a counter-intuitive hypothesis, since we live in a 3D world with no immediate perception that 4D space exists at all, *e.g.*, if we walk along one of the curves of a 4-ball, we think are crossing a straight trajectory, not recognizing that our environment is embedded in higher spatial dimensions. The cause/effect relationships of the entangled system occurs in the fourth dimension: for this reason, we are not able to detect it by ordinary means. We are able to look just at the 3D part part of the S^3 system and such an incomplete viewpoint gives us the false impression of a weird picture, apparently incompatible with our common sense. In conclusion, the Borsuk-Ulam theorem sheds new light on quantum entanglement. It explains how the two entangled particles on a hypersphere yield observations about particles that reside on a lower dimensional sphere, thus leading to a quantum information system.

REFERENCES

- 1) Jaeger, G. *Quantum information. An overview* (Springer, New York-Berlin, 2007).
- 2) Gruska, J. Quantum entanglement as a new information processing resource. *New Generation Computing* **21**, 279-295 (2003).
- 3) Hauke, P., Tagliacozzo, L. Spread of correlations in long-range interacting quantum systems. *Phys Rev Lett.* **111**, (20):207202 (2013).
- 4) Horodecki, P., Horodecki, M. Entanglement and thermodynamical analogies *Acta Physica Slovaca* **3**, 141-56 (1998).
- 5) Borsuk, K. Drei saetze ueber die n-dimensionale euklidische sphaere. *Fundamenta Mathematicae* **XX**, 177-190 (1933).
- 6) Cohen, M.M. *A course in simple homotopy theory* (Springer-Verlag, New York-Berlin, 1973).
- 7) Schroedinger, E. Discussion of probability relations between separated systems. *Proceedings of the Cambridge Philosophical Society* **31**, 555-563 (1935).
- 8) Peters, J.F. *Computational Proximity. Excursions in the Topology of Digital Images, Intelligent Systems* (Reference Library, Springer, 2015, to appear).
- 9) Weisstein, E.W. Antipodal points (<http://mathworld.wolfram.com/AntipodalPoints.html>, 2015).
- 10) Henderson, D.W. *Experiencing Geometry: In Euclidean, Spherical, and Hyperbolic Spaces* (Second edition 2001).
- 11) Naimpally, S.A., Peters, J.F. Preservation of continuity. *Scientiae Mathematicae Japonicae* **76**, 305-311 (2013).
- 12) Willard, S. *General topology* (Dover Pub., Inc., Mineola, New York, 1970).
- 13) Collins, G.P. The shapes of space. *Sci. Am.* **291**, 94-103 (2004).
- 14) Borsuk, M., Gmurczyk A. On homotopy types of 2-dimensional polyhedral. **109**, 123-142 (1980).
- 15) Dodson, C.T.J., Parker, P.E. *A user's guide to algebraic topology* (Kluwer, Dordrecht, Netherlands, 1997).
- 16) Leinaas, J.M., *et al.* Geometrical aspects of entanglement, arXiv, 0605079v1, 1-31 (2006).
- 17) Borsuk, M. Concerning the classification of topological spaces from the standpoint of the theory of retracts. **XLVI**, 177-190 (1958-1959).
- 18) Borsuk, M. Fundamental retracts and extensions of fundamental sequences. **64**, 55-85 (1969).
- 19) Krantz, S.G. *A guide to topology.* (The Mathematical Association of America, Washington, D.C. 2009).
- 20) Manetti, M. *Topology.* (Springer, Heidelberg, 2015).
- 21) Peters, J.F. *Topology of Digital Images. Visual Pattern Discovery in Proximity Spaces. Intelligent Systems* (Reference Library, **63**, Springer, 2014).
- 22) Weisstein, E.W. Pathwise-connected (Mathworld, <http://mathworld.wolfram.com/Pathwise-Connected.html>, 2015).
- 23) Zhang, Y. *et al.* Simulating quantum state engineering in spontaneous parametric down-conversion using classical light. *Opt Express.* **22**, 17039-17049 (2014).
- 24) Quesada, N., Sipe, J.E. Time-ordering effects in the generation of entangled photons using nonlinear optical processes. *Phys Rev Lett.* **114**, 093903 (2015).

COMPUTATIONAL GEOMETRY PROVIDES INDIRECT EVIDENCE OF DARK MATTER LOCATION IN COSMIC STRUCTURES

The elusive dark matter is the best candidate in order to explain gravitational effects such as, for example, the motion of stars in galaxies. We introduce a novel method for the measurement of information in cosmic images called maximal nucleus clustering (MNC) *i.e.*, nucleus clustering's Rényi entropy derived from strong proximities in feature-based Voronoi tessellations. MNC is a novel, fast and inexpensive image-analysis technique, independent from other detectable signals. It permits the assessment of changes in gradient orientation into zones of two-dimensional cosmic images that generally are not taken into account by other techniques. In order to evaluate the potential applications of MNC, we looked for the presence of MNC's distinctive hallmarks in the plane surface of astronomic images. We found that Rényi entropy is higher in MNC areas of cosmic images than in the surrounding regions, and that these patterns are correlated with cosmic zones containing a lesser amount of dark energy. Therefore, computational geometry provides a bridge made of affine connexions and proximities between features of a two-dimensional pictures and physical features of the Universe.

A diffuse presence of invisible dark matter in the Universe is required by current cosmological models, in order to explain features such as the experimentally detected movement of stars in the peripheries of galaxies (Penrose, 2011; Aad et al., 2013; Khachatryan et al, 2015). Here we introduce a novel technique of cosmic image analysis in the plane surface of 2D images. The method, called computational proximity, takes into account maximal nucleus clustering in Voronoi tessellations (Peters, 2016, Peters and Inan, 2016). Cosmic images are subdivided in contiguous polygons, termed "Voronoi polygons" (without interstices or overlap). They yield a density map, called "tessellation", that makes it possible to make an objective measurement of the spatial distribution of polygon areas and helps to define "random", "regular" and "clustered" distributions (Franck and Hart, 2010; Edelsbrunner, 2014; Peters and Guadagni, 2015; Peters et al., 2016). Voronoi tessellations have been already used in cosmology, *i.e.*, in order to investigate spatial cosmic matter distribution on scales of a few up to more than a hundred Megaparsec (van de Weygaert, 2007). In a Voronoi tessellation of a cosmic image, of particular interest is the presence of maximal nucleus clusters (MNC), *i.e.*, cosmic zones with the highest number of adjacent polygons (Peters and Inan, 2016). The MNC clustering approach includes a main feature of level set methods, namely, a nucleus boundary that is embedded in a family of nearby level sets (Saye and Sethian, 2011). MNC reveals regions of the Universe, independent from other techniques, characterized by different gradient orientation and gradient magnitude (edge strength) of region pixels. Here we evaluate the power and potentialities of this novel, easy and inexpensive approach. We also establish a link between MNCs and the presence of the otherwise undetectable dark matter in cosmic images.

MATERIALS AND METHODS

Cosmic images. We used public domain astronomic pictures from the NASA website (<http://apod.nasa.gov/apod/archivepix.html>). Here follows a list of the cosmic structures we evaluated using computational geometry techniques.

- 1) Starburst Galaxy Messier 94 (**Figure 1**). It lies 15 million light-years distant in the northern constellation of Canes Venatici. The galaxy's compact nucleus and prominent inner dust lanes are surrounded by a ring of young, massive stars, likely less than 10 million years old (Image Credit: ESA/Hubble and NASA).
- 2) The "classical" image depicting the cosmic microwave background (**Figure 2A**), which is the almost isotropic thermal radiation left over from an early stage in the development of the Universe, about 380,000 years after the Big Bang (Penzias and Wilson, 1965; Gawiser and Silk, 2000; Fixsen, 2009).
- 3) the SDSS 3-dimensional map of the distribution of galaxies (**Figure 2B**). Earth is at the center, and each point represents a galaxy, containing about 100 billion stars. The outer circle is at a distance of two billion light years. Both slices contain all galaxies within -1.25 and 1.25 degrees declination. (Image Credit: M. Blanton and the Sloan Digital Sky Survey, https://www.sdss3.org/science/gallery_sdss_pie2.php).
- 4) Cosmic structures from the in the long-necked, northern constellation of Camelopardalis. In particular, we evaluated the the spiral galaxy NGC 2403 (**Figure 3A**), which stands within the boundaries of the constellation (Image Credit & Copyright: Eric Coles and Mel Helm), and the Hidden Galaxy IC 342 (**Figure 3B**), similar in size to large spiral galaxies in our neighborhood. IC 342 may have undergone a recent burst of star formation activity and has gravitationally influenced the evolution of the Milky Way (Image Credit & Copyright: Fabiomassimo Castelluzzo).

- 5) IRG-NGC303, magnitude 14.3, lenticular Galaxy (**Figure 3C**).
- 6) the Red Square Nebula MWC9 22 (**Figure 4**). The featured image combines infrared exposures from the Hale Telescope on Mt. Palomar in California, and the Keck-2 Telescope on Mauna Kea in Hawaii. A hypothesis for the unusual square shape is that the central stars expelled cones of gas during their late developmental stage. These cones incorporated nearly right angles and were visible from the sides. Supporting evidence for the cone hypothesis includes radial spokes in the image that might run along the cone walls. (Image Credit & Copyright: Peter Tuthill & James Lloyd).
- 7) NGC 1068 (**Figure 5A**). This spiral galaxy, located in the Cetus constellation 47 million light-years away, contains a supermassive black hole (detected by NASA’s Nuclear Spectroscopic Telescope Array, or NuSTAR, and the European Space Agency’s XMM-Newton space observatory).
- 8) Markarian 231 (**Figure 5B**). This Hubble Space Telescope image reveals a bright glow in the center of the interacting galaxy Markarian 231, the nearest quasar to the Earth. Quasars are powered by a central black hole that heats gas around it to unleash tremendous amounts of energy. Hubble spectroscopic observations infer the presence of two supermassive black holes whirling around each other (Credit: NASA, ESA, the Hubble Heritage Team (StScI/AURA)-ESA/Hubble Collaboration, and A. Evans (University of Virginia, Charlottesville/NRAO/Stony Brook University).
- 9) SDSSJ1126-2944 (**Figure 5C**). This galaxy is the result of a merger between two smaller galaxies, which brought together a pair of supermassive black holes. One of the black holes is surrounded by a typical amount of stars, while the other is strangely “naked” and has a much lower number of associated stars than expected (Comerford 2015). (Image Credit & Copyright: Julie Comerford and NASA Chandra Xray Observatory).

Nucleus clustering in Voronoï tessellations. The plane surfaces of cosmic structures’ pictures were subdivided into contiguous polygons, the so-called “Voronoi polygons” (**Figure 1A**). Geometrically, a Voronoi tessellation is a collection of non-overlapping convex polygons (Edelsbrunner, 2006). Each point p in the tiling represents a generating point (called a site) with particular features, such as corners, centroids, gradient orientation and brightness (some of them are depicted with the letter p in **Figure 1A**). A Voronoi region contains every point in the plane that is closer to the point p than to any other site. In technical words, each polygon is a Voronoi region $V(s)$ of a generating point $s \in S$, which is a set of all points nearer s than to any other point in S . We achieve a “tessellation”, *i.e.*, a density map that allows an objective measurement of the polygon areas’ spatial distribution. A central Voronoi region is called the cluster nucleus (some of the cluster nuclei are depicted with the letter N in **Figure 1A**) and contains all the points on the plane surface that are nearer to the generating point p than to any other generating point on the surface (**Figure 1B**). A *Voronoi nucleus cluster* is a collection of Voronoi polygons that are adjacent to their central cluster nucleus (Peters, 2016): that is, each polygon which is strongly near a cluster nucleus has an edge in common with its polygon (Edelsbrunner, 2014). In a Voronoi tessellation carried out in a so called “strong” proximity space (Peters 2016), of particular interest is the presence of maximal nuclei, *i.e.*, zones with the highest number of sides and of adjacent polygons (**Figure 1C**, letter M). The maximal nucleus plus its adjacent polygons is called maximal nucleus cluster (MNC): in sum, the latter is a Voronoi cluster in which the cluster nucleus is a polygon which displays the highest number of sides (in **Figure 1E**, a MNC is embedded in the white oval). In technical terms, this clustering approach includes a main feature of level set methods, namely, a nucleus boundary that is embedded in a family of nearby level sets. Strongly near Voronoi polygons is an application of the notion of strong proximity between sets of points: for further details and the algorithms, see Peters (2016) and Peters and Inan (2016).

Summarizing, in a tessellated image, Voronoi tessellation serve as indicator of high object concentration and inhomogeneity distributions, while MNCs as indicators of gradient orientations.

Steps to Construct Maximal Nucleus Clusters on a Tessellated Cosmic Image. Here we give the steps to construct MNCs on a tessellated cosmic image (see **Figure 1.0**). The basic approach is to find those polygonal regions in a cosmic image that yield the most information and the reflect the fact that the site (generating point) each Voronoi region has a gradient orientation and gradient magnitude (edge strength) that is different from all of the other generating points. The nucleus of an MNC has a singular character, since the number of Voronoi regions along the borders of the nucleus is maximal. It is this maximality that is a signature of cosmic regions that yield the greatest information levels.

Algorithm 1: Construct Cosmic Maximal Nucleus Cluster

Input : Cosmic image img .

Output: MNCs on cosmic image img .

```

1  $img \mapsto TitledImg$  /*(Voronoi tessellation)*/;
2 Choose a Voronoi region in  $TitledImg$ : *;
3  $ngon \leftarrow TitledImg$ ;
4  $NoOfSides \leftarrow ngon$ ;
5 /* Count no. of sides in  $ngon$  & remove it from  $TitledImg$ . */;
6  $TitledImg := TitledImg \setminus ngon$ ;
7  $ContinueSearch := True$ ;
8 while ( $TitledImg \neq \emptyset$  and  $ContinueSearch$ ) do
9    $ngonNew \leftarrow TitledImg$ ;
10   $TitledImg := TitledImg \setminus ngonNew$ ;
11   $NewNoOfSides \leftarrow ngonNew$ ;
12  if ( $NewNoOfSides > NoOfSides$ ) then
13    |  $ngon := ngonNew$ ;
14  else
15    | /* Otherwise ignore  $ngonNew$ : */
16  if ( $TitledImg = \emptyset$ ) then
17    |  $ContinueSearch := False$ ;
18    |  $maxN := ngon$ ;
19    | /* Cosmic image MNC found; Discontinue search */;

```

Figure 1.0. The steps in the method used to construct the mesh MNCs on a cosmic image shown in **Figure 1D**.

Rényi entropy assessed information content in cosmic Nucleus Clusters. We showed in the previous paragraphs that the major new elements in the evaluation of cosmic images are nucleus clusters, maximal nucleus clusters, strongly near maximal nucleus clusters, *e.g.*, convexity structures that occur whenever max nucleus clusters intersect (Peters and Inan, 2016). In a Voronoi tessellation, of particular interest is the presence of *maximal nucleus clusters* (MNC), *i.e.*, clusters with the highest number of adjacent polygons. In this section, we introduce a measure of the information that MNCs in cosmic images yield. We demonstrate that MNC reveal regions of the Universe with higher levels of information, in comparison with non-MNC regions, that uniformly yield less information.

In a series of papers, Rényi (Rényi, 1961; Rényi, 1966), introduced a measure of information of a set random events. Let X be a set random events such as the occurrence of polygonal areas in a Voronoi tessellation and let $\beta > 0, \beta \neq 1, p(x)$ the probability of the occurrence of x in X . Then Rényi entropy $H_\beta(X)$ is defined by

$$X = \{x_1, \dots, x_n\},$$

$$H_\beta(X) = \frac{1}{1-\beta} \log_2 \sum_{i=1}^n p^\beta(x_i).$$

Because of the relationship between Rényi entropy of a set of events and the information represented by events, Rényi entropy and information are interchangeable in practical applications (Rényi, 1982; Bromiley et al., 2010). In fact, it has

been shown that Rényi entropy $H_\beta(X)$ is a monotonic function of the information associated with X . This means that Rényi entropy can be used as a measure of information for any order $\beta > 0$.

Let X_{MNC}, X_{nonMNC} be sets of MNC polygon areas and non-MNC polygon areas in a random distribution of tessellation polygon areas. Also, let $p(x) = \frac{1}{x}, p(y) = \frac{1}{y}$ be the probability of occurrence of $x \in X_{MNC}, y \in X_{nonMNC}$. Notice that the nuclei in MNCs have the highest concentration of adjacent polygons, compared with non-MNC polygons. Based on measurements of Rényi entropy for MNC vs. non-MNC observations, we have confirmed that Rényi entropy of nucleus polygon clusters is consistently higher than the set of non-MNC polygons (**Figures 3 and 4**). This finding indicates that MNCs yield higher information than any of the polygon areas outside the MNCs.

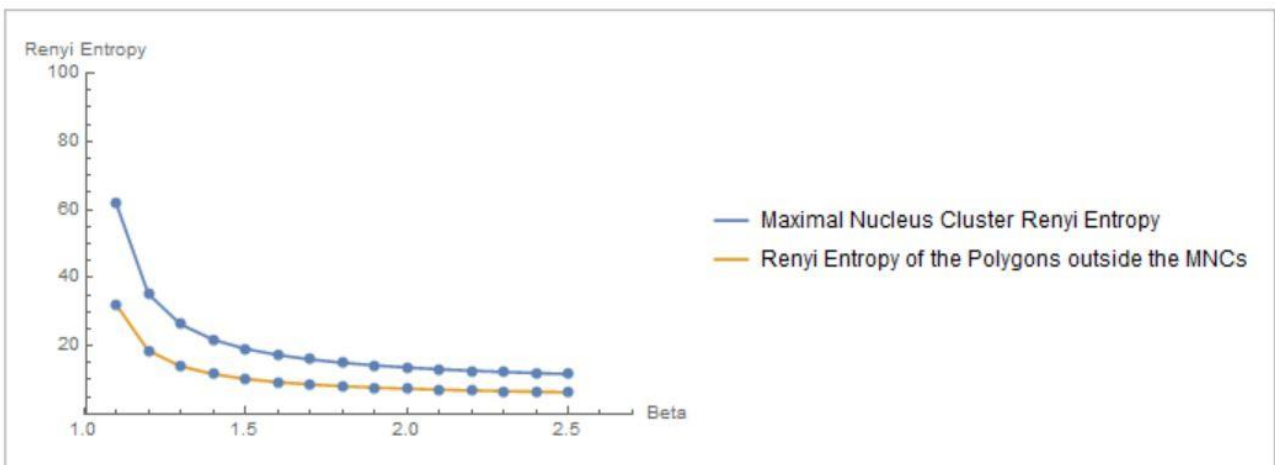


Figure 3. Rényi entropy values of maximal nucleus clusters, compared with the surrounding areas of cosmic images. The x axis displays the values of the Beta parameter for $1.1 \leq \beta \leq 2.5$.

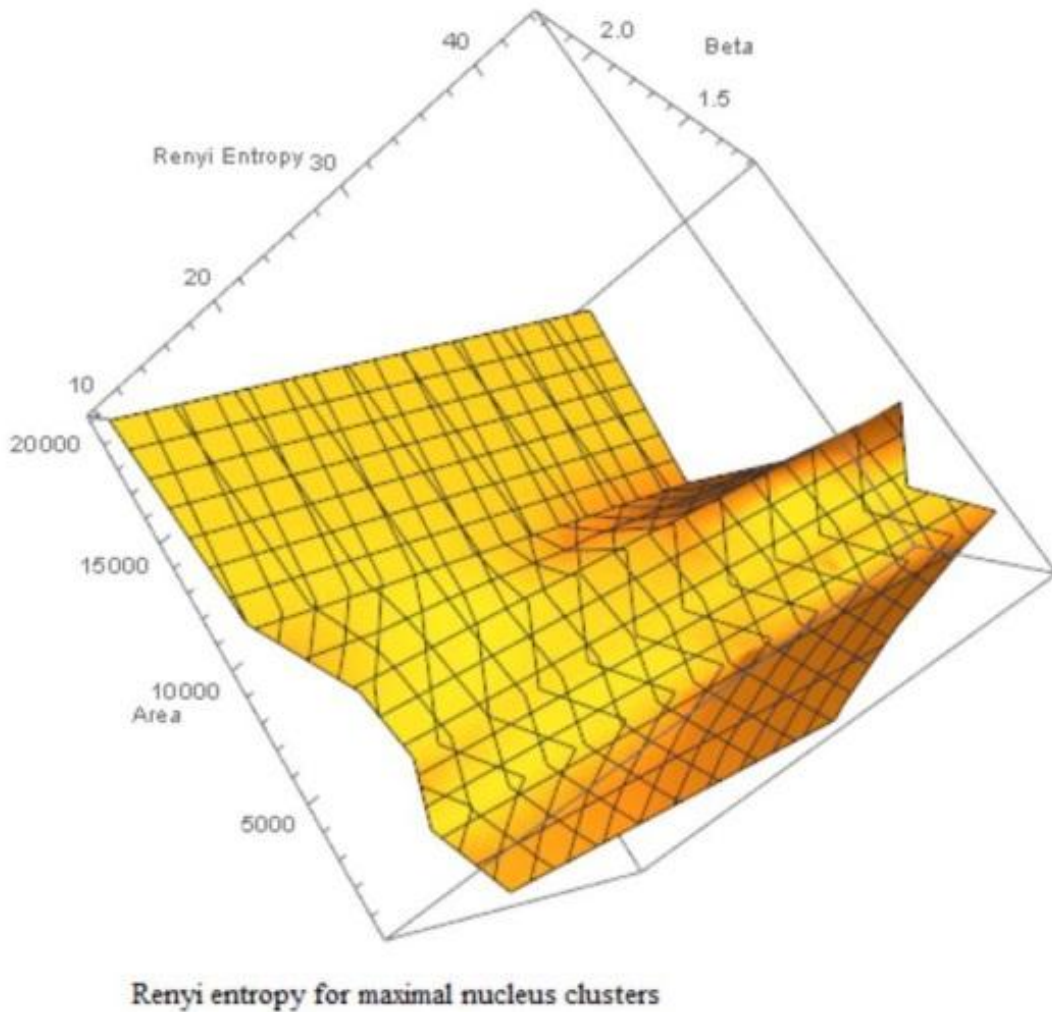


Figure 4. Rényi entropy values vs. number polygon areas vs. $1.1 \leq \beta \leq 2.5$ of maximal nucleus clusters in cosmic images. MNC Nuclei surrounded by polygons with smaller areas have higher Rényi entropy, which tells us that smaller MNC areas yield more information than MNCs with larger areas.

In sum, Rényi entropy provides a measure of the information in maximal nucleus clusters and the surrounding zones of cosmic images. This means that the information from areas occupied by MNCs vs. non-MNC areas can be measured and compared. This also means that the maximal nucleus clusters are equipped with higher entropy values (and corresponding higher information), which contrasts with measure of information in the surrounding non-MNC zones. Hence, MNCs make it possible to pinpoint the highest source of information in images of the Universe.

Dark matter comes into play. MNCs indicate zones where singular generating points lie which are equipped with gradient orientations and gradient magnitudes different from the rest of the cosmic image. This means, in our case, that the homogeneity of the galaxies is broken in some points, where a different gradient orientation angle occurs. A deformation of the spacetime occurs in the zones of MNCs. What is the cause of such local inhomogeneities? We can assess the discrepancies in terms of symmetry breaks, locally disrupting the general symmetry of the cosmic structures' experimentally detected movements. Symmetries, in turn, are dictated by the mutual interactions between visible and dark matter. Symmetry breaks could be due to factors that obstruct the natural settings of stars in galaxies, which results from the subtle interaction of visible and dark masses. Indeed, a variant of the virial theorem (Pollard, 1964) states that:

$$v = \sqrt{GM/r}$$

where v is the velocity of stars, G is the gravitational constant, M is the mass and r is the distance of the star from the center of the galaxy. It means that an increase of dark matter, believed as located out of the galaxies, increases the value of the mass M , in order that stars speed v does not decrease as could be expected when their distance r from the center of the Galaxy increases. Therefore, MNCs might stand for zones where the ratio visible/dark matter is different, compared

with others. It leads to the subtle differences in gradient orientation detected by MNCs. In sum, the concentration of dark matter in MNCs cosmic zones is different from the surrounding ones. The next answer is: once established that in MNCs zones the concentration of dark matter is diverse from the surrounding zones, could we assess whether it is higher or lower? The increase of Rényi entropy in the MNCs zones suggests that information is higher into such zones and lower outside. Because visible matter is detectable, while dark matter is not, it is expected that an increase in information in MNCs is dictated by larger concentrations of visible matter. In sum, MNC zones contain more visible matter than the surrounding zones, and it means less dark matter. In sum, MNCs in a tessellated cosmic image point to cosmic regions that has a diminished presence of dark matter.

RESULTS

At first, we evaluated the presence of MNC in the coarse graining, large-scale image of the cosmic microwave background (**Figure 2A**). We found that MNCs, rather than being scattered everywhere, are localized in clusters embedding specific zones of the Universe. It is noteworthy that the MNC pattern is not as isotropic as the microwave background. The SDSS 3-dimensional map displays instead a symmetrical pattern of MNCs (**Figure 2B**). Note that the maximal nuclei lie in zones with lesser concentration of galaxies. The MNC tessellation of more recent, lower-scale cosmic bodies (**Figure 3**), revealed that MNCs, rather than being embedded in the very core of the galaxies, generally lie in their outer branches. Note that the MNCs are generally not embedded in the youngest astronomic bodies (see, e.g., **Figure 1**). Clusters of MNCs micro-zones are scattered throughout the pictures (**Figures 4 and 5**). In order to quantitatively assess MNCs' size, we also provided the nuclei areas in square light years (see the legends of **Figures 2 and 3**). Interestingly, the galactic zones containing black holes displayed less MNCs than the surrounding structures (**Figure 5**). In sum, MNCs clusters, equipped with higher Rényi entropy compared with the surrounding zones, are scattered throughout different cosmic areas. It means that some micro-areas of a specific cosmical zones contain more information than the adjacent ones.

CONCLUSIONS

We showed that computational proximity (i.e., strongly near nucleus mesh clusters) is able to reveal, in 2D fMRI images, hidden patterns of Rényi entropy, enabling us to detect functional information from morphological data. There is a difference in Rényi entropy between MNC and the surrounding zones, these data pointing towards diverse levels of dark matter. Therefore, in different coarse-grained images of the Universe at different times of evolution, MNC is able to detect the presence of zones in which the concentration of dark matter is lower. This result paves the way towards novel approaches to cosmological evaluation, because MNC elucidates the zones of the Universe more likely to contain dark matter. MNC tessellation allows us to confine the zones of the sky in looking for such elusive matter: this could also help reduce the number of dark matter candidates. The holographic principle states that informational content of all the objects that have fallen into a black hole might be entirely contained in surface fluctuations of the event horizon (Susskind, 2004; Pourhasan et al., 2014). It means that the black hole surface needs to have less information than the surrounding cosmological structures. Our data show that this is the case: indeed, in the zones of the black hole, the information is lower. In conclusion, by uncovering evidence of dark matter in different cosmic images, our study shows that a novel and fairly inexpensive image-analysis technique of simple planar images gives insights into the expansion of the Universe. Further, MNC allows the detection of informational entropy which does not necessarily correspond to the zones of the image that we repute more significant. This means that MNC provide a basis for quantifying high-yield information areas in cosmic image features that are normally "hidden" from our attention.

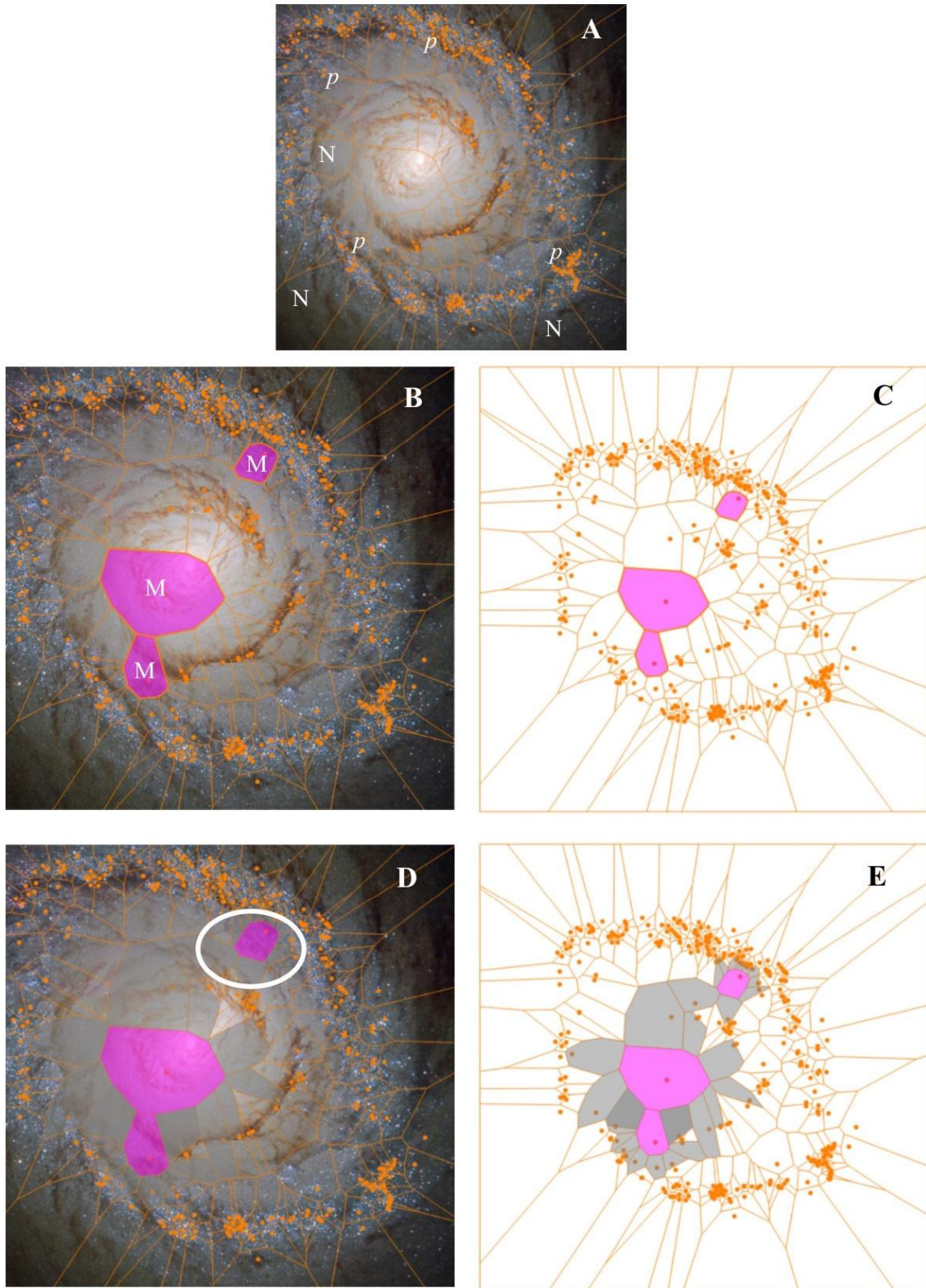
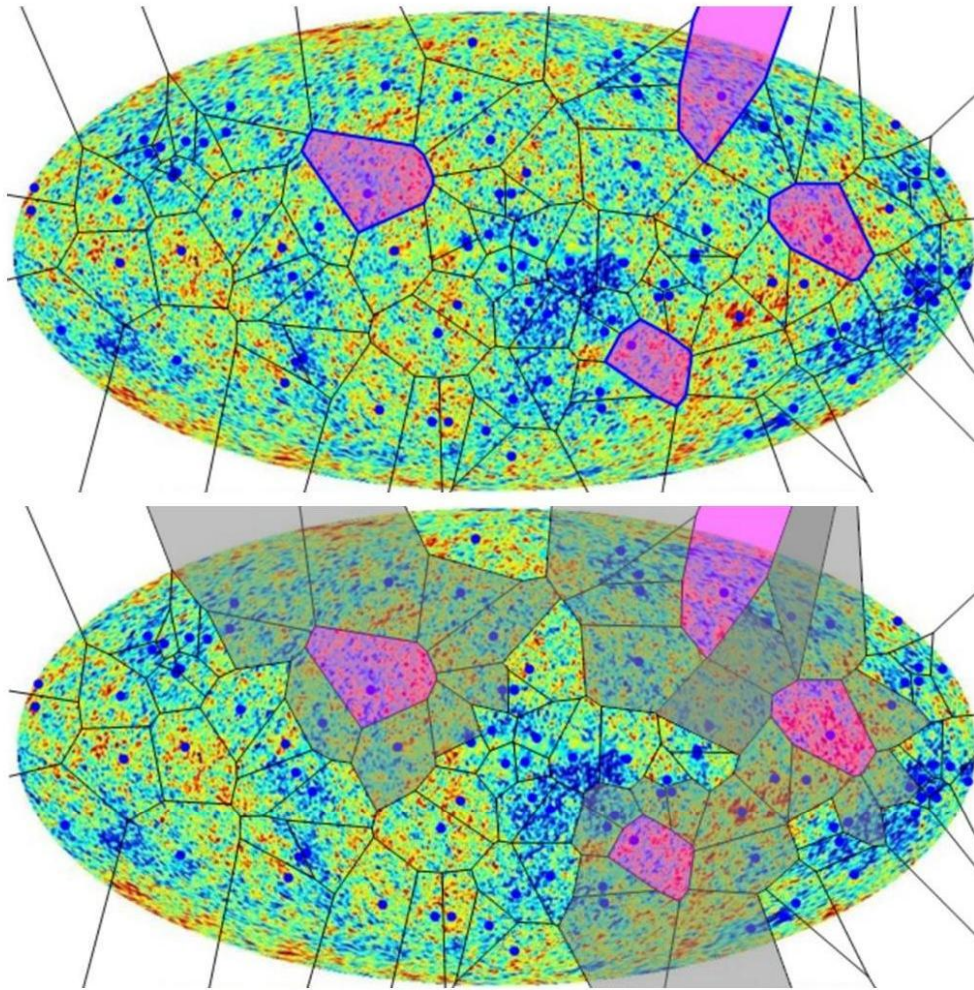


Figure 1. Computational proximity methods on a cosmic image (Starburst Galaxy Messier 94). **Figure 1A** depicts a Voronoi tessellation, **Figure 1B** three cluster nuclei and **Figure 1C** their surface tiling (without the original picture), which allows an easier evaluation. **Figure 1D** shows the three maximal nucleus clusters and **Figure 1E** their surface tiling. See main text for further details.

A



B

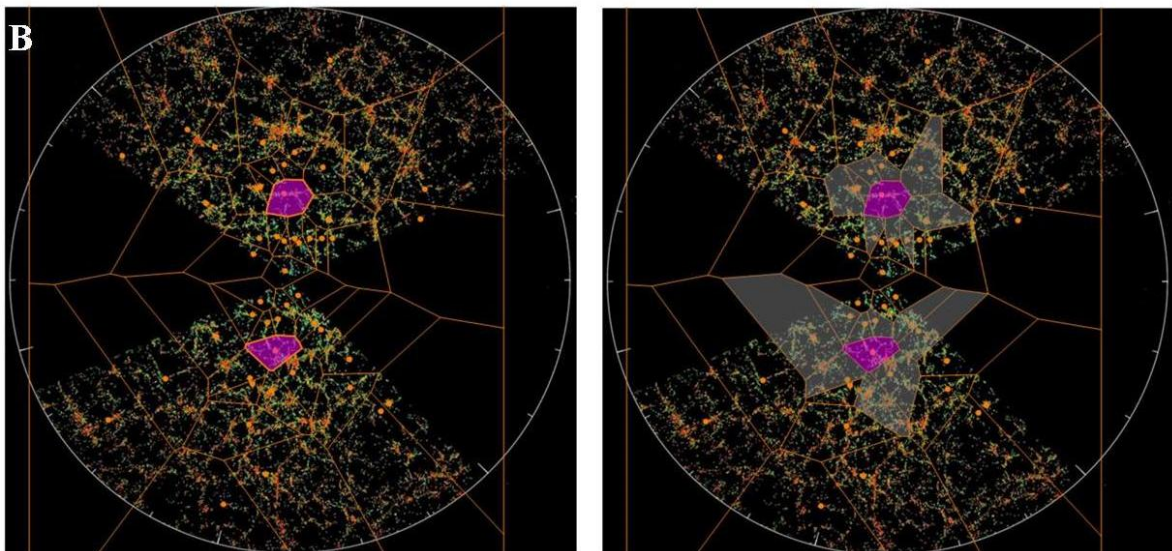


Figure 2A: cluster nuclei and MNC of a picture taken from the cosmic microwave background. **Figure 2B:** cluster nuclei and MNC of a picture taken from the SDSS 3-dimensional map of the distribution of galaxies.

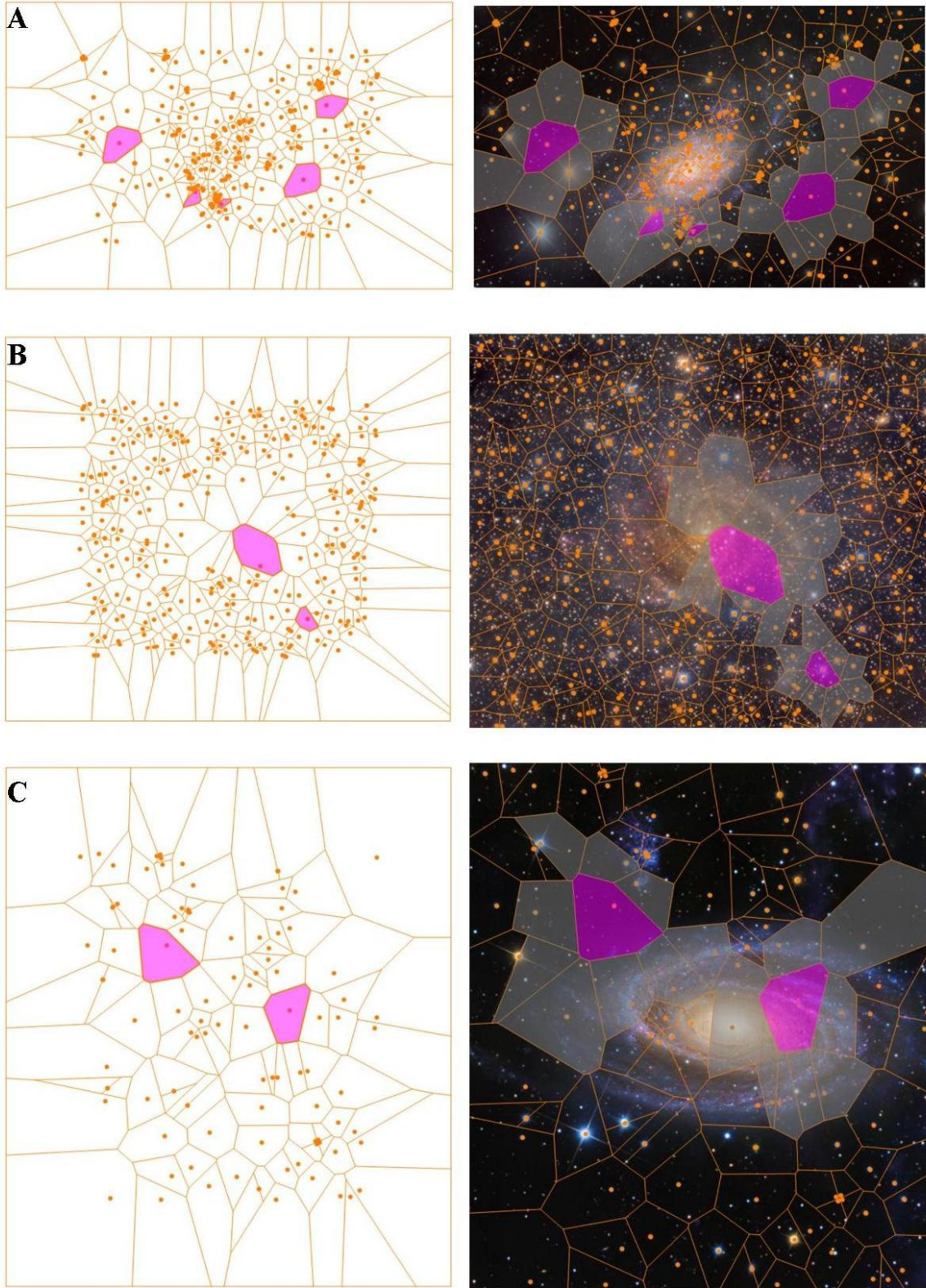


Figure 3. Cluster nuclei and MNC of pictures taken from different cosmic structures. **Figure 3A:** NGC 2403. The nuclei areas in square light years (l_{yr}^2) are: N1 area= 14979.1 l_{yr}^2 ; N2= 14861.9; N3 = 9074.54; N4 = 2774.25; N5= 1179.78. The nuclei are marked with numbers (not shown in Figure) N1-N5 from right to left. **Figure 3B:** the Hidden Galaxy IC 342. Nuclei areas: N1 = 29375.9, N2 = 5624.46. **Figure 3C:** IRG-NGC303 Galaxy. Nuclei areas: N1 = 21654.8, N2 = 17403.7.

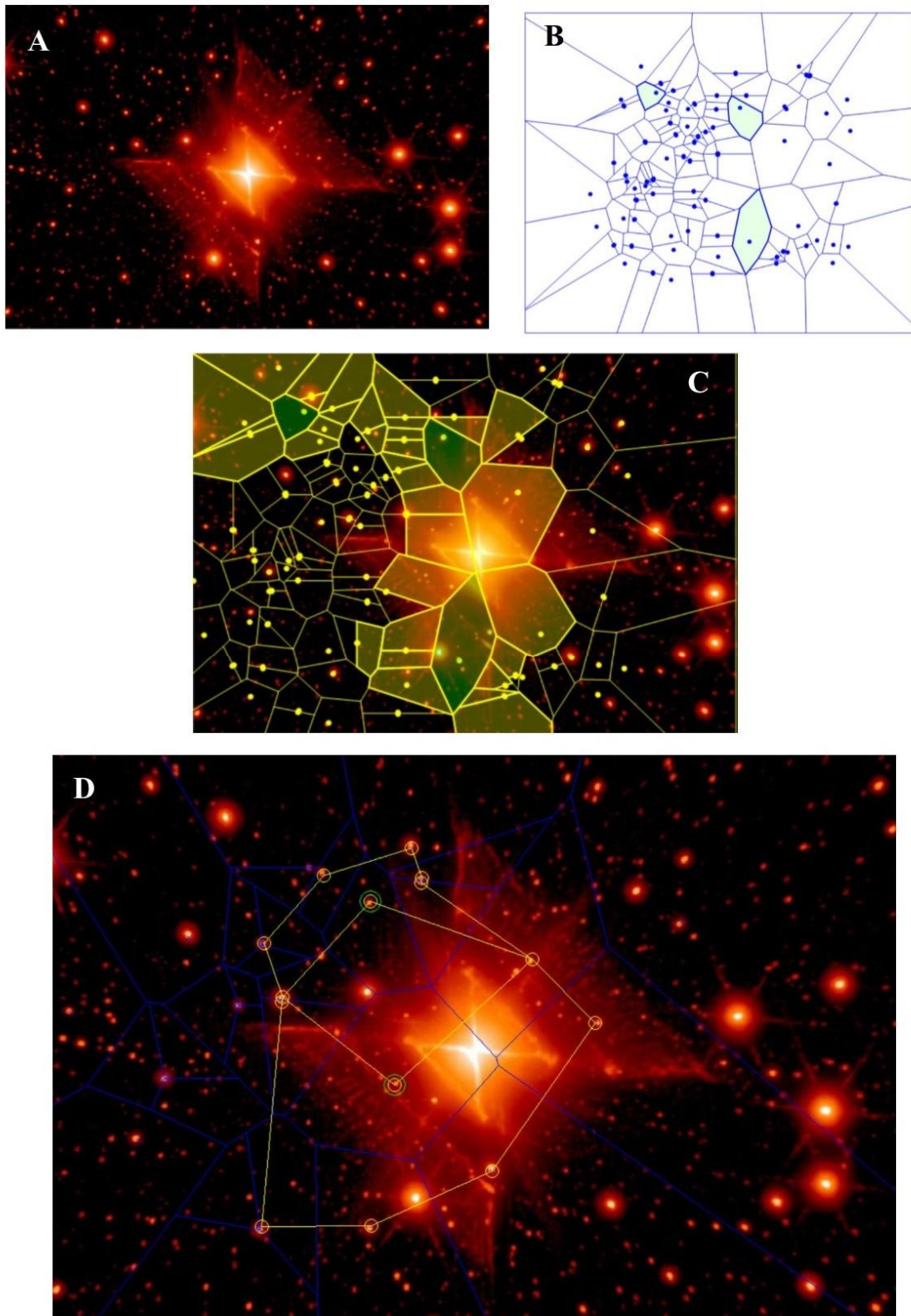



Figure 4. Tessellation of the Red Square Nebula MWC9 22. **Figure 4A** illustrates the original image, **Figure 4B** its three cluster nuclei and **Figure 4C** the corresponding three MNCs. **Figure 4D** shows two Voronoi nuclei. The concentric circles  represent nuclei generating points, while the non-concentric circles (endpoints of the straight edges in this mesh) are the generating points of the adjacent Voronoi regions. This means that this pair of MNCs overlaps.

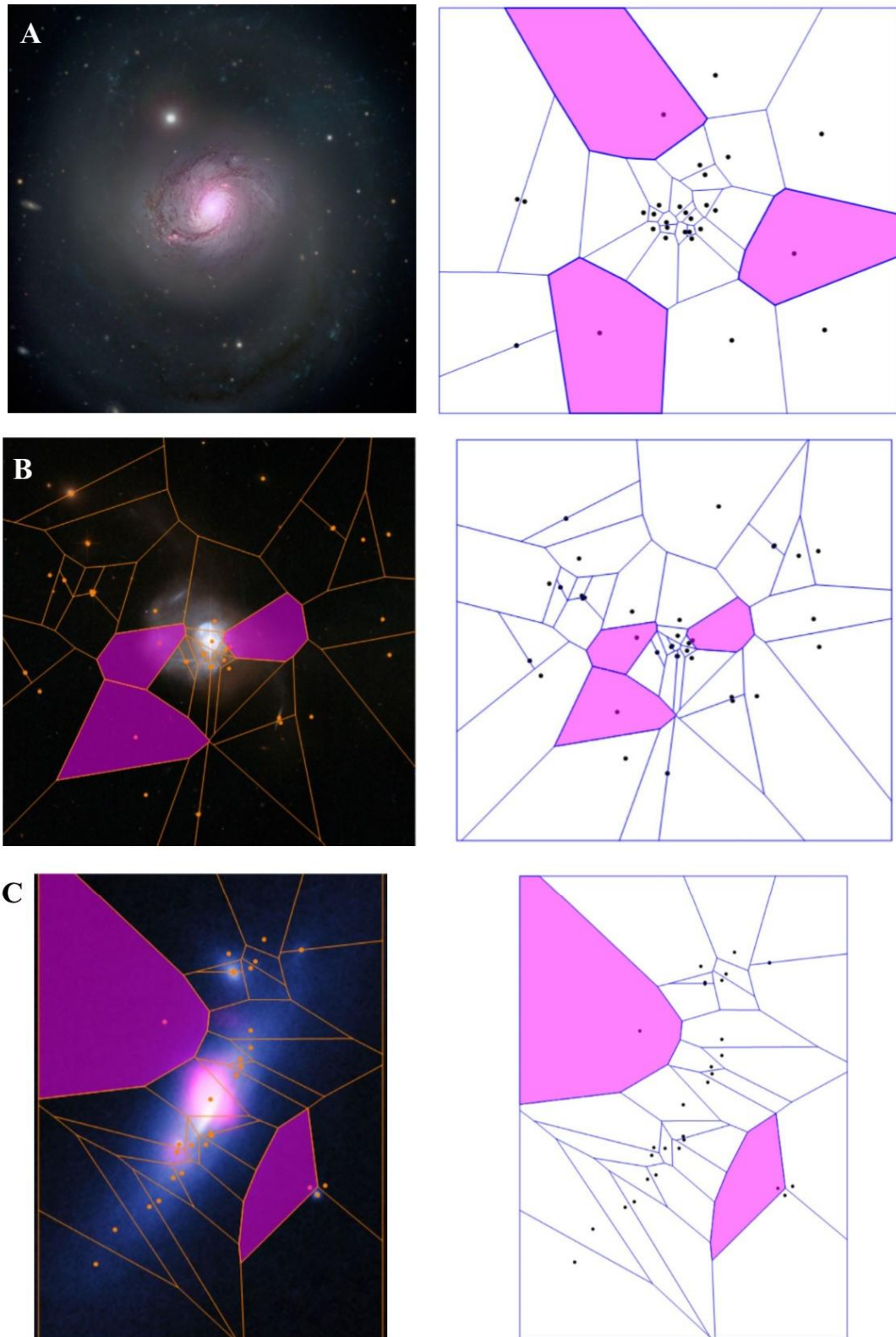


Figure 5. Tessellation of three different galactic structures containing black holes: NGC 1068 (**Figure 5A**), Markarian231 (**Figure 5B**) and SDSSK1126-2944 (**Figure 5C**). Note that the MNCs always occur outside the black holes.

REFERENCES

- 1) Aad G, Abajyan T, Abbott B, Abdallah J, Abdel Khalek S, et al. 2013. Search for dark matter candidates and large extra dimensions in events with a photon and missing transverse momentum in pp collision data at 7 TeV with the ATLAS detector. *Phys Rev Lett.* 110(1):011802. Epub 2013 Jan 3.
- 2) Bromiley PA, Thacker NA, Bouhova-Thacker E. 2010. Shannon entropy, Renyi entropy, and information. *Tina 2004-004, Statistic and Inf Series, Imaging Sci. and Biomed. Eng., Univ. of Manchester, UK*
- 3) Edelsbrunner H. 2006. *Geometry and Topology for Mesh Generation* (Cambridge University Press, Cambridge, U.K.)
- 4) Edelsbrunner H. 2014. *A Short Course in Computational Geometry and Topology* (Springer Briefs in Applied Sciences and Technology, Springer, Cham)
- 5) Fixsen DJ. 2009. The Temperature of the Cosmic Microwave Background. *The Astrophysical Journal* 707 (2): 916–920. doi:10.1088/0004-637X/707/2/916.
- 6) Frank NP, Hart SM. 2010. A dynamical system using the Voronoi tessellation. *The Amer Math Monthly* 117(2):92–112.
- 7) Gawiser E, Silk J. 2000. The cosmic microwave background radiation. *Physics Reports.* 333–334: 245–267. doi:10.1016/S0370-1573(00)00025-9.
- 8) Khachatryan V, Sirunyan AM, Tumasyan A, Adam W, Bergauer T, et al. 2015. Search for dark matter, extra dimensions, and unparticles in monojet events in proton-proton collisions at ... *Eur Phys J C Part Fields.* 75(5):235. Epub 2015 May 29.
- 9) Penrose R. 2011. *Cycles of Time. An Extraordinary New View of the Universe.* Alfred A. Knopf, NY, 2011.
- 10) Penzias AA, Wilson RW. 1965. A Measurement of Excess Antenna Temperature at 4080 Mc/s. *The Astrophysical Journal* 142 (1): 419–421. doi:10.1086/148307.
- 11) Peters JF, Guadagni C. 2015. Strong proximities on smooth manifolds and Voronoi diagrams, *Advances in Math.* 4, no. 2, 97-107.
- 12) Peters JF. 2016. *Computational Proximity. Excursions in the Topology of Digital Images.* (Springer, Intelligent Systems Reference Library 102, Berlin, ISBN 978-3-319-321662), *in press.*
- 13) Peters JF, İnan E. 2016. Strongly near Voronoi nucleus clusters. arXiv 1602(03734): 1-7.
- 14) Peters JF, Tozzi A, Ramanna S. 2016. Brain Tissue Tessellation Shows Absence of Canonical Microcircuits. *Neuroscience Letters* 626: 99–105. doi:10.1016/j.neulet.2016.03.052.
- 15) Pollard H. 1964. A sharp form of the virial theorem. *Bull. Amer. Math. Soc.* LXX (5): 703–705.
- 16) Pourhasan R, Afshordi N, Mann RB. 2014. Out of the white hole: a holographic origin for the Big Bang. *Journal of Cosmology and Astroparticle Physics.* JCAP04(2014)005 (<http://iopscience.iop.org/1475-7516/2014/04/005>)
- 17) Rényi A. 1961. On measures of entropy and information. *Proc. Fourth Berkeley Symp. Math. Stat. and Probability*, vol. I, Berkeley, CA, University of California Press, 547-457, **MR0132570**.
- 18) Rényi A. 1966. On the amount of information in a random variable concerning an event. *J. Math. Sci.* 1, 30-33, MR0210263.
- 19) Rényi A. 1982. *Tagebuch über die Informationstheorie.* VEB Deutcher der Wissenschaften, Berlin, 173 pp., MR0707097.
- 20) Saye RI, Sethian JA. 2011. The Voronoi implicit interface method for computing multiphase physics. *Proc. Nat. Acad. of Sci.* 108(49): 19498-19503, doi/10.1073/pnas.111155708.
- 21) Susskind L. 2004. *An Introduction to Black Holes, Information and the String Theory Revolution: The Holographic Universe.* (World Sci. Pub., Singapore, ISBN-13 978-9812561312).
- 22) van de Weygaert R. 2007. *Voronoi Tessellations and the Cosmic Web: Spatial Patterns and Clustering across the Universe.* arXiv:0707.2877v1.

TOPOLOGICAL FRAMEWORK FOR BRANE COSMOLOGY

Our Universe could either lie on a spatial three-dimensional brane embedded in a higher dimensional bulk, or could be flanked by one or more multi-dimensional branes of different possible sizes and shapes. Here we demonstrate, based on novel topological findings, that disconnected strings with matching descriptions moving on a 4-brane (or more) project to a single string on a 3-brane. This means that strings travelling on the bulk or on higher dimensional branes necessarily display a counterpart in our 3D world, and vice versa. Furthermore, based on the concept of homotopy equivalence, we show how it is possible for branes to stitch together to become condensed branes. Our framework allows a topological duality among different brane theories, because it holds for all the types of branes, independent of their hypothetical shape, curvature, size and boundaries. Furthermore, a topological approach allow branes assessment in the general terms of particle trajectories taking place on donut-like manifolds. Indeed, every high-dimensional brane, independent on the subtending cosmological model, can be described in terms of multi-dimensional toruses mapping to branes with lower spatial dimensions.

1. INTRODUCTION

In brane cosmology, a *brane* is a domain of the Universe with number of dimensions lower than the surrounding or bordering space (Baulieu et al., 2001; Burgess and Van Nierop, 2013). Several brane theories have been developed throughout the years (Candelas et al., 1985; Arkani-Hamed et al., 1998; Randall and Sundrum, 1999; Hitchin, 2003; Hashimoto, 2012). Some scientists believe that our visible four-dimensional Universe is a restricted 3-brane world endowed in a space extending in all directions, called the *bulk*, equipped with any number of spatial dimensions more than three. At least some of the extra-dimensions are extensive (possibly infinite) and branes may be moving through them. Brane-world scenarios might involve more than one, either warped or large, multi-dimensional branes, giving rise to a so-called *multiverse*. A 3-brane can be either the boundary wall of a bulk spanning every dimension both on and off the brane, or a non-boundary domain flanked by one or more branes. Other brane models state that the additional dimensions are compact and our Universe contains the extra-dimensions, so that no reference to the bulk is needed. The concept of *braneworlds* is based on the assumption that some strings are confined to lower-dimensional branes, trapped there by physical laws. They cannot travel in other dimensions and their forces influence just other strings confined to the same brane. Brane-bound forces would spread out only along their brane, and brane-bound particles would be exchanged solely along its dimensions. Not all strings are confined to a single brane, because some of them might be free to travel throughout the bulk. Gravity, for example, is never confined to a brane. This means that, at least via gravity, braneworlds must interact with the bulk, or must be connected to extra-dimensional branes. Interactions with the bulk, and possibly with other branes, can influence our world, introducing effects not detectable by standard cosmological models.

Here we explore the possibility to assess branes, bulks and multiverse bulks in terms of algebraic topology. We demonstrate, based on novel topological findings, that disconnected strings with matching description embedded in a 4-brane (or more) map to a single string on a 3-brane. Therefore, strings moving on higher dimensional brane necessarily display a counterpart in our 3D world, and vice versa. This leads also to novel scenarios, where branes are able to scatter, collide and combine, so that they merge together in an assessable way. Our framework holds for all the types of branes, independent of their hypothetical shape, curvature, size and boundaries. It means that all the hypothesized branes are dual under topological transformation. Here we show how such duality allows branes assessment in the general terms of particles trajectories taking place on donut-like manifolds. Indeed, every high-dimensional branes' model can be described in guise of multi-dimensional toruses, projecting and mapping to branes which display lower spatial dimensions.

2. TOPOLOGY, STRINGS AND BRANES

Here we assess a geometric structure, e.g., a string (denoted str) or *worldline* (Olive and Landsberg, 1989), which is a region on the surface of either abstract geometric spaces or non-abstract physical spaces. A string displays zero or non-zero width ([30], [6], [13]) and either bounded or unbounded length. A string is the path followed by a particle moving through a brane, or different branes, or the bulk (Olive, 1987). Our 3D brane can be depicted as a n -dimensional normed linear space, while the bulk (or the higher-dimensional brane) as a n -dimensional hypersphere. Various continuous mappings from an n -dimensional hypersphere S^n to a feature space that is an n -dimensional Euclidean space R^n lead to a

string-based incarnation of the Borsuk-Ulam theorem (BUT) (Borsuk 1933; Krantz, 2009; Tozzi and Peters, 2016a). It states that:

Every continuous map $f : S^n \rightarrow R^n$ must identify a pair of antipodal points (on S^n).

Points on S^n are *antipodal*, provided they are diametrically opposite (Weisstein, 2016). If we simply evaluate branes or strings instead of *points*, BUT leads naturally to the possibility of a region-based brane geometry. The two opposite points could stand not just for the description of simple topological points (Marsaglia, 1972), but also of brane or strings features, such as spatial or temporal patterns, tensors, signals, particle trajectories (Peters, 2016). Therefore, we can describe branes or strings features as antipodal points on n -manifolds. Signal shapes can be compared, because the two antipodal points can be assessed at higher-dimensional levels of observation, while single points at lower levels (Tozzi and Peters, 2016b). The two points (or regions) do not need necessarily to be antipodal, in order to be described together (Peters, 2016). Indeed, BUT can be generalized also for the assessment of non-antipodal features, provided there are a pair of regions on a n -sphere with the same feature value (Peters and Tozzi, 2016a). We are allowed to consider also homotopic regions on an n -sphere that are either adjacent or far apart. Despite BUT was originally described just for positive-curvature n -spheres, we are allowed to look for antipodal points also on manifolds equipped with non convex curvatures (Mitroi-Symeonidis, 2015; Tozzi, 2016). Whether branes display concave, convex or flat geometry, it does not count, because we may always find the points with matching description predicted by BUT. Furthermore, a S^n manifold might not map just to a R^{n-1} Euclidean space, but straight to a S^{n-1} manifold, e.g. a lower-dimensional surface of the same S^n . In other words, either the Euclidean space and other manifolds could be omitted in brane theory. We do not need anymore a S^n manifold curving into a dimensional space R^n : we may think the brane just as existing by itself. Indeed, some brane theories do not require two branes at all (Randall and Sundrum, 1999): by an intrinsic point of view, a single brane might exist in - and on - itself and does not need to lie in a bulk (Weeks, 2002). It means that the mapping of two antipodal points to a single point in a dimension lower becomes a projection internal to the same brane. For technical readers, see also: Dodson and Parker (1997), Matousek (2003), Crabb and Jaworowski (2013).

In the evaluations of strings confined to a brane, we take into account antipodal sets instead of antipodal points (Peters and Naimpally, 2012), because in a point-free geometry regions replace points as the primitives (Di Concilio, 2013; Di Concilio and Gerla, 2006). If we assess a string in terms of a spatial regions on the surface of an n -sphere, or in an n -dimensional normed linear space, the same string can be defined as *antipodal*, provided the regions encompassing the strings belong to disjoint parallel hyperplanes. Put simply, strings have no points in common (**Figure 1**). A region is called a *worldsheet*, or a brane, if everyone of its subregions contains at least one string. In other words, the term *worldsheet* or brane designates a nonempty region of a space completely covered by strings, in which every member is a string (Peters and Tozzi, 2016b). A 2D plane worldsheet can be rolled up to form the lateral surface of a 3D cylinder, termed a *worldsheet cylinder*. Further, a *worldsheet cylinder* maps to a *worldsheet torus*, formed by bending the former until the ends meet. In sum, a flattened *worldsheet* maps to a *worldsheet cylinder* and a flattened *worldsheet cylinder* maps to *worldsheet torus*. It means that a bounded *worldsheet cylinder* is homotopically equivalent to a *worldsheet torus*, so that every brane can be described in terms of particle movements along the surface of multi-dimensional toruses. Although strings on different *worldsheets* are antipodal and descriptively near, e.g., they share matching description, there is however a difference between the strings embedded in branes of diverse dimensions. The higher the dimension of the *worldsheet*, the more the information encompassed in strings on the same region, because the number of coordinates is higher. Strings contain more information than their projections in lower dimensions. It means that BUT allows us to evaluate systems features in higher-dimensions, in order to increase the amount of detectable information. Vice versa, dropping down a dimension means that each region in the lower-dimensional space is simpler. Hence, BUT provides a way to evaluate changes of information among different branes and bulk in a topological, other than thermodynamical, fashion.

Next, consider Brouwer's fixed point theorem (FPT), which states that every continuous function from a n -sphere of every dimension to itself has at least one fixed point (Volovikov and Yu, 2008). FPT applies, for example, to any disk-shaped area, where it guarantees the existence of a fixed point, which behaves like a sort of whirlpool attracting moving particles. Su (1997) gives a coffee cup illustration of the FPT: no matter how you continuously slosh the coffee around in a coffee cup, some point is always in the same position that it was before the sloshing began. And if you move this point out of its original position, you will eventually move some other point in the sloshing coffee back into its original position. In BUT terms, it means that not only we can always find a n -sphere, e.g. a brane, containing a string, but also that every string with a particular shape comes together with another string, termed a *wired friend*. These observations lead to a *wired friend theorem*: every occurrence of a *wired friend* string with a particular shape on the structure S^n maps to a fixed description, e.g. to another string that belongs to a manifold or Euclidean space with different dimensions. Every *wired friend* is recognizable by its shape, because the shape of a string is the silhouette of a *wired friend* string. Therefore, we are allowed to achieve a map of *wired friend* strings, projecting from the 2D *worldsheet* to the 3D *cylinder* and *torus* *worldsheets*. The mean achievement is that we can always find a string embedded in a higher-dimensional brane which is the description of another string in a lower dimensional brane, and vice versa.

our 3-brane

4-brane (or bulk)

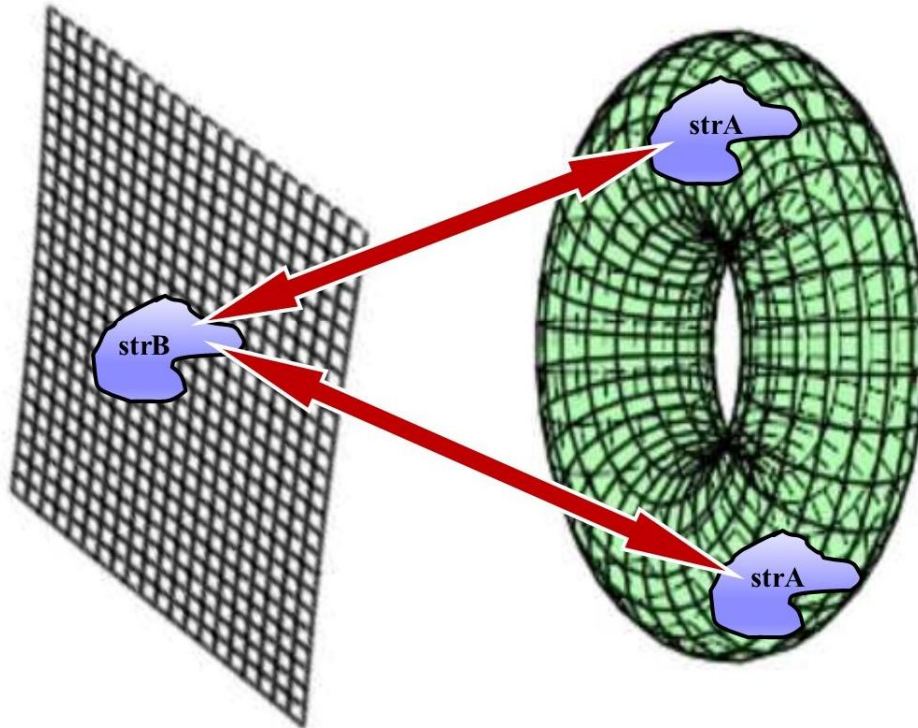


Figure 1. Samples of strings with finite length are represented by the bounded strings strA and strB. Regions strA, strB are examples of antipodal strings. Note that the torus might depict, according to the different brane theories, either a 4-brane adjacent our 3D brane, or a 4D bulk in which our 3-brane is embedded. The branes are depicted, for sake of clarity, one dimension lower than the real ones.

3. BRANES AND HOMOTOPY EQUIVALENCE

In the previous paragraph, we showed why different branes necessarily have at least a few features in common. Here we illustrate how, in topological terms, brane shapes are continually transforming into new homotopically equivalent shapes. Branes might influence each other by scattering, colliding and combining, to create bounded regions into the bulk. Hence, it is possible for branes to stick together to become *condensed branes*, e.g., worldsheets (operationally assessable in terms of the torus described above) which depict the behaviour of a collection of interacting and scattering elements.

Homotopy Equivalence.

Let $f, g : X \rightarrow Y$ be a pair of continuous maps. For example, let $f(X)$ and $g(X)$ be two branes with fixed endpoints. A *homotopy* (Cohen, 1973) between f and g is a continuous map $H : X \times [0,1] \rightarrow Y$ so that $H(x,1) = g(x)$ and $H(x,0) = f(x)$. The interest here is in the possibility of deforming (transforming) one brane with a particular shape into another with a different shape. It means that in the birth of branes, that evolve out of the interaction of initially disjoint branes, is allowed. Let $id_X : X \rightarrow X$ denote an identity map defined by $id_X(x) = x$. Similarly, $id_Y : Y \rightarrow Y$ is defined by $id_Y(t) = t$. The composition $f \circ g(X)$ is defined by $f \circ g(X) = f(g(X))$

. Similarly, $g \circ f(X)$ is defined by $g \circ f(X) = g(f(X))$. The sets X and Y are homotopically equivalent, provided there are continuous maps so that $g \circ f \sqsupseteq id_X(x)$ and $f \circ g \sqsupseteq id_Y(y)$. The sets X and Y are the same homotopy type, provided X and Y are homotopically equivalent (Peters and Inan, 2016). The interest here is in evolving branes that have the same homotopy type. In effect, homotopically equivalent brane shapes have the same homotopy type (Peters and Nainpally, 2012). This leads to a comparison of branes with seemingly varying shapes and sizes that are homotopically equivalent.

Example. Homotopically Equivalent Shapes.

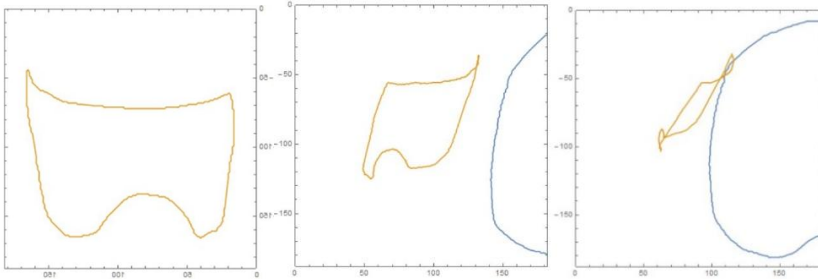


Fig. 2.A 3-Brane

Fig. 2.B Two branes

Fig. 2.C interacting branes

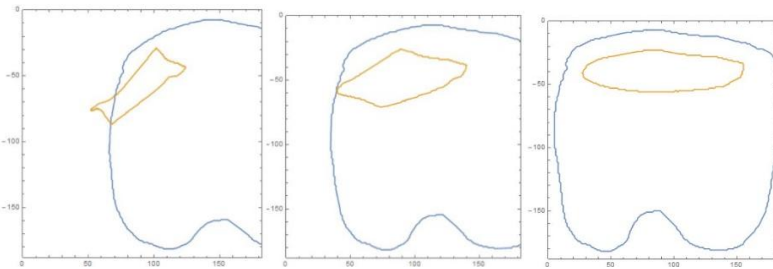


Fig. 2.D dual branes

Fig. 2.E concentric branes

Fig. 2.F tooth brane

Figure 2. Eventually brane will deform into another, as a result of the collision of a pair of separate branes. Let a brane be represented by the 3-brane in **Fig. 2.A**. This brane evolves over time as it twists and turns through the outer reaches of the bulk. An inking twisting brane appearing in the neighbourhood of the first one is shown in **Fig. 2.B**. The two branes begin interacting, so that the first now has a region of space in common with the second in **Fig. 2.C**. In effect, as a result of the interaction between the branes, they are partially stitched together in **Fig. 2.C**. The partial absorption of one brane in another is shown in **Fig. 2.D**. Here, a very large region of bulk space occupied by the first brane is absorbed by the second and we have the birth of a condensed brane. The two branes become at first concentric in **Fig. 2.E**, then a complete condensed brane is formed with a tooth shape in **Fig. 2.F**. When the two branes are completely transformed into a new one, we have instance of their homotopy of equivalence, with the second that has completely absorbed the first.

A stitching action on a pair of branes is homotopic mapping of one brane into another. This is a further instance of the duality principle in brane cosmology. That is, one brane is the dual of another brane, provided the first can be deformed into the second. The brane in **Fig. 2.E** is an example of a Edelsbrunner-Harer nerve (Peters and Inan, 2016), which is a collection $Nrv\mathfrak{S}$ such that all nonempty subcollections of $Nrv\mathfrak{S}$ have a non-void common intersection, i.e.,

$$Nrv\mathfrak{S} = \{X \in \mathfrak{S} : \bigcap X \neq \emptyset\}.$$

Lemma 1. Branes of the same homotopy type are stitched together to form a condensedbrane.

Proof. Let A, B be branes with the same homotopy type. Then brane A can be deformed into brane B . In effect, brane B absorbs brane A . By definition, brane B is a condensed brane. This phenomenon is true in general for homotopically equivalent branes that have the potential to be stitched together. Hence, the desired result follows.

Theorem 1. A condensed brane is an instance of an Edelsbrunner-Harer nerve.

Proof. From Lemma 1, a condensed brane is an instance of an Edelsbrunner-Harer nerve.

Theorem 2. Every brane is a Edelsbrunner-Harer nerve.

Proof. Let A be a brane. Every brane is a collection of strings. Each of the strings have brane A in common. That is, all sub-branes of brane A have nonempty intersection. Consequently, A is an Edelsbrunner-Harer nerve. Hence, the desired result follows.

4. DISCUSSION

Extra dimensional branes can come in different numbers of sizes and shapes and may display either warped or large extra-dimensions. If the bulk separates one brane from another, some strings might be embedded in the bulk, while others are confined to branes. Here we introduced novel topological variants that elucidate the features of different types of extra dimensional setups. We achieve generalizations that allow the assessment of every possible cosmological brane, independent on its shape, size or boundaries. Our results show that sets of strings, equipped either with antipodal or non-antipodal matching description and embedded in d -dimensional branes M^d , map to a single set of strings in M^{d-1} branes, and vice versa. The term matching description means the strings display common feature values, e.g., all the branes, even if embedded in different dimensions, must have features in common. It has been hypothesized that there exist different branes that are too far apart ever to communicate with one another, so that strings bounded on distant branes would never have direct contact. However, our topological investigation reveals that this scenario is unfeasible, because there must be at least one element in common among branes that are very distant one each other too. Further, all the branes and bulks will always have some element in common, not just gravity: branes do not exist in isolation, rather they are part of a larger interconnected whole with which they interact.

In brane cosmology, particle movements are described as functions occurring on manifolds equipped with different possible geometric curvatures. We showed that M may stand for a multi-dimensional brane with any kind of curvature, either concave, convex or flat. M^{d-1} may also be a part of M^d , or in other words, embedded in M^d or lying on its surface. Such rather general BUT dictates encompass almost all the brane models. Indeed, cosmic theories claiming different curvatures of the Universe (from hyperbolic anti-deSitter Cosmos, to inflationary models, to flat Riemannian 4D Universes) and brane theories describing branes with small or large extra-dimensions (from warped scenarios and Calabi-Yau manifolds, to extralarge and infinite dimensions) are DUAL: e.g., their topological description is the same, despite the huge differences in the subtending manifolds. Therefore, the shape is not important in the evaluation of branes, because it is fully interchangeable. This also means that projections between dimensions describe phenomena spanning from the smallest to the highest scales: the distinction in brane size in different theories does not count anymore.

Some branes theories predict the existence of open strings, e.g., strings equipped with two ends lying on diverse branes. For our definition of antipodality, the two strings need to be separated. An appropriate projection mapping shows that, if two strings have matching features (shape, length, width, area), the two strings are the same. This calls for the Brouwer fixed point and wired friend theorems. In sum, two strings with matching description embedded on two branes of different dimensions are the same string and are not divided. Strings with matching ends (regions) in different dimensions might also help to explain Einstein–Rosen–Podolski bridges.

The fundamental problem with conventional approaches to duality is starting with points instead of regions. It carries over in string theory, where one *stitches* together strings to obtain a new string. This problem is solved in a framework of region-based spacetime geometry (Lentzen, 1939; Disalle, 1995; Henderson, 1996).

Our results also entail that every kind of high-dimensional brane can be described in terms of donut-like structures (Peters and Tozzi, 2016b). We showed that, while strings' features in our 3D Universe can be described in terms of particle trajectories on 3D sheets, strings' features in higher-dimensional branes can be assessed in the generic terms of particle trajectories traveling on multi-dimensional toruses. This methodological advance could be useful in order to uniform the operationalization of the countless theories in brane cosmology.

By way of application of the proposed framework, the closed paths described by BUT and FPT variants represent branes occurring in different dimensions. Every pathway in a brane is a closed string intertwined with strong proximities with other strings in other branes. Indeed, we showed that the branes' components are densely connected with the rest of the Universe. The tight coupling among different branes features gives rise to cosmic systems that are in charge of receiving and interpreting signals from other branes, in closely intertwined relationships.

REFERENCES

- 1) Arkani–Hamed N, Dimopoulos S, Dvali G. 1998. The hierarchy problem and new dimensions at a millimetre. *Physics Letters B*, 429(3):263–272, doi:10.1016/S0370-2693(98)00466-3.

- 2) Baulieu L, Green M, Picco M, Windey P. 2001. *Progress in String Theory and M-Theory*, Springer, Berlin, DOI 10.1007/978-94-010-0852-5.
- 3) Borsuk M. 1933. Drei Satze Uber Die N-Dimensionale Euklidische Sphere. *Fundamenta Mathematicae* XX: 177–90.
- 4) Burgess CP, van Nierop L. 2013. Technically natural cosmological constant from supersymmetric 6D brane backreaction. *Physics of the Dark Universe*,2(1):1–16, doi:10.1016/j.dark.2012.10.001
- 5) Candelas P; Horowitz G, Strominger A, Witten E. 1985. Vacuum configurations for superstrings. *Nuclear Physics B*, 258: 46–74, Bibcode:1985NuPhB.258...46C, doi:10.1016/0550-3213(85)90602-9
- 6) Cohen MM. 1973. *A Course in Simple Homotopy Theory*. New York-Berlin: Springer-Verlag.
- 7) Crabb MC, Jaworowski J. 2013. Aspects of the Borsuk-Ulam Theorem. *J. of Fixed Point Theory and Applications* 13 (2013), 459–488, DOI 10.1007/s11784-013-0130-7, MR3122336.
- 8) Di Concilio A. 2013. Point-free geometries: Proximities and quasi-metrics, *Math. in Comp. Sci.* 7, 1, 31–42, MR3043916.
- 9) Di Concilio A, Gerla G. 2006. Quasi-metric spaces and point-free geometry. *Math. Structures Comput. Sci.* 16, 1, 115137, MR2220893.
- 10) Disalle R. 1995. Spacetime theory as physical geometry. *Erkenntnis*, 42(3):317–337.
- 11) Dodson CTJ, Parker PE. 1997. *A User’s Guide to Algebraic Topology*. Dordrecht, Netherlands: Kluwer Academic Publishers.
- 12) Edelsbrunner H. 2014. *A Short Course in Computational Geometry and Topology*. Berlin: Springer-Verlag.
- 13) Hashimoto K. 2012. D-Brane. Superstrings and New Perspective of Our World. Springer-Verlag, Berlin, DOI 10.1007/978-3-642-23574-0.
- 14) Henderson DW. 1996. *Experiencing Geometry on Plane and Sphere*. New York: Prentice Hall.
- 15) Hitchin N. 2003. Generalized Calabi–Yau manifolds. *The Quarterly Journal of Mathematics*, 54 (3): 281–308.
- 16) Krantz SG. 2009. *A Guide to Topology*. Edited by The Mathematical Association of America. Washington DC.
- 17) Lenzen VF. 1939. Physical geometry, *Amer. Math. Monthly* 46, 324–334, MR0000214.
- 18) Marsaglia G. 1972. “Choosing a Point from the Surface of a Sphere.” *Annals of Mathematical Statistics* 43 (2): 645–46. doi:10.1214/aoms/1177692644.
- 19) Matoušek J. 2003. Using the Borsuk–Ulam Theorem. *Lectures on Topological Methods in Combinatorics and Geometry*. Berlin Heidelberg: Springer-Verlag.
- 20) Mitroi-Symeonidis FC. 2015. Convexity and Sandwich Theorems. *European Journal of Research in Applied Sciences* 1 (March): 9–11.
- 21) Naimpally SA, Peters JF. 2013. *Topology with applications. Topological spaces via near and far*. World Scientific, Singapore, Amer. Math. Soc. MR3075111.
- 22) Olive DI. 1987. Algebras, lattices and strings 1986. Unification of fundamental interactions. *Proc. Royal Swedish Acad. Sci.*, Stockholm, 19–25, MR0931580.
- 23) Olive DI, Landsberg PT. 1989. Introduction to string theory: its structure and its uses. *Physics and mathematics of strings*, *Philos. Trans. Roy. Soc. London* (1989), 319–328, MR1043892.
- 24) Peters JF. 2016. *Computational Proximity. Excursions in the Topology of Digital Images*. Edited by Intelligent Systems Reference Library. Berlin: Springer-Verlag. doi:10.1007/978-3-319-30262-1.
- 25) Peters JF, Guadagni, C. 2015. Strongly near proximity and hyperspace topology, arXiv 1502, no. 05913.
- 26) Peters JF, Guadagni, 2015. C. Strongly proximal continuity & strong connectedness, arXiv 1504, no. 02740.
- 27) Peters JF, Inan E. 2016. Strongly proximal Edelsbrunner-Harer nerves. *Proc. Jangjeon Math. Soc.* 19(3):563-582.
- 28) Peters JF, Naimpally SA. 2012. Applications of near sets, *Notices of the Amer. Math. Soc.* 59(4):536–542, DOI: <http://dx.doi.org/10.1090/noti817>.
- 29) Peters JF, Tozzi A. 2016a. Region-Based Borsuk-Ulam Theorem. arXiv.1605.02987
- 30) Peters JF, Tozzi A. 2016b. String-Based Borsuk-Ulam Theorem. arXiv:1606.04031
- 31) Randall L, Sundrum R. 1999. Large Mass Hierarchy from a Small Extra Dimension. *Phys. Rev. Lett.* 83, 3370.
- 32) Su FE. 1997. Borsuk-Ulam implies Brouwer: A direct construction. *Amer. Math. Monthly* 104 (9): 855–859, MR1479992.
- 33) Tozzi A. 2016. Borsuk-Ulam Theorem Extended to Hyperbolic Spaces. In: *Computational Proximity. Excursions in the Topology of Digital Images*, edited by J F Peters, 169–171. doi:10.1007/978-3-319-30262-1.
- 34) Tozzi A, Peters JF. 2016a. Towards a Fourth Spatial Dimension of Brain Activity. *Cognitive Neurodynamics* 10 (3): 189–199. doi:10.1007/s11571-016-9379-z.
- 35) Tozzi A, Peters JF. 2016b. A Topological Approach Unveils System Invariances and Broken Symmetries in the Brain. *Journal of Neuroscience Research* 94 (5): 351–65. doi:10.1002/jnr.23720.
- 36) Volovikov, Yu A. 2008. Borsuk-Ulam Implies Brouwer: A Direct Construction Revisited. *American Mathematical Monthly* 115 (6): 553–56. doi:10.2307/2975293.
- 37) Weeks JR. 2002. *The shape of space*, IInd edition. Marcel Dekker, inc. New York-Basel.
- 38) Weisstein EW. 2016. Hyperplane, Mathworld. A Wolfram Web Resource. <http://mathworld.wolfram.com/Hyperplane.html>.

TOWARDS A MONSTER GROUP ENCOMPASSING THE UNIVERSE

(symmetries, information and monster groups before and after the big bang)

The Monster group, the biggest of the sporadic groups, is equipped with the highest known number of dimensions and symmetries. Taking into account variants of the Borsuk-Ulam theorem and a novel topological approach cast in a physical fashion that has the potential to be operationalized, the Universe can be conceived as a lower-dimensional manifold encompassed in the Monster group. Our Universe might arise from spontaneous dimension decrease and symmetry breaking that occur inside the very structure of the Monster Module. We elucidate how the energetic loss caused by projection from higher to lower dimensions and by the Monster group's non-abelian features is correlated with the present-day asymmetry in thermodynamic arrow. By linking the Monster Module to theoretical physical counterparts, we are allowed to calculate its enthalpy and Lie group trajectories. Our approach also reveals how a symmetry break might lead to a Universe based on multi-dimensional string theories and CFT/AdS correspondence.

*The Mode is an enclosed, detectable manifestation of the Substance...
The Substance is equipped with infinite attributes (Spinoza, Ethica, pars I)*

INTRODUCTION

The Fischer-Griess Monster group, the largest among the twenty-six sporadic groups, is equipped with 196,883 dimension and an order of about 10^{54} elements (Conway et al., 1986). It is noteworthy that the Monster Module displays the highest known number of symmetries (du Sautoy). It has been recently proposed that the symmetries, widespread invariances occurring at every level of organization in our Universe, may be regarded as the most general feature of physical systems, perhaps also more general than thermodynamic constraints (Tozzi and Peters, 2016a, Roldán 2014). Therefore, giving insights into the Monster symmetries would provide a very general approach to systems function, Universe evolution and energetic dynamics. Here we show how a novel symmetry-based, topological approach sheds new light on Monster's features. We provide a foundation for the Monster's physical counterparts, cast in a fashion that has the potential to be operationalized, which can be used for the assessment of our Universe's evolution and, in particular, pre-big bang scenarios.

This paper comprises four sections. In the first section, we describe a generalized version of the Borsuk-Ulam theorem, in order to provide the topological machinery for further evaluations of the Monster in the context of theoretical physics. Section two explains how the Universe might originate from the Monster Module, due to a dimension loss, linking the Monster group to theoretical physics counterparts. Furthermore, taking into account energetic arguments dictated by topological dimension decrease, the section explains why and how our Universe is equipped with the symmetry breaks which give rise to the thermodynamic arrow. Section three elucidates various physical features of the Monster. In the final section, we raise a number of still open questions.

1) TOPOLOGICAL TOOLS

The standard version of the Borsuk-Ulam theorem (BUT).

The Borsuk-Ulam Theorem (Borsuk 1933) states that:

Every continuous map $f : S^n \rightarrow R^n$ must identify a pair of antipodal points (on S^n).

This means that the sphere S^n maps to the Euclidean space R^n , which stands for an n -dimensional Euclidean space (Beyer; Matoušek). See Tozzi and Peters (2016b) for further details. The original formulation of BUT displays four versatile ingredients which can be modified, resulting in different guises: a continuous function, two antipodal (or non-antipodal) points with matching description, an n -sphere equipped with different n values and, last but not the least, a mapping from a higher to a lower dimension that is invertible.

BUT variants. We resume some BUT variants described by Peters (2016) and Tozzi and Peters (2016a). The concept of antipodal points can be generalized to countless types of signals. Two opposite points encompass not just the

description of simple topological points, but also of spatial and temporal patterns, vectors and tensors, functions, signals, thermodynamical parameters, trajectories, symmetries (Peters and Tozzi, 2016a). The two antipodal points standing for different systems features are assessed at one level of observation, while the single point is assessed at a lower level. The antipodal points restriction from the *classical* BUT is no longer needed, because the applications on an n -sphere can be generalized not just for the evaluation of diametrically opposite points, but also of non-antipodal ones. We are allowed to take into account homotopic regions on an n -sphere that are either adjacent or far apart. This means that the points (or regions) with the same feature value do not need necessarily to be antipodal, in order to be described together (Peters 2016). The original formulation of BUT describes the presence of antipodal points on spatial manifolds in every dimension, provided the n -sphere is a convex, positive-curvature structure. However, many physical functions occur on manifolds endowed with other types of geometry: for example, the hyperbolic one (Watanabe; Sengupta et al., 2016). Whether the manifold displays a concave, convex or flat activity, it does not count: we may always find the points with matching description predicted by BUT. Although BUT has been originally described just in case of n being a natural number which expresses a spatial dimension, its value in S^n can also stand for other types of numbers. The n value can be also cast as an integer, a rational or an irrational number. It allows us to use the n parameter as a versatile tool for the description of systems symmetries (Tozzi and Peters, 2016a). A BUT variant tells us that we can find a pair of opposite points an n -dimensional sphere, that display the same encoding not just on a R^n manifold, but also on an $n-1$ sphere. A symmetry break occurs when the symmetry is present at one level of observation, but *hidden* at another level (Roldàn). This means that symmetries can be found when evaluating the system in a proper dimension, while they disappear (are hidden or broken) when the same system is embedded in just one dimension lower.

Here we introduce recently developed, unpublished BUT variants. The first is a BUT corollary, which states that a S^n manifold does not map just to a R^{n-1} Euclidean space, but straight to a S^{n-1} manifold. In other words, the Euclidean space is not mentioned in this formulation. Indeed, in many applications, *e.g.*, in fractal systems, we do not need a Euclidean manifold at all. A manifold, in this case S^n , may exist in - and on - itself, by an intrinsic, *internal* point of view, and does not need to be embedded in any dimensional space (Weeks). Therefore, we do not need a S^n manifold curving into a dimensional space R^n : we may think that the manifold just does exist by itself. An important consequence of this BUT version is that a n -sphere may map on itself. The mapping of two antipodal points to a single point in a dimension lower can be a projection internal to the same n -sphere.

The second and foremost variant is termed **Energy-BUT**. There exists a physical link between the abstract concept of BUT and the real energetic features of systems formed by two spheres S^n and S^{n-1} . An n -sphere S^n is equipped with two antipodal points, standing for symmetries according to BUT. When these opposite points map to a n -Euclidean manifold where S^{n-1} lies, a symmetry break/dimensionality reduction occurs, and a single point is achieved (Peters and Tozzi, 2016b). It is widely recognized that a decrease in symmetry goes together with a reduction in entropy and free-energy (in a closed system). It means that the single mapping function on S^{n-1} displays energy parameters lower than the sum of the two corresponding antipodal functions on S^n . Therefore, a decrease in dimensions gives rise to a decrease of energy and energy requirements. BUT and its variants are physical quantities, because we achieve a system in which the energetic changes do not depend anymore on thermodynamic parameters, rather on topological features such as affine connections and homotopies. The energy-BUT concerns not just energy, but also information. Indeed, two antipodal points contain more information than their single projection in a lower dimension. Dropping down a dimension means each point in the lower dimensional space is simpler, because each point has one less coordinate. In sum, energy-BUT provides a way to evaluate the decrease of energy in topological, other than thermodynamical, terms.

Another novel variant of BUT is the string-based BUT (briefly, **strBUT**). The usual continuous function required by reBUT (region-based BUT in Peters and Tozzi, 2016a) is replaced by a proximally continuous function, which guarantees that, whenever a pair of strings (regions that are world lines) are close (near enough to have common elements), then we always know that their mappings will be also be close. A string is a region of space with zero width and either bounded or unbounded length. As a particle moves through space following a world line (Olive and Landsberg, 1989). Interactions occur at the junctions of world lines. Let τ the proper time of a particle, measured by clock travelling with a particle and integration along the world line of the particle. The *action*_{particle} of a freely moving particle is defined by

$$action_{particle} = -mc^2 \int d\tau.$$

As time evolves, a particle leaves a trace of its movements along a surface that are “remembered”. A string is then a remembered parts of a hypersphere surface over which a particle travels. In terms of quantum theory, a string is a path defined by a moving particle. Put another way, a string is path-connected and its path is defined by a sequence of adjacent *fat* surface points. The points are *fat* because they are physical as opposed to abstract geometric points. In other words, a string A (briefly, **strA**) is a thin region of space that has describable features such as connectedness, length, open-ended or closed-ended, and shape. Strings $strA, \neg strA$ are antipodal, provided $strA$ and $\neg strA$ are disjoint and yet have the same description. Strings $strA, \neg strA$ are examples of antipodal sets (Petty, 1971). The description of $strA$ (briefly, $\Phi(strA)$) is a feature vector in R_n , where that each component of $\Phi(strA)$ is a feature value of $strA$.

Quantum String Axioms

1. Every string has an action.
2. If $\text{str}A, \neg\text{str}A$ are antipodal, then $\text{action}_{\text{str}A} = \text{action}_{\neg\text{str}A}$.
3. Separate strings with k features with the same description are antipodal.
4. There is a set $\{\neg\text{str}A\}$ of antipodal strings for every string $\text{str}A$.

Let X be a topological space equipped with descriptive proximity δ_ϕ . $\text{str}A \delta_\phi \neg\text{str}A$ reads $\text{str}A$ and $\neg\text{str}A$ have the same description. Let 2^{S^n} denote the family of sets on the surface of a hypersphere S^n and $\text{str}A, \neg\text{str}A \in 2^{S^n}$ are antipodal strings on S^n . A function $f : 2^{S^n} \rightarrow R^n$ is proximally continuous, provided $\text{str}A \delta_\phi \neg\text{str}A$ implies $f(\text{str}A) \delta_\phi f(\neg\text{str}A)$. With these observations about strings, we obtain the following results.

Lemma [strBUT]. If $f : 2^{S^n} \rightarrow R^n$ is proximally continuous, $f(\text{str}A) = f(\neg\text{str}A)$ for some $\text{str}A$ in 2^{S^n} .

Proof. Case $n = 1$. Let each $\text{str}A$ have 1 feature, namely, action. Assume antipodal strings $\text{str}A, \neg\text{str}A$ with n features are descriptively close, i.e., $\text{str}A \delta_\phi \neg\text{str}A$. Since f is proximally continuous, we have $f(\text{str}A) \delta_\phi f(\neg\text{str}A)$. From Axiom 2, $\text{action}_{\text{str}A} = \text{action}_{\neg\text{str}A}$. Hence, from the definition of the descriptive proximity δ_ϕ , $f(\text{str}A) = f(\neg\text{str}A)$.

Case $n > 1$. The proof is symmetric with case $n = 1$ and Axiom 3. \square

Theorem 1. If $f : 2^{S^n} \rightarrow R^k$, $k > 0$ is proximally continuous, $\text{action}_{\text{str}A} = \text{action}_{\neg\text{str}A}$ for some $\text{str}A$ in 2^{S^n} .

Proof. We consider only the case for $k = 1$, for strings whose only feature is action. The desired result is immediate from the strBUT Lemma and Axiom 2. This result is easily extend to the case where $k > 1$ for strings with k features. \square

Theorem 2. If $f : 2^{S^n} \rightarrow 2^{R^k}$, $k > 0$ is proximally continuous, $f(A) = f(\neg A)$ for each $\neg\text{str}A$ in the set of antipodes $\{\neg\text{str}A\} \in 2^{S^n}$.

Proof. Immediate from the Theorem 1 and Axiom 4. \square

In order to map S^n to $S^{\{n-1\}}$, we need to work with lower dimensional spaces containing regions where each point in $S^{\{n-1\}}$ has one less coordinate than a point in S^n .

Let X be a topological space equipped with Lodato proximity δ (Peters, 2016). $\text{str}A \delta \neg\text{str}A$ reads $\text{str}A$ and $\neg\text{str}A$ are close. Dochviri and Peters (2016) introduce a natural approach in the evaluation of the nearness of sets in topological spaces. The objective is to classify levels of nearness of sets relative to each given set. The main result is a proximity measure of nearness for disjoint sets in an extremely disconnected topological space. Let $\text{int}(\text{str}A)$ be the set of points in the interior of $\text{str}A$. Another result is that if strings $\text{str}A, \neg\text{str}A$ are nonempty semi-open sets such that $\text{str}A \delta \neg\text{str}A$, then $\text{int}(\text{str}A) \delta \text{int}(\neg\text{str}A)$.

An important feature is that the manifolds M^d and M^{d-1} are topological spaces equipped with a strong descriptive proximity relation. Recall that in a topological space M , every subset in M and M itself are open sets. A set E in M is open, provided all points sufficiently near E belong to E (Bourbaki, 1966). The description-based functions in genBUT are strongly proximally continuous and their domain can be mathematical, physical or biological features of world line shapes. Let A, B be subsets in the family of sets in M (denoted by 2^M) and let $f : 2^M \rightarrow R^n$, $A \in 2^M$, $f(A)$ = a feature vector that describes A . That is, $f(A), f(B)$ are descriptions of A and B . Nonempty sets are *strongly near*, provided the sets of have elements in common. The function f is strongly proximally continuous, provided A strongly near B implies $f(A)$ is strongly near $f(B)$. This means that strongly near sets have nonempty intersection. From a genBUT perspective, multiple sets of objects in M^d are mapped to $f(A \cap B)$, which is a description of those objects common to A and B . In other words, the functions in genBUT are set-based embedded in a strong proximity space. In particular, each set is set

of contiguous points in a path traced by a moving particle. The path is called a world line. Pairs of world lines have squiggly, twisted shapes opposite each other on the surface of a manifold. Unlike the antipodes in a conventional hypersphere assumed by the BUT, the antipodes are now sets of world lines that are discrete and extremely disconnected. Sets are extremely disconnected, provided the closure of every set is an open set (Dochviri and Peters, 2016), is in the discrete space and the intersection of the closure of the intersection of every pair of antipodes is empty. The shapes of the antipodes are separated and belong to a computational geometry. That is, the shapes of the antipodal world lines approximate the shapes in conventional homotopy theory (Borsuk, 1969). The focus here is on the descriptions (sets of features) of world line shapes. Mappings onsets with matching description, or, in other words, mappings on descriptively strongly proximal sets, here means that such mappings preserve the nearness of pairs of sets. The assumption made here is that antipodal sets live in a descriptive Lodato proximity (DLP) space. Therefore, antipodal sets satisfy the requirements for a DLP (Peters, 2016). Let δ be a DLP and write $A \delta B$ to denote the descriptive nearness of antipodes A and B . And let f be a DLP continuous function. This means $A \delta B$ implies $f(A) \delta f(B) = f(A) \cap f(B) \neq \emptyset$.

Example: Assume that antipodes A and B have symmetries (shape, bipolar, colour, overlap, path-connectedness), and f is DLP strongly continuous function, then $A \delta B \Rightarrow f(A) \delta f(B)$

This means that, whenever A and B are descriptively close, then A is mapped to $f(A)$ and B is mapped to $f(B)$ and $f(A) \delta f(B)$. If we include in the description of A and B the location of the discrete points in A and B , then the DLP mapping is invertible. That is, $f(A)$ maps to A , $f(B)$ maps to B and $f(A) \delta f(B)$ implies $A \delta B$.

Figure 1 provides an example of antipodal sets in case of a pair of closed regions, e.g., strings.

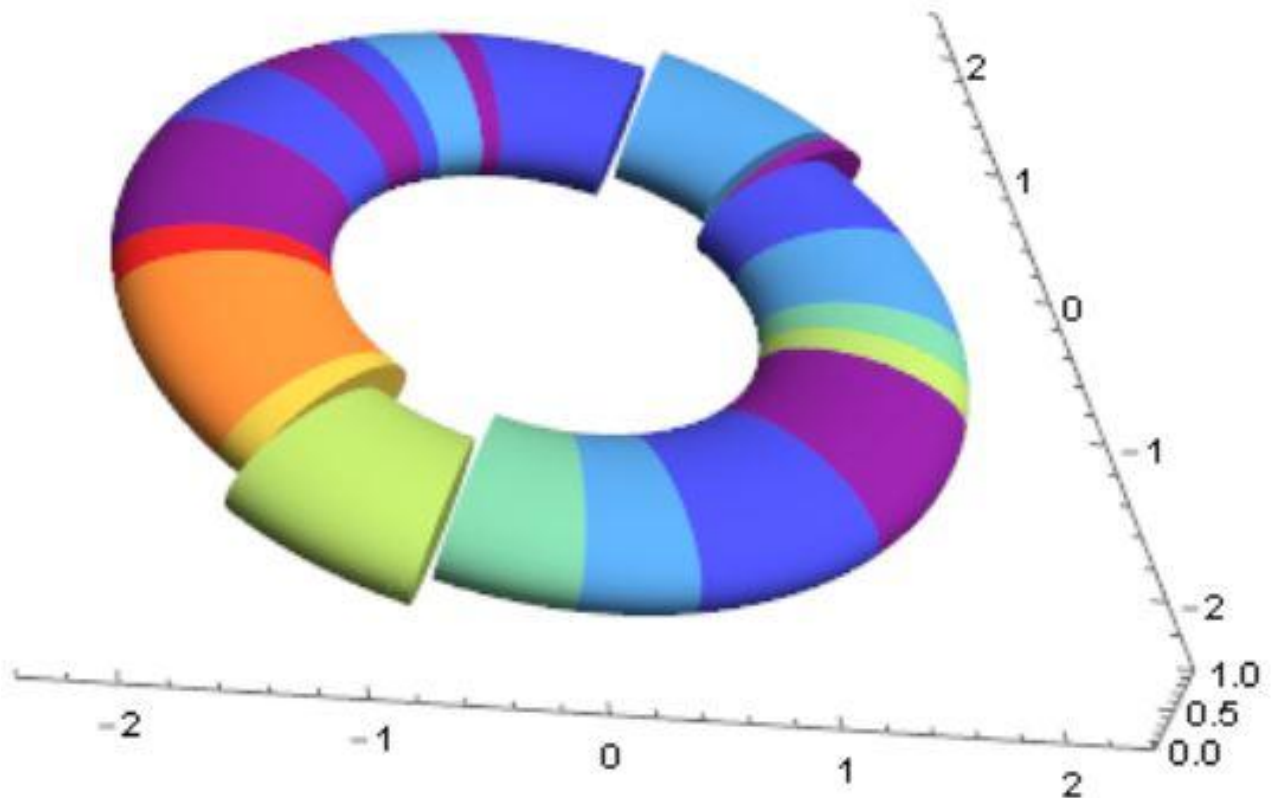


Figure 1. Torus Antipodal Strings. World lines with matching description preserve the nearness of pairs of sets. See text for further details.

Generalized BUT (genBUT). We conclude this section by introducing generalized version of BUT, which encompasses all the previously described variants. This version allows the study of the Monster in the context of theoretical physics. Gen-BUT states that:

Multiple sets of objects with matching descriptions in a d -dimensional manifold M^d are mapped to a single set of objects in M^{d-1} and vice versa. The sets of objects, which can be mathematical, physical or biological features, do not need to be antipodal and their mappings need not to be continuous. The term *matching description* means the sets of objects display common feature values or symmetries.

M stands for a manifold with any kind of curvature, either concave, convex or flat. M^{d-1} may also be a part of M^d . The projection from S to R is not anymore required, just M is required. The notation d stands for a natural, or rational, or irrational number. This means that the need for spatial dimensions of the classical BUT is no longer required. The process is reversible, depending on energetic constraints. Note that a force, or a group, an operator, an energetic source, is required, in order to project from one dimension to another.

2) EMBEDDING THE MONSTER GROUP IN M^{d-1}

The Monstrous Moonshine conjecture suggests a puzzling relationship between the Fourier coefficients of the normalized elliptic modular invariant, e.g., the hauptmodul J , which value is 19884, and the simple sums of dimensions of irreducible representation of the Monster group M , which is 196883 (Frenkel et al, 1984). It would seem that a relationship between the symmetries in the plot (range) of the j -function and symmetries in the Monster group products occurs. We might speculate that, in physical terms, the j -function could stand for an activity occurring into to the Monster Module during the movements of the Lie Monster Group. In an infinite-dimensional space, the action of the J function is correlated with the the Monster vertex operator Virasoro algebra, e.g., the Monster Module (Duncan et al., 2015).

A topological approach helps to elucidate such an unusual relationship. In the BUT framework, the J function and the Monster Module are sets of objects with matching description embedded in a M^d manifold, where d stands for their abstract dimension 196,884. Encompassing the two parameters in a M^d manifold allows us to provide a topological commensurability between the Monster Module and the J function. When we reduce the dimensions to $S^{196,883}$, we achieve a single function, e.g., the Monster Lie group. It easy to see that, if we map the two functions to a dimension lower, in this case $M^{196,883}$, we achieve a single function which retains the features of both. This single function stands for the Monster Group, which is the automorphic Lie group acting on the Monster Module (**Figure 2, upper part**). In topological terms, as always, two functions on a S^n sphere lead to a single function on a S^{n-1} sphere.

3) OF MONSTERS AND UNIVERSES

Dimensions reduction. Here we propose a BUT model of our Universe located inside the Monster Module. We argue, based on topological and energetic claims, that our Universe might arise from a spontaneous loss of dimensions, e.g., an automorphism, occurring into the very structure of the supersymmetric, multidimensional Monster Module. According to energy-BUT, the more the symmetries, the more the energy, so that every increase of symmetric level doubles the energy of the previous, less symmetric one. If the Monster stood before the Big-Bang, we are in front of a manifold with the highest possible energy, because it displays the highest number of symmetries.

The group Monster encompasses several subgroups, also classified into the sporadic groups (e.g., Mathieu groups, Leech lattice groups, and so on) (Gannon., 2006). It is worth of mention that the symmetries in a hypothetical M^d encompassing our Universe do not need to be necessarily of the huge order of 10^{54} . In such a vein, one might think two possible physical scenarios:

- a) The Monster group is progressively formed starting from its subgroups, with a gradual building from blocks.
- b) The Monster group is the initial structure. It then might split into its subgroups.

Because the entropy is increasing in the Universe, the second hypothesis is more reasonable. It would be better to take a starting point before the Big Bang with a higher energetic manifold, and not vice versa. Our Universe goes towards gradually lower energetic levels. At the Big- Bang, a loss of dimensions and thermodynamic free-energy occurred. There was, going from a dimension to a lower one, a sort of quantum jump towards lesser levels, of which one is the half of the other. It is a testable hypothesis. Like an electron orbit, a jump towards more internal levels occurred. This explains the arrow of entropy. A loss of dimensions came together with a loss of symmetries. Indeed, at the low-dimensional level of our Universe, just the symmetries embedded in the preserved dimensions are kept, while the other are apparently lost. The original lost symmetries could in theory be restored, inverting the process from lower dimensions to the higher

ones of the Monster Module, but it would require a source of energy able to perform the inverse projection, and this is not the case of our Universe.

Topological relationships between the Monster and string theories. Moonshine can be regarded as a collection of related examples where algebraic structures have been associated with automorphic functions or forms, because it is also displays relationships with the Lie group $E^8(C)$ and a lattice vertex operator algebra equipped with a rank 24 Leech lattice (Borcherds, 1992; Frenkel, 1988). Several features of the Monster, either the Module, or the group and the subgroups, have been associated with different physical scenarios. Some examples are depicted in **figure 2 (lower part)**. Links between Monstrous Moonshine and string theories have been described. The Monster might stand for the symmetry of a string theory for a Z^2 -orbifold of free bosons on a Leech lattice torus, in the context of a conformal field theory equipped with partition function j . Recent papers link other sporadic groups with modular forms, suggestive of a more central role for the Umbral Moonshine (Eguchi et al., 2011). Witten proposed that pure gravity in AdS_3 (anti deSitter) space with maximally negative cosmological constant is AdS/CFT dual to a holomorphic CFT (conformal field theory), with the numbers of the Moonshine coming into play (Witten, 2007). CFT/AdS is dual to string theories, and is involved in the many models: CFT, Chern-Simon-Matter, Super Jang-Mills, Superconformal algebras. The AdS/CFT correspondence means that conformal field theory is like a hologram, which captures information about the higher-dimensional quantum gravity theory. It is exactly a picture which could be described in the BUT framework. The Witten's conjecture of a duality between pure quantum gravity and external holomorphic CFT predicts the existence of a hyperbolic anti-DeSitter Universe equipped with a strongly negative cosmologic constant. The relationships between Universe's negative curvature and Monster Moonshine have been recently explored in the above mentioned, unpublished paper (*Tozzi and Peters, unpublished data; under review for Eur Phys J C*).

The problem of singularity. A problem which arises is how to explain the event, commonly called *singularity* (Chow, 2008), which caused an apparent loss of dimensions in parts of the Monster, giving rise to our Universe. It must be taken into account that the trajectory on a hypersphere, or in general on a manifold, does not need necessarily to be closed, because a particle could just travel along a shortest path, and not along the entire surface (Collins, 2004). We might think of world lines traced by a moving particle: this line evolves, whereas the line in the chart is static. A hypothetical particle embedded into the Monster Module follows the movements dictated by the Monster Lie group. However, the particle cannot travel everywhere, due to the huge amount of dimensions. The complete ergodicity of particle pathways on the Monster Module cannot be guaranteed, due to the countless possible trajectories. When a particle travels on the ergodic Monster manifold's huge phase space, it might simply take a random direction towards any dimensions and not others. In other words, the particle follows (probably random) paths equipped with dimension decrease. We provide an example which takes into account the well-studied model of a 26D bosonic string theory. Such a model, although partially dismissed, provides a good example of our model. Bosons' trajectories in a 24D Leech lattice may follow paths of 196,884 dimensions. Notice that the Leech lattice is almost ubiquitous in the description of sporadic groups, thus offers an interesting example. When particles go towards preferential trajectories, they follow paths involving just some of the total Monster's dimensions. They fall into trajectories lying into the lower dimensions of our Universe. When bosons' paths fall into some of the Monster's dimensions, they lose energy for energy-BUT. It might explain the Big Bang, equipped with high energetic levels that decrease with time passing. Therefore, the singularity might be explained simply by random particles' movements. Note that, because random paths might occur everywhere on the Monster Module, it means that countless Universe are allowed, every one equipped with just some of the primeval symmetries. Our (and others) Big Bang might just have been occurred naturally, when a particle fell into a dimension instead of another. It also means that the path chosen by a particle is equipped with just some of the Monster symmetries, while the others are lost (or, better, hidden, because they might reappear at the level higher than the ones where they are embedded). If a particle travels along a path embedded just in a few dimensions (our Universe), the loss of the other primeval dimensions gives rise in our Universe to symmetry breakings, including the thermodynamical arrow. In order to elucidate why a decrease in symmetries and dimensions leads to our Universe equipped with symmetry breakings, another important argument must be taken into account. Indeed, almost all the finite groups are *non-abelian*: it explains how the multisymmetric Monster loses dimensions and leads to our Universe, in which the rules are dictated by *asymmetric* laws. The intrinsic non-abelian structure of the Monster itself ensures that the patterns are not reversible. Once taken a path, for the non-abelian and energetic arguments, it is not possible to reverse the process in our Universe, unless other energy is supplied. The presence of an ergodic, homogeneous Monster Module before the big bang also solves the so called horizon problem. A few Planck times after the Big Bang, the Universe consisted of 10^{90} Planckian size, disconnected regions (Veneziano, 1998). Currently, those regions make up our observable Universe and resemble one another. The presence of the homogeneous Monster Module before the Big Bang explains why the initial disconnected regions had all the same conditions.

The Monster and the spacetime. The Monster is a manifold which, for the BUT variants, can be also described as a hypersphere, and thus equipped with closed trajectories. Therefore, our Universe is *internal* to the Monster. The loss of dimensions occurs *into* the Monster, giving rise to the Big Bang. That's why the fossil background cosmic radiation comes from everywhere, when we look at it (Fixsen, 2009). A problem arises: how can a string-like manifold give rise and contain the whole Universe? A possible solution is that the Monster is not in the space, and the space occurs together with the Universe. Concerning the time, the things are more complicated. Indeed, in touch with Veneziano's pre big bang scenarios (Veneziano, 1998), the time could exist before the Big Bang, and not arise together with the Universe. The Monster group needs to be embedded into the time, because it, acting as a Lie group, needs to perform symmetric movements which may just occur in a given time. It might however be speculated that the time is not required at the Monster Module level, and the Wheeler-DeWitt equation might be valid at such level. By a physical point of view, you start from two algebraic structures and reach a Lie group, which needs to perform an action. It means that the level S^{196883} requires that the introduction of the parameter time, while the Monster Module in S^{196884} lies in infinite dimensions, and is atemporal.

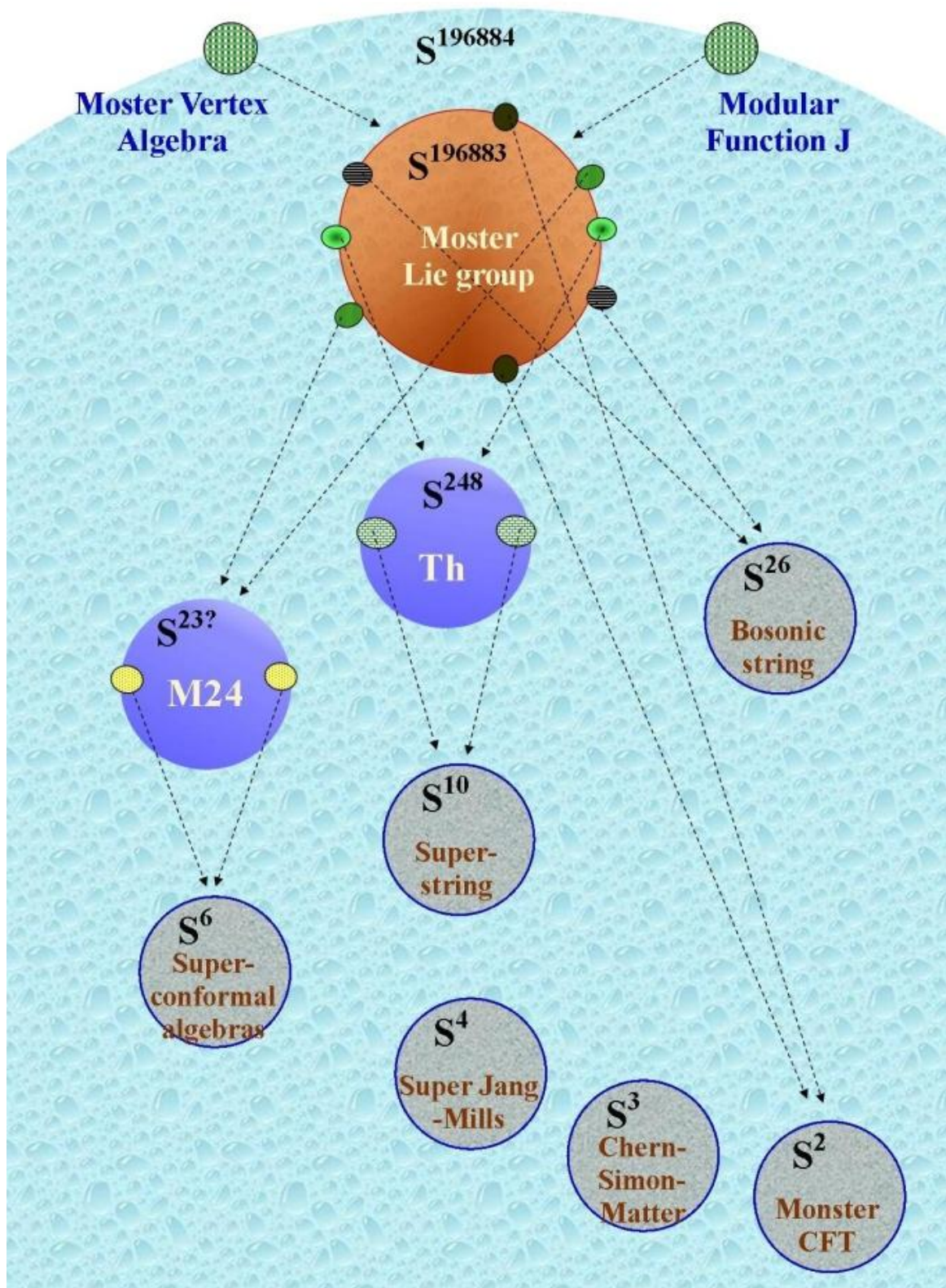


Figure 2. Progressive loss of dimensions in sporadic groups can be encompassed in a BUT framework. Note also the loss of symmetries from the highest dimension levels to the lowest ones. The Figure also illustrates how every sporadic group might display a theoretical physical counterpart.

3) QUANTIFYING PHYSICAL MONSTER'S PARAMETERS

Towards the Monster's enthalpy. We are allowed to use the energy BUT in order to calculate the energetic requirements of Monster Modules in a physical context. Thermodynamics says that:

$$H = F + T \times E$$

Where H is the Enthalpy, F the free-energy, T the temperature (trascurable) e E the entropy. We assume that our Universe is closed. We will evaluate the possible values at the Big Bang (H_0, F_0, T_0, E_0) and at the present time (H_1, F_1, T_1, E_1). The current level E_1 of entropy in the Universe is estimated in $2.6 \pm 0.3 \times 10^{122}$ k (Egan and Lineweaver, 2010; Frampton et al, 2008), while T_1 is neglectable. If the Universe displays four dimension as currently believed, every dimension contains approximately an average entropy of:

$$E_1/4.$$

As shown in Figure 10 of Egan and Lineweaver (2010), the current Universe displays almost the highest possible values of entropy. Also in the future, the entropy will be just slightly larger than the current value E_1 , because a monotonical increase already occurred. It means that E_1 is more or less the maximum value of entropy achievable in the whole life of the Universe, and also means that the free-energy F_1 is currently very low. It also means that:

$$E_1 = H_1.$$

At the Big Bang, on the contrary, E_0 was close to zero and F_0 very high.

Therefore the current E_1 almost equals the total enthalpy H_1 of the Universe. Vice versa, at the Big Bang, F_0 and T_0 were very high and E_0 the lowest possible. It means that, at the Big Bang:

$$F_0 = H_0 - T_0.$$

If the Monster occurred before the Big-Bang, we are in front of a manifold with the highest possible energy, because it displays the higher number of symmetries. If the Monster gave rise to our Universe, and the Monster displays 196,883 dimensions, the Entropy of the Monster E_M is:

$$E_M = E_1/4 \times 196,883.$$

Thus, the enthalpy of the Monster H_M stands roughly for the same value:

$$H_M = E_1/4 \times 196,883$$

The loss of dimensions into the Monster Module, due to the non-abelian movements of the Monster Lie group and the energy-BUT, give rise to different Universes with dimensions lower than the Monster, and equipped with less energy and information.

Through the Conway atlas of finite groups, we know the dimensions and the order of every group, including the sporadic ones. It is not difficult to calculate how many dimensions have been lost. We know this number, e.g., $196,883 - 4$, the dimensions of our Universe, we know how many symmetries are preserved, and we know, for energy-BUT, that every decrease of a single symmetric level denotes the loss of half of the energy. If the pre-Big Bang manifold, e.g., the Monster Module, is equipped with 196,884 dimensions and 10^{54} elements, and if our Universe has 4 dimensions (the spacetime), we have 10^{50} elements in our Universe.

Summarizing, once hypothesized a high-energy Monster Module before the rise of our Universe, the next step is to reduce the symmetries from the Monster vertex operator to the Monster group, which is the Lie group acting on it. A further step gives rise to a dimensions and symmetries reduction until our Universe, equipped with the Standard Model.

Information. The energy-BUT states that it is not possible to achieve higher information, starting from a lower dimensional level. It means that we need to start from the Monster Module, and not vice versa. The process must be top-down, e.g., from the Monster to the Universe, and not bottom-up. According to the energy-BUT, a loss of information occurs together with a decrease in dimensions. It means that, from the Monster to our Universe, it occurs a loss of information. You cannot move a particle in our Universe from lower to higher dimensions, unless you, for energy BUT, do not *inject* novel free-energy or enthalpy. You can do it just locally in the Universe, for example when biological entities are formed in limited niches, but not everywhere, because the total entropy increases together with a decrease in free-energy. It also means that from the highest to the lower levels there is a *reduction*, and not an *emergence* of information.

Watching the Monster: vertex algebra. In order to incorporate the j-function into a general context and to visualize the movements of the Monster Group on the Monster Module, we built a simplified 3D model equipped with a hypersphere and a vertex algebra operator. We achieved a low-dimensional model of j-function and its group, embedded into a vertex algebra's manifold. Briefly, a vertex algebra provides a mathematical formulation of the chiral part of 2-dimensional conformal field theory. The axioms of a vertex algebra are obtained from the properties of quantum field theories and operator product expansions (OPEs). The main tactic flowing from OPEs is that a product of local operators defined at nearby locations can be expanded in a series of local operations (Ekstrand, 2011). A graphical representation of an OPE

is represented in **Figure 3A**. Let ω_1, ω_2 be periods of a doubly periodic function with $\tau \equiv \frac{\omega_1}{\omega_2}$. Then Klein's absolute invariant is defined by

$$J(\omega_1, \omega_2) = \frac{g_2^3(\omega_1, \omega_2)}{\Delta(\omega_1, \omega_2)},$$

where g_2 is the invariant of the Weierstrass elliptic function. If H is the upper half plane and $\tau \in H$, then $J(\tau) \equiv J(1, \tau) = J(\omega_1, \omega_2)$.

The function $J(\tau)$ is the j-function modulo a constant multiplicative factor (Weisstein, 2016). A dynamical system with a strange attractor and invariant tori (Sprott, 2014) initialized with the j-function is illustrated in **Figure 3B**.

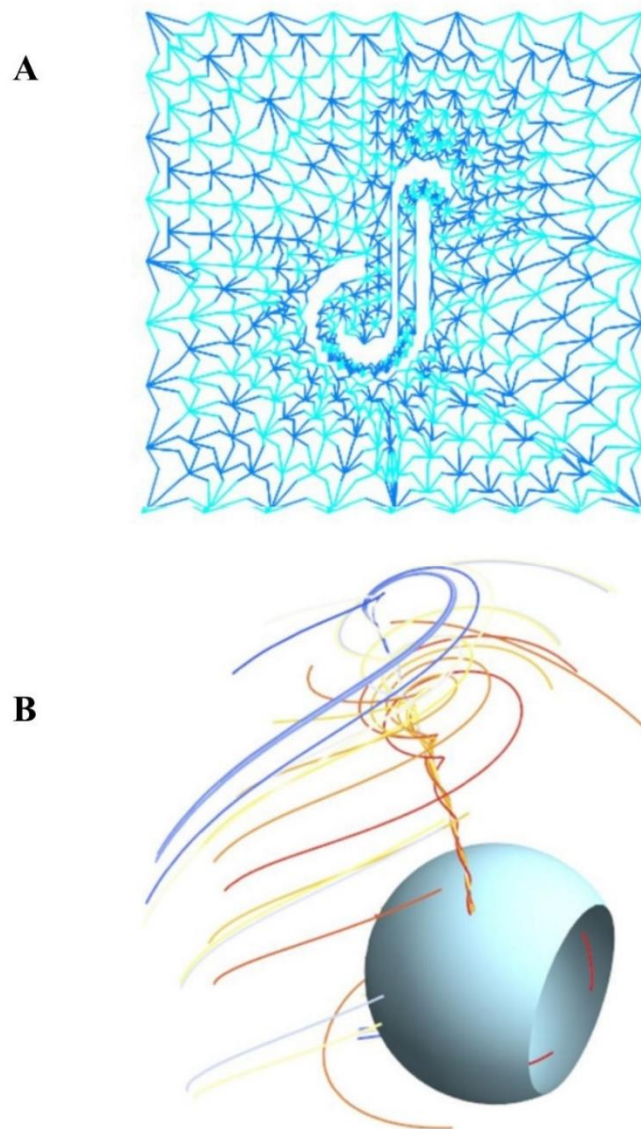


Figure 3. Defining a vertex algebra on a torus helps us to visualize otherwise abstract structures. Starting from a vertex operator algebra (a very small portion is described in **Figure 3A**) we made use of the attractors and the corresponding

ODEs described by Sprott (2014). In **Figure 3B**, the j -function on the attractor torus displays one coordinate initialized with a j -function value.

4) QUESTIONS AND CONCLUSIONS

Starting from a *Spinozian* global system, shaped in guise of a multidimensional and multisymmetric manifold equipped with a structural order of relationships, we were able to analyse, through a loss of dimensions dictated by the intrinsic features of the Monster Module and its Lie group, the individual history of the Universe. The Universe can be thus conceived as a manifold at lower dimensions encompassed in higher ones. The Monster Module is a manifold equipped with absolutely the highest dimensions - that is, a manifold consisting in the highest number of symmetries. The Monster Moonshine manifold is prior to its modifications. We may mean the nature and the flow of events in the Universe as a Monster's self-projection towards less dimensions. The Universe stands for a local symmetry, e.g., modifications of the Monster manifold. The Monster Module cannot exist in, and cannot be conceived through, an higher manifold other than itself. Every manifold in the Universe exists either in itself or in some higher manifold else, e.g., the Monster Module. The knowledge of a lower dimension manifold in the Universe depends on and involves the knowledge of higher dimensions mapping the lower manifold. In the meantime, the Monster Module, which n -dimensions are untouched, is still there. If different trajectories on the Monster Module give rise to different local losses of dimensions, it means that countless Universes are possible, each one equipped with different or overlapping symmetries.

We would like to bring to an end with a few unsolved problems.

- a) Where does the Monster take such a huge amount of enthalpy? It takes us in pre, pre- Big Bang scenarios. This is the same problem of inflaton models, that do not explain where does the energy of the required false vacuum come from. A link between the Monster group and the false vacuum might be speculated.
- b) Which is the role of the J function in the pre Big Bang period? Does it provide energy?
- c) How does the Monstruos Moonshine look like? We might either imagine a timeless, immutable manifold where just the Monster Group movements take place, or as we did, a dynamical, time-dependent structure.
- d) Does the curvature of the Monster Module change with time passing? It could be a very useful information, in order to elucidate the predicted passage from an ancient anti DeSitter hyperbolic Universe to the current, flat one.
- e) Our Universe might not arise directly from the Monster, but by one of its subgroups, e.g., Th , which is correlated with the successful superstring 10D theory. Is it possible to split the Leech lattice in which the Monster group is embedded, in order to achieve the lower dimensional E_8 lattice where the Th group's movements take place? Remind that the step from E_8 lattice to the Leech requires $\times 3$ multiplication and peculiar rotations.
- f) The topological step from the vertex operator algebra to the Lie Monster Group requires a continuous function. Are we in front of a *super* gauge field? In other words, is there a gauge field which causes the first projection depicted at the top of the **Figure 2**? In a topological framework, the feature which links the symmetries at a higher level with the single point at a lower level is the continuous function. If we assess two antipodal points as symmetries, and the single point as symmetry breaks and local transformations, a gauge field could be required, in order to *restore* the (apparently hidden) symmetry.

REFERENCES

- 1) Beyer WA, Zardecki A. The early history of the ham sandwich theorem. *American Mathematical Monthly*, 111, n. 1, 2004, 58-61
- 2) Borcherds R (1992), "Monstrous Moonshine and Monstrous Lie Superalgebras", *Invent. Math.* 109: 405-444, doi:10.1007/bf01232032
- 3) Borsuk, M. Drei s'atze "uber die n -dimensionale euklidische sph"are, *Fundamenta Mathematicae* XX (1933), 177-190.
- 4) Borsuk, M. Fundamental retracts and extensions of fundamental sequences, 64 (1969), no. 1, 55-85.
- 5) Bourbaki, N. (1966). *Elements of Mathematics. General Topology 1, Chapters 1-4*. Translated from the French. Reprint of the 1966 edition. *Springer-Verlag, Berlin*, 1989. viii+437 pp. ISBN: 3-540-19374-X, MR0979294.
- 6) Chow, T.L. (2008). *Gravity, Black Holes, and the Very Early Universe. An Introduction to General Relativity and Cosmology*. New York, Springer, x+280 pp.
- 7) Collins, G.P. The shapes of space, 291 (2004), 94-103.

- 8) Conway JH, Curtis RT, Norton SP, Parker RA, Wilson RA. 1985. Atlas of Finite Groups: Maximal Subgroups and Ordinary Characters for Simple Groups. Conway JH (Editor). Clarendon press, Oxford, USA
- 9) Dochviri, I. and Peters, J.F. (2016). Topological sorting of finitely near sets. *Math. in Comp. Sci.*, *in press*.
- 10) du Sautoy M. Finding Moonshine, A Mathematician's Journey Through Symmetry. Fourth Estate, 2008 ISBN 0-00-721461-8
- 11) Duncan JFR, Griffin MJ, Ono K. Moonshine. *Research in the Mathematical Sciences* (2015) 2:11. DOI 10.1186/s40687-015-0029-6
- 12) Egan CA, Lineweaver CH. 2010. A Larger Estimate of the Entropy of the Universe. arXiv:0909.3983v3
- 13) Eguchi, T, Ooguri, H, Tachikawa, Y: Notes on the K3 Surface and the Mathieu group M₂₄. *Exper. Math.* 20, 91–96 (2011)
- 14) Ekstrand, J. Lambda: A Mathematica package for operator product expansions in vertex algebras. *Computer Physics Communications* 182 (2011), 409-418, doi:10.1016/j.cpc.2010.09.018
- 15) Fixsen, D. J. (2009). "The Temperature of the Cosmic Microwave Background". *The Astrophysical Journal* 707 (2): 916–920. doi:10.1088/0004-637X/707/2/916.
- 16) Frampton P, Hsu SDH, Kephart TW, Reeb D. What is the entropy of the universe? 2008 arXiv:0801.1847
- 17) Frenkel, I, Lepowsky, J, Meurman, A: A natural representation of the Fischer-Griess Monster with the modular function J as character. *Proc. Nat. Acad. Sci. U.S.A.* 81(10), 3256–3260 (1984). MR 747596 (85e:20018)
- 18) Frenkel IB.; Lepowsky j, Meurman A (1988). *Vertex Operator Algebras and the Monster*. Pure and Applied Math. 134. Academic Press.
- 19) Gannon, T (2006), *Moonshine beyond the Monster: The Bridge Connecting Algebra, Modular Forms and Physics*, ISBN 0-521-83531-3
- 20) Matoušek, J. Using the Borsuk–Ulam Theorem. *Lectures on Topological Methods in Combinatorics and Geometry*. Springer-Verlag Berlin Heidelberg, 2003
- 21) Olive DI, Landsberg PT. Introduction to string theory: Its structure and its uses. *Philos. Trans. of the Royal Soc. of London, Series A, Mathematical and Physical Sciences* 329 (1989), 319-328.
- 22) Peters JF. 2016. *Computational Proximity. Excursions in the Topology of Digital Images*. Edited by Intelligent Systems Reference Library. Berlin: Springer-Verlag. doi:10.1007/978-3-319-30262-1.
- 23) Peters JF, Tozzi A. 2016a. "Region-Based Borsuk-Ulam Theorem." arXiv, 1605.02987.
- 24) Peters JF, Tozzi A. 2016b. "Quantum Entanglement on a Hypersphere." *Int J Theoret Phys*, 1–8. doi:10.1007/s10773-016-2998-7.
- 25) Petty, CM. Equivalent sets in Minkowsky spaces. *Proc. Amer. Math. Soc.* 29(2), 1971, 369-374.
- 26) Roldán E, Martínez IA, Parrondo JMR, Petrov D. Universal features in the energetics of symmetry breaking. *Nature Physics* 10, 457–461 (2014) doi:10.1038/nphys2940
- 27) Sengupta, Biswa, Arturo Tozzi, Gerald K. Cooray, Pamela K. Douglas, and Karl J. Friston. 2016. "Towards a Neuronal Gauge Theory." *PLOS Biology* 14 (3): e1002400. doi:10.1371/journal.pbio.1002400.
- 28) Sprott, JC. A dynamical system with a strange attractor and invariant tori. *Physics Letters A* 378 (2014), 1361-1363.
- 29) Tozzi A, Peters JF. 2016a. "A Topological Approach Unveils System Invariances and Broken Symmetries in the Brain." *Journal of Neuroscience Research* 94 (5): 351–65. doi:10.1002/jnr.23720.
- 30) Tozzi A, Peters JF. 2016b. "Towards a Fourth Spatial Dimension of Brain Activity." *Cognitive Neurodynamics* 10 (3): 189–99. doi:10.1007/s11571-016-9379-z.
- 31) Veneziano G. (1998) A Simple/Short Introduction to Pre-Big-Bang Physics/Cosmology. arXiv:hep-th/9802057v2
- 32) Watanabe T, Masuda N, Megumi F, Kanai R, Rees G. 2014 Energy landscape and dynamics of brain activity during human bistable perception. *Nat. Commun.* 28, 5:4765. (doi: 10.1038/ncomms5765)
- 33) Weeks, J.R. The shape of space. Second edition. Marcel Dekker, inc. New York-Basel (2002).
- 34) Weisstein E.W. 2016. Klein's absolute invariant, <http://mathworld.wolfram.com/KleinsAbsoluteInvariant.html>
- 35) Witten E (2007). "Three-dimensional gravity revisited". arXiv:0706.3359

TIME SYMMETRY BREAKING IN PRE-BIG BANG VACUUM STATE

The vacuum catastrophe refers to the discrepancy between the predicted and detected values of repulsive vacuum energy. To tackle the issue, we start from a model of inflation in a time-symmetric quantistic vacuum, which, due to the Mandelstamm-Tamm inequality, leads to a trapping of a part of the original vacuum during the formation of our closed Universe. We show how the energy of our cosmos is stored in two different compartments, the microscopic quantistic vacuum and the macroscopic detectable cosmos. If we take into account, at the time of the Big Bang, the occurrence of time symmetry breaking into our Universe, we achieve a macroscopic energetic system governed by the second law of thermodynamics, where time acts like a continuous gauge field able to progressively increase the entropy. Our framework makes it possible to assess, among other issues, the vacuum catastrophe, to calculate the minimum three-dimensional volume of the pre-Big Bang vacuum and to make previsions for the future evolution of the two energetic compartments.

Our Universe started with the Big Bang, expanding from a very high density and high temperature state (Penrose, 2011). At the age of 10^{-43} seconds, the Universe was very hot (10^{34} K). By then, the temperature halved every double expansion. The Universe underwent an inflationary expansion at 10^{-35} sec, which is the current explanation for cosmic features such as isotropicity, homogeneity, symmetry and zero curvature. Another gentler inflationary period started approximately 4.5 billion years ago, due to the prevalence of the anti-gravitational vacuum energy (e.g., the repulsive dark energy corresponding to the cosmological constant), that overtook the decrease of matter and radiation due to cosmic dilation (Ellwanger, 2012). The *vacuum catastrophe* refers to the discrepancy between the predicted and real values of the repulsive vacuum energy. Currently, 13.79 billions years after its birth, our Universe is still accelerating, slowly proceeding towards thermal death (Bars and Terning, 2009).

Our Universe displays four known dimensions, three temporal and one spatial. Here we focus on the time. It has been recently suggested that time exists just for observers inside the universe, because it is an emergent phenomenon arising from quantum entanglement (Moreva et al., 2013). Any god-like observer outside the cosmos sees a static, unchanging Universe, just as the Wheeler-DeWitt equations predict. In such a vein, it is noteworthy that time plays a role neither in such equations, nor in the formulation of the entangled states (Peters and Tozzi, 2016). Here we propose a time symmetry-based mechanism, which elucidates how and why, during the Big Bang, part of the original pre-Big Bang vacuum was sequestered into our time-asymmetrical Universe. The mechanism gave rise to two different types of energy in our cosmos: a microscopic one acting at quantum levels, and a macroscopic one acting at relativistic and non-relativistic scales. Our framework, which focuses on time symmetry breaking, suggests that the arrow of time works like a gauge field, leading to progressive increase of entropy. Furthermore, our approach makes it possible for us to assess different features of our Universe, from the very first phases of the Big Bang to the final doom, from the required cosmic energetic requirements to the vacuum catastrophe. Also, our model makes predictions about the size of the original vacuum that gave rise to our Universe.

Pre-Big Bang vacuum with T-invariance. An overall description of vacuum energy is given as an energy tensor of the form

$$T_v = \lambda g \text{ for } \lambda = \infty, \text{ or } \lambda = 0, \text{ or } \lambda \approx t_v^{-2},$$

where t_v is Planck time and g is a mathematical tensor quantity (Penrose, 2011). The vacuum catastrophe refers to the huge discrepancy in our Universe between the detected values of vacuum energy, and the theoretical previsions, that suggest a huge value. Indeed, the vacuum energy of free space has been estimated to be 10–9 joules (10–2 ergs), per cubic meter, e.g., $0.683\rho_{\text{crit}}$, while theoretical arguments require it to have a much larger value of 10^{113} joules per cubic meter (Hobson et al., 2006). Some Authors believe that our Universe arose from an inflationary event taking place in the quantistic vacuum (Veneziano, 1998). If we assume that an inflative event in the quantistic vacuum gave rise to the Big Bang and our Universe, we are allowed to hypothesize a pre-Big Bang quantistic “original vacuum”, e.g., a vacuum state equipped with the massive levels of dark energy predicted by theoreticians. This original vacuum is equipped both with false vacuum, e.g., high-energy fields with vacuum expectation value different from zero, and real vacuum, e.g., low-energy fields that do not allow the production of real particles. The original vacuum is a n -manifold, bounded or unbounded. The term manifold is commonly used in this context, referring to a spatial structure with a smooth, rubber sheet geometry. A CPT symmetry occurs in the original vacuum. While real charged particles cannot exist in such an empty vacuum, however charged virtual particles are produced. Every one blinks into existence with its antimatter counterpart, then both quickly annihilate and fall back into the original vacuum. Therefore, the energetic balance in the

original vacuum is always zero. In the original quantistic vacuum, a time reversal symmetry (also called time-reversal invariance or T -symmetry) occurs, *e.g.*, many variables do not change under a time reversal transformation (right part of **Figure 1**). To make some examples in our observable Universe, time-reversal invariant parameters include: coupling constants except those associated with the weak force, electric potential and field, density of electric charge, electric polarization, some particle features (position in three-space, acceleration, force, energy), microscopic level of physical systems, including microscopic reversibility in physical and chemical kinetics, laws of mechanics and, last but not the least, the same observable Universe in equilibrium states. On the other hand, some variables in our observable Universe change under a time reversal transformation (a feature also called time reversal symmetry violation, T -asymmetry): violations of either C , or, P or T , the time when an event occurs, power, electromagnetic vector potential, magnetic field, density of electric current, magnetization, weak force, some particle features (velocity, linear momentum, angular momentum), macroscopic levels of physical systems and the observable Universe in non-equilibrium states.

In the original vacuum, the Mandelstamm-Tamm inequality for quantistic systems holds (Mandelstam and Tamm, 1945). The inequality assesses the rate evolution of an isolated quantum state, allowing us to calculate how long does it take for a quantum system like the original vacuum to evolve to an orthogonal state (Vaidman 1992). There is a general lower bound for the lifetime of all quantum states in terms of reasonable measures of uncertainty in energy, even if the standard deviation is infinite. Indeed, according to a formulation of the Heisenberg principle, energy and time in the original vacuum can be related by the formula:

$$\Delta E \Delta T \geq \frac{\hbar}{4\pi}$$

where ΔE is a non-infinite uncertainty in energy that is independent of time (Uffink, 1993). This means that a significant change in energetic conformation may occur in a very short time interval. The original vacuum is time-invariant, and therefore time can be both positive or negative, or even “frozen” and close to T_0 . These short time intervals lead to huge fluctuations in energy. One of such common, almost instantaneous, fluctuations could have produced the inflation that gave rise to our Universe.

Vacuum trapped in an inflationary T -asymmetric Universe. We stated that, in very short times, huge energetic differences may occur in the original vacuum. One (or more) large fluctuations are able to put in motion the well-described process of inflation. In the original vacuum, a high energetic state of false vacuum abruptly falls towards the low energetic basins of real vacuum (left part of **Figure 1**). This process leads to an inflationary mechanism, *e.g.*, the production of a huge amount of anti-gravitational energy that leads to cosmic dilation and the generation of real particles and fields in our Universe. Such inflationary event that occurred in the original vacuum is different from the one that occurred 10^{-35} sec after the birth of Universe. Both might be explained by huge energetic oscillations occurring in almost frozen times. Therefore, our Universe (and probably countless others, equipped with cosmological constants and physical laws different from ours) is born, like a closed bubble arising from the original vacuum. It is noteworthy that, in our framework, the closed inflationary Universe encompasses parts of the original vacuum that was trapped into the bubble during its formation. Indeed, our bubble includes, apart from particles and energy, also a certain amount of vacuum, “stolen” from the original one (right part of **Figure 1**). Such vacuum, that we will term “trapped vacuum”, is equipped with a much lower energetic level than the original one. Such a level matches the experimentally detected value of $0.683\rho_{\text{crit}}$. Therefore, our closed Universe is equipped with a certain amount of energy, provided by two sources: a) the observable particles, fields and energy produced by the inflationary events occurred in the original vacuum during the Big Bang; and b) the dark energy enclosed in the trapped vacuum. The energetic behaviors of the open original vacuum and the trapped one are different. They display a completely different evolution (**Figure 1**). The cause of this discrepancy lies in the very structure of the closed bubble and its subtle differences from the original vacuum. While the original vacuum displays T -symmetry, in our Universe the time invariance is lost. Indeed, our time, is not anymore symmetric. The arrow of time becomes positive and cannot be reverted, splitting the past from the future. In such a way, the sudden appearance of a novel single parameter, *e.g.*, a T -symmetry violation in the trapped vacuum, is able to explain why high energy particles, once produced in the T -symmetric original vacuum during the Big Bang, give rise to our Universe, instead of promptly disappear. Time, together with other factors, makes it possible for the bubble to not implode, rather progressively to dilate (stretch) indefinitely.

In our Universe, due to time asymmetry, the two energies of the trapped vacuum and the observable Universe have different developments (**Figure 1**). In the macroscopic Universe, the energy becomes enthalpy and drives the cosmos towards progressively higher levels of entropy. Indeed, our observable Universe is subjected to the second law of thermodynamics. It means that our cosmos’ asymmetric time dimension acts like a constraint, allowing just the trajectories that lead towards an increase of entropy in the macroscopic Universe. We will describe this macroscopic process in the following paragraphs. On the other side, in the microscopic compartment of the trapped vacuum, energy oscillations progressively decrease with time passing, due to the quantistic Mandelstamm-Tamm inequality. For the first law of thermodynamics, this vacuum energy is conserved. However, the large energetic oscillations that could lead to false vacuums and subsequent inflationary processes disappear, because the energetic variations are progressively

flattened. It is noteworthy that, in very long timescales, the Universe reaches a final state of equilibrium, where time symmetry is restored. Indeed, a system at equilibrium displays time reversal invariance.

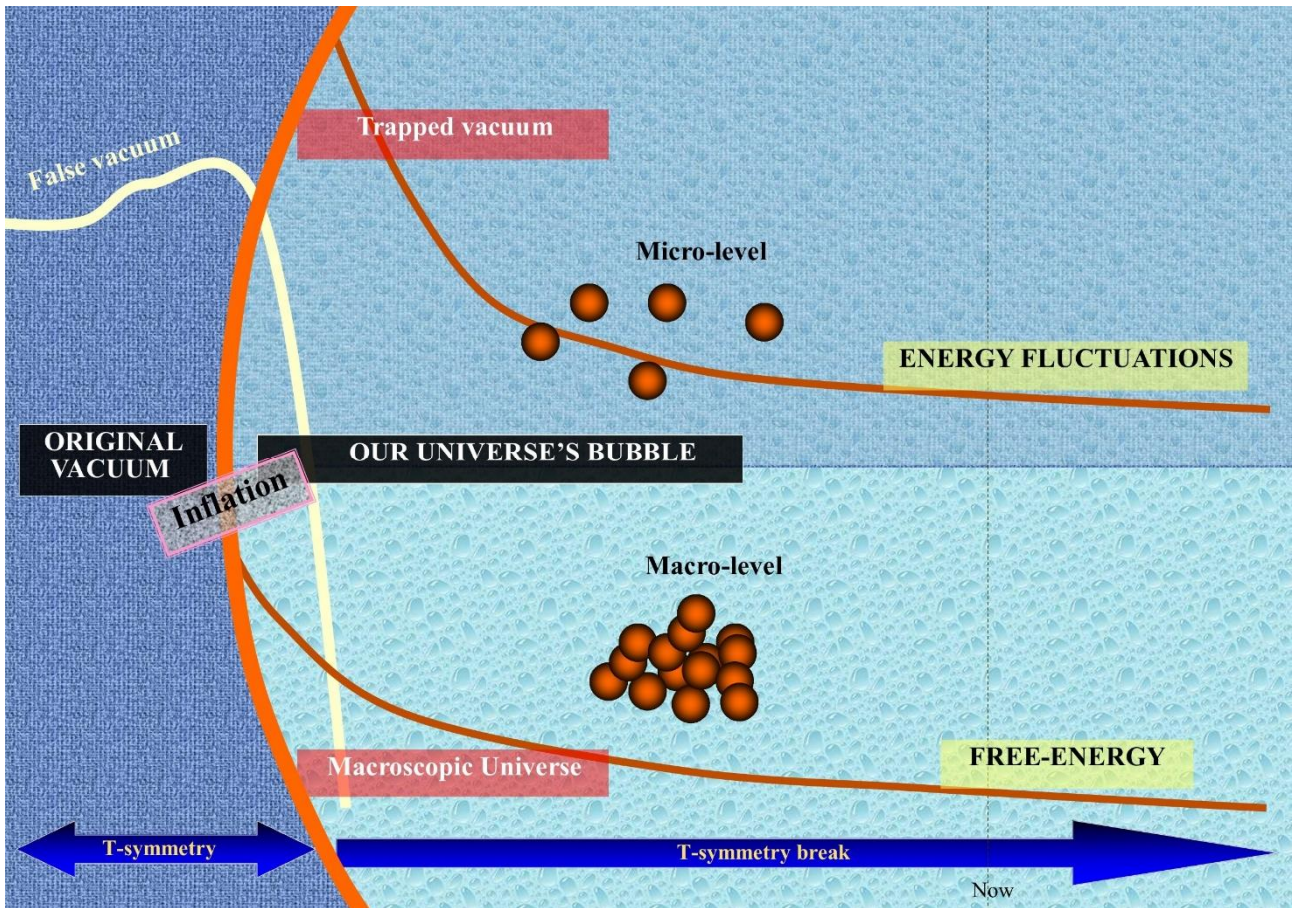


Figure 1. Evolution from the original time symmetric vacuum to our time asymmetric Universe. Our Universe is splitted into two compartments with different energetic features: the trapped vacuum and the macroscopic Universe. See the text for further details.

Energetic evolution of the macroscopic Universe. Macroscopic physical systems like the observable Universe are not just regulated by stochastic variables and random fluctuations⁴, but also by constraints given by the arrow of time. The same stands for biological system: to make an example, protein-folding final conformation is dictated by the minimum frustration principle on long evolutionary timescales, which states that proteins' energy decreases more than expected, as they assume conformations progressively more like the native state (Bryngelson and Wolynes, 1987; Ferreiro et al., 2011; Tozzi et al., 2016). Despite the large number of different scenarios, the processes governing time constraints of physical and biological systems may be generalized, taking into account a universal principle: the second law of thermodynamics, which states that “*every process occurring in nature proceeds in the sense in which the sum of the entropies of all bodies taking part in the process is increased*” (Planck’s formulation). Therefore, the positive arrow of time observed in the macroscopic Universe (due to the time-reversal symmetry violation) is strictly correlated with the second law of thermodynamics. In other words, the arrow of time acts, in long timescales, like a constraint dictating the evolution of the Universe towards an increase of entropy.

In this framework, it is interesting to see what happens to physical paths when time is kept fixed (**Figure 2A**). In a graph plotting time t on the X-axis and the space x on the Y-axis, take two trajectories which both display a starting position at x_0 and an ending position at x_2 . In **Figure 2A**, the black solid curve $x(t)$ stands for the trajectory describing the real path followed by a particle in the macroscopic Universe. This path is dictated by the second law of thermodynamics and the arrow of time. Note that such a real trajectory is constrained along the line of the time: it cannot go back from t_1 to t_0 ,

e.g., time cannot be reversed (Goldstein, 1980; Torby, 1984). On the contrary, the dotted black curve x^1 displays one of the possible virtual trajectories, e.g., a trajectory different from the real one, that might take place when the time is kept fixed and $\delta t = 0$ (Sommerfeld, 1952; Landau and Lifshitz, 1976). Starting from the position x_1 and time t_1 , the virtual displacement δx , e.g., from x_1 to the point c , is shown in **Figure 2A** (green arrow). Therefore, in very short timescales, virtual changes in physical/biological trajectories might occur far from the real path. It might be also hypothesized that virtual trajectories stand for singularities and timeless perturbations in our Universe: they could be regarded, for example, as places in which life occurs. Virtual constraints are central, because they allow us to understand the current state of our Universe. Indeed, an observer cannot understand whether a trajectory she is observing lies on a virtual or a real path, therefore she cannot predict the real, final trajectory that will necessarily take place according to the second law of thermodynamics. In very short timescales, the macroscopic paths bear a resemblance to Feynman's diagrams describing subatomic particles' behaviour: the possible trajectories are countless, although just a very few are the most probable in the real life. The next paragraph, just for technical readers, provides a mathematical explanation of virtual constraints.

Technical interlude: virtual constraints. In analytical mechanics, a virtual displacement is an assumed change of system coordinates occurring while time is held constant. It is called "virtual" rather than "real", since no actual displacement takes place without the passage of time. The key concept of virtual constraints is a dynamically imposed outer feedback control, so that the trajectory of a particle or an agent in the system's phase space can be "forced" towards the desired orbits and outputs (Canudas-de-Wit, 2004). Virtual constraints reduce the degrees of freedom, coordinating the evolution of the various links throughout a single variable. A closed-loop mechanism is achieved, wherein dynamic behaviour is fully determined by the evolution of simplest lower-dimension system (Stepp et al., 2010). The resulting system is called a "virtual limit system".

In mathematical terms, we define a set of $n - 1$ outputs (or constraints):

$$y = \varphi(p, q) = \bar{q} - h(\theta, p) = \bar{q} - h(\theta, p(t)),$$

where y and $\varphi(p, q)$ are the outputs or constraints, $\bar{q} \in R^{n-1}$ is a vector describing the actuated coordinates and velocities, p is the set of the design parameters, $\theta \in R$ is the unactuated variable, $h(q)$ is a function of the generalized coordinates of q . The latter equation describes the most general condition.

An inner-feedback loop is used to perform output feedback linearization in a local domain, where the matrix is invertible:

$$\psi(q)u = k(q; \dot{q}) + v,$$

where v is the outer feedback loop. Note that the equation includes a term \dot{q} which depends on time, where the upper

dot stands for the partial time derivative, i.e., $\dot{q} = \frac{\partial q}{\partial t}$ (Canudas-de-Wit et al., 2003).

If an outer feedback loop v is designed to zeroing the output y , we get a partially linearized system in the form:

$$\ddot{y} = v.$$

Then the full system dynamic is captured by the solutions of:

$$\alpha(\theta)\ddot{\theta} + \beta(\theta)\dot{\theta}^2 + \gamma(\theta) = 0,$$

together with the imposed constraint for mean q -value:

$$\bar{q} = h(\theta, p),$$

where $h(q)$, $\alpha(\theta)$, $\beta(\theta)$ and $\gamma(\theta)$ are scalar functions depending on the inner feedback loop.

In conclusion, the virtual constraints are forces external to the system's phase space, able to modify an internal trajectory towards the required one. This process allows one to deal with high-dimensional systems with underactuated degree one, by only analyzing this second-order nonlinear equation.

In analytical mechanics the researchers cope with under-actuated Lagrangian systems of the form:

$$\frac{d}{dt} \left(\frac{\partial L}{\partial \dot{q}} \right) - \frac{\partial L}{\partial q} = B(q)u,$$

where q and \dot{q} are vectors of generalized coordinates and velocities, $L(q; \dot{q})$ is a Lagrangian of the system, $B(q)$ is a matrix function of an appropriate dimension, with rank equal to the number of inputs and u is a vector of independent control inputs. The under-actuation means that $\dim u < \dim q$, i.e., the number of actuators is less than the number of its degrees of freedom.

Prediction of macroscopic trajectories in long cosmic timescales. Here we, elucidating the close relationships among virtual displacements, probabilities and time, show how we can assess whether observed trajectories are real or virtual and, in case they are virtual, how long does it take to become real. Real displacements are governed by the second law of thermodynamics because in every closed system, either physical or biological, the thermodynamical entropy

relentlessly increases from time T_0 to $T_2 = \infty$, until its maximum value. It is however preferable to use the informational entropy, instead of the thermodynamical one. Indeed, the two entropies are linked through the formula:

$$S = k H$$

in which S is the thermodynamical entropy, k is the Boltzmann constant and H is the Shannon informational entropy. The informational entropy, apart from the invaluable advantage of quantifying the macroscopic states without a perfect knowledge of the microscopic ones, is not linked with time. Therefore, Shannon entropy allows us to neglect the parameter time from our system, in order to assess its behavior not taking into account its evolution. However, to evaluate whether the trajectory we observe in different time frames is real or virtual, we need to superimpose the arrow of time on the “classic” two-dimensional plane containing the Shannon curve. Indeed, we are allowed to add a third dimension to the 2-D plot of Shannon entropy (**Figure 2B**). The vector of time ζ lies in a plane forming an angle A with the 2-D plane of Shannon entropy. This procedure allows the observer to evaluate how much time is needed, for the particle she is observing, to reach the real final state. To make an example, in the system Universe, T_0 on the vector of time ζ stands for the state of minimum entropy, e.g., the initial Big Bang, while $T_2 = \infty$ stands for the state of maximum entropy, e.g., the hypothetical final macroscopic state of the Universe. The real trajectory follows the Shannon curve: the highest probabilities can be found at $p=0$ and 1, while the maximum entropy at $p=0.5$. Starting from the probability of a virtual constraint observed in a point c , the corresponding point T_1 on the arrow of time can be detected. Therefore, we can calculate how much time is required to the vector of time ζ to reach $T_2 = \infty$, which stands for the Universes’s “real” final state at the energetic equilibrium. In order to proceed, there is a still unknown parameter left: the value of the angle A . The latter can be calculated by sketching a differential geometry-based theory (Tozzi and Peters, 2016). We need to ponder the Universe as a system where real displacements, e.g., the real trajectory of particles or events, stand for the continuous, global symmetry. This symmetry stands for the energetic constraints dictated by the second law of thermodynamics, e.g., an energetic gradient flow occurring just in long timescales. In turn, in the very instant in which T is “frozen”, fixed and equals to zero, virtual displacements occur. The latter stand for continuous groups of local transformations, able to “break” the above mentioned symmetry. The local loss of symmetry, e.g., a disturbance of the gradient flow, can be restored by introducing a continuous field, the time, able to re-establish the gradient flow. The time, in such a framework, stands for a field which is continuous, by the point of view of an inertial observer. There are many possible ways to deal with real and virtual displacements in a differential geometric sense, for example by analysing them in terms of sections of fibre bundles, jet manifolds and Ehresmann connections (Ehresmann, 1950; Abraham and Marsden, 1978; Lang, 1995; Kolar and Michor, 1993). One of the procedures is described in Sengupta et al. (2016). In sum, we can make accurate predictions about the time required for a trajectory in order to converge towards the most probable pattern, e.g., to increase its thermodynamical entropy. Our scheme resembles a physical gauge theory, retaining its tenets (Higgs, 1964; DeWitt, 1967; ’t Hooft, 1971; Zeidler, 2011):

- d) The system is equipped with a continuous, preserved “global” symmetry (and a corresponding Lagrangian).
- e) The system displays a continuous group of “local” transformations, equipped with a Lie group.
- f) The Lagrangian is kept invariant under such local transformations by a “gauge field”, i.e. a continuous force acting on the system.

However, our framework draws an important distinction from a classical gauge theory. Our concept of Lagrangian is slightly different: instead of referring to the principle of least action and the “preservation” of a physical quantity as usual in gauge theories and in Noether theorem, our Lagrangian refers to the “dissipation” of a physical quantity through a gradient flow. In other words, we provide a framework in which a Universe trajectory can be predicted in long timescales, by introducing the arrow of time in guise of a gauge field that keeps invariant the second law of thermodynamics. Such gauge field counterbalances the effects of local energetic peaks caused by the virtual transformations that might occur in very short timescales.

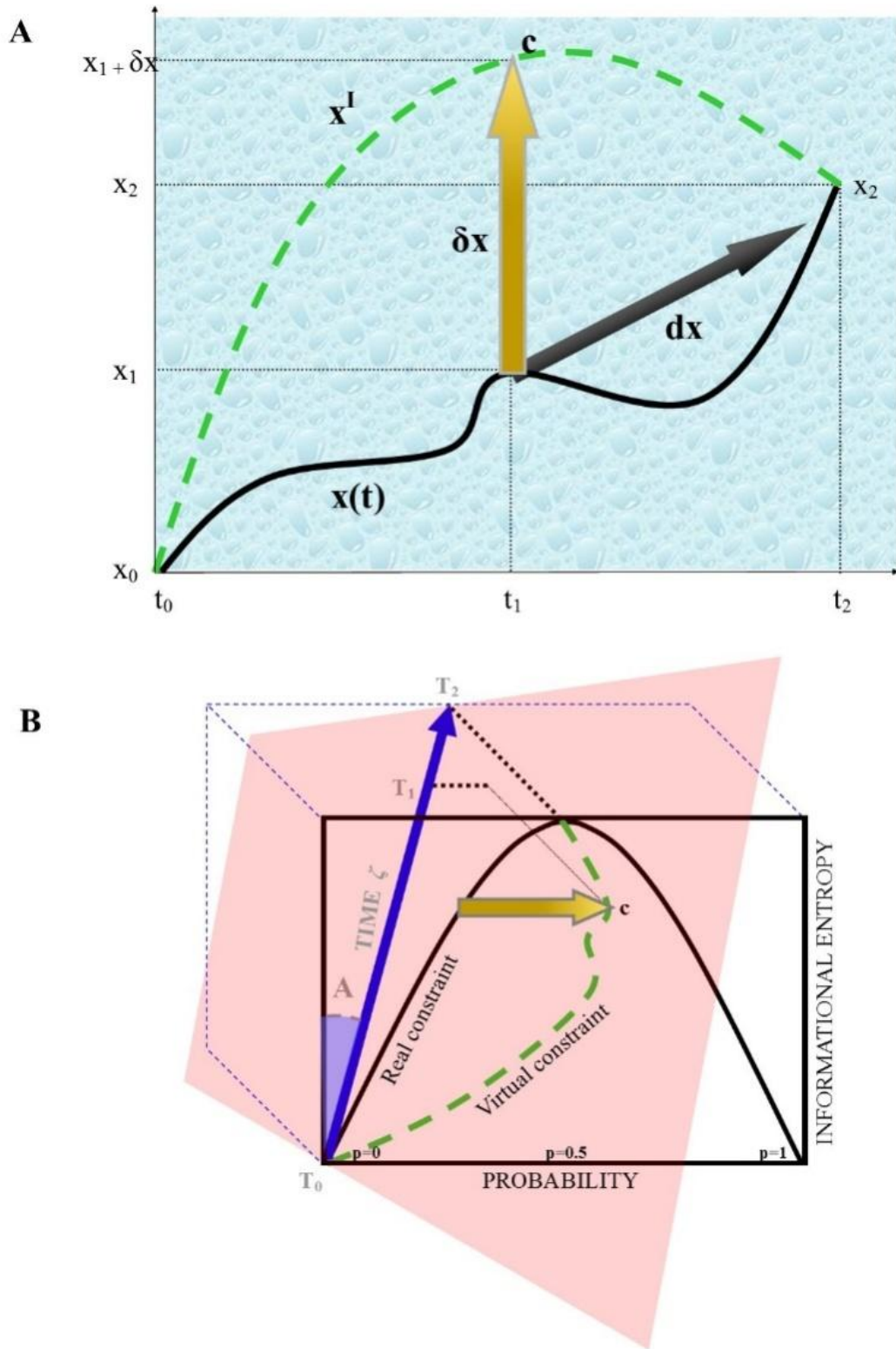


Figure 2A. Graph of the macroscopic observable Universe plotting time t on the X-axis and the space x on the Y-axis. The regular displacement dx is a vector pointing in the direction of the motion (black arrow), which arises from differentiating with respect to time parameter along the path of the motion. In contrast, the virtual displacement δx is a tangent vector to the constraining manifold at a fixed time, because it arises from the differentiation with respect to the enumerating paths of the motion, varied in a manner consistent with the constraints. See text for further details.

Figure 2B. Informational entropy is plotted as a function of the random variable p , in the case of two possibilities with probabilities p and $(1-p)$. The solid line black stands for the Shannon entropy (under ergodic conditions). The values $p=0$ and $p=1$ stand for the minimum entropy, $p=0.5$ for the maximum entropy. The arrow of time ζ (blue solid line) lies on a third coordinate of the phase space and forms the angle A . Due to the energetic gradient flows dictated by the second law of thermodynamics, time, in its real route from T_0 to $T_2 = \infty$, must be correlated with an increase in informational entropy. Given a virtual displacement c on the virtual trajectory (dotted black line), the corresponding value of T_1 on the arrow of time can be calculated, provided the value of the angle A is known.

CONCLUSIONS

We described the peculiar features of energy and time in the original vacuum and in our Universe. The latter encompasses trapped vacuum and is equipped with T-symmetry break. Further, we showed that the vector of time may stand for the macroscopic Universe's energetic gradient, locally "broken" by virtual timeless perturbations. Our framework allows us to elucidate controversial issues in cosmology and to make a few empirically testable previsions.

The problem of the vacuum catastrophe is solved straightforwardly: just a small amount of the original vacuum is embedded in our Universe. It means that the trapped vacuum displays the low experimentally detected values of dark energy, while the original vacuum the very high predicted ones. Therefore, we are allowed to calculate the size of the original vacuum that gave rise to our Universe: if 10^{-9} joules (10^{-2} ergs) per cubic meter are trapped in the size of our Universe before inflation, e.g., 3×10^{25} cm, it means that the total dark energy of 10^{113} joules per cubic meter is trapped in an original vacuum with spatial dimensions (in cubic meters) of more than 100 orders of magnitude. Such calculation does not take in to account the possible decrease of dark energy occurred in the Universe lifetime until the current age. However, this loss of energy is not likely to happen in the trapped vacuum, because of the first law of thermodynamics. The concepts of "constraints" and "virtual displacement" from analytical mechanics shed new light on the role of time and timescales in physical systems such as the Universe. Here we proposed a covariant version of a gauge theory, in which the required global symmetry stands for the real constrained trajectories, i.e., the energetic gradient flows dictated by the second law of thermodynamics. The virtual displacements, occurring while time is held constant, stand for the local transformations acting on the Universe. In this framework, time stands for a continuous gauge field. At the end of the Universe, before the thermal death, the quantum fluctuations in the trapped vacuum are close to zero. Indeed, our framework suggests that, with time passing, the vacuum will progressively loose its dark energy oscillations. It means that the spontaneous production of real matter and energy from quantistic vacuum will decrease. The energy located in the false vacuum will not have further possibilities to fluctuate, then it will not be able to give rise to novel inflationary events. Therefore, other inflations will not be possible when our Universe will approximate its end. However, in the very last phases of thermal death, a state of energetic equilibrium will be achieved, both in the trapped vacuum and in the observable Universe. This means that an almost complete T-symmetry could be restored. Some questions remain unanswered: at thermal death, does another Big Bang take place? Or does the trapped vacuum join the original one? Further studies will elucidate such issues.

REFERENCES

- 1) Abraham RH, Marsden JE. 1978. Foundations of mechanics. Benjamin-Cummings, London.
- 2) Bars I, Terning J. 2009. Extra Dimensions in Space and Time. Springer. ISBN 978-0-387-77637-8.
- 3) Bryngelson JD, Wolynes PG. 1987. Spin glasses and the statistical mechanics of protein folding. Proc Natl Acad Sci U S A. 84, 7524-7528.
- 4) Canudas-de-Wit C. 2004. On the concept of virtual constraints as a tool for walking robot control and balancing. Annual Reviews in Control 28, 157-166.
- 5) Canudas-de-Wit C, Tsiotras P, Velenis E, Basset M, Gissinger G. 2003. Dynamic tire friction models for vehicle traction/braking control. Vehicle System Dynamics 39(3),189-226.
- 6) DeWitt BS. 1967. Quantum Theory of Gravity II. The Manifestly Covariant Theory. Phys. Rev. 160, 1195-1239.
- 7) Ehresmann C. 1950. Les connexions infinitesimales dans un espace fibrée différentiable. Colloque de Topologie, Bruxelles, 29-55.
- 8) Ellwanger U. 2012. From the Universe to the Elementary Particles. A First Introduction to Cosmology and the Fundamental Interactions Springer-Verlag Berlin Heidelberg. ISBN 978-3-642-24374-5.
- 9) Ferreira DU, Hegler JA, Komives EA, Wolynes PG. 2011. On the role of frustration in the energy landscapes of allosteric proteins. Proc Natl Acad Sci U S A. 108, 3499-503.
- 10) Goldstein H. 1980. Classical Mechanics. Addison-Wesley Publishing Co., Reading, Massachusetts.
- 11) Higgs PW. 1964. Broken Symmetries and the Masses of Gauge Bosons. Phys Rev Lett 13, 508.

- 12) Hobson MP, Efstathiou GP, Lasenby AN. 2006. *General Relativity: An introduction for physicists* (Reprint ed.). Cambridge University Press. ISBN 978-0-521-82951-9.
- 13) Kolar I, Michor PW. 1993. *Natural operations in differential geometry*. Springer-Verlag, Berlin, 1993.
- 14) Landau LL, Lifshitz M. 1976. *Mechanics*. Pergamon Press, Oxford.
- 15) Lang S. 1995. *Differential and Riemannian manifolds*. Springer-Verlag, Berlin, New York.
- 16) Mandelstam L, Tamm I. 1945. The uncertainty relation between energy and time in nonrelativistic quantum mechanics. *J. Phys. (USSR)* 9, 249–254.
- 17) Moreva EV, Brida G, Gramegna M, Giovannetti V, Maccone L, Genovese M. 2013. Time from quantum entanglement: An experimental illustration. *Physical Review A* 89,052122.
- 18) Penrose R. 2011. *Cycles of Time. An Extraordinary New View of the Universe*. Alfred A. Knopf, NY.
- 19) Peters JF, Tozzi A. 2016. Quantum Entanglement on a Hypersphere. *Int J Theoret Phys*, 1–8. doi:10.1007/s10773-016-2998-7.
- 20) Sengupta B, Tozzi A, Coray GK, Douglas PK, Friston KJ. 2016. Towards a Neuronal Gauge Theory. *PLOS Biology* 14 (3): e1002400. doi:10.1371/journal.pbio.1002400.
- 21) Sommerfeld A. 1952. *Mechanics, Lectures on Theoretical Physics*, vol. I. Academic Press, New York.
- 22) Stepp CE, Hillman RE, Heaton JT. 2010. A virtual trajectory model predicts differences in vocal fold kinematics in individuals with vocal hyperfunction. *J Acoust Soc Am*. 127, 3166-3176.
- 23) 't Hooft G. 1971. Renormalizable Lagrangians for massive Yang-Mills fields. *Nuclear Physics B* 35, 167–188.
- 24) Torby B. 1984. *Energy Methods. Advanced Dynamics for Engineers*. HRW Series in Mechanical Engineering. CBS College Publishing, United States of America.
- 25) Tozzi A, Peters JF. 2016. A Topological Approach Unveils System Invariances and Broken Symmetries in the Brain. *Journal of Neuroscience Research* 94 (5): 351–65. doi:10.1002/jnr.23720.
- 26) Tozzi A, Fla Tor, Peters JF. 2016. Building a minimum frustration framework for brain functions in long timescales. *J Neurosci Res*. 94(8): 702–716.
- 27) Uffink J. 1993. The rate of evolution of a quantum state. *Am. J. Phys.* 61, 935. <http://dx.doi.org/10.1119/1.17368>
- 28) Vaidman L. 1992. Minimum time for the evolution to an orthogonal quantum state. *Am J Phys*, 60, 182–183.
- 29) Veneziano G. 1998. A Simple/Short Introduction to Pre-Big-Bang Physics/Cosmology. arXiv:hep-th/9802057v2
- 30) Zeidler E. 2011. *Quantum Field Theory III: Gauge Theory*. Springer-Verlag, Berlin, Heideberg.

A THEOREM FROM TOPOLOGY UNVEILS THE MYSTERY OF FRACTALS AND POWER LAWS

The (spatial) fractals and (temporal) power laws are ubiquitously displayed by large classes of biological systems. Nevertheless, they are controversial phenomena with still unexplained genesis. From the far-flung branch of topology, a helpful concept comes into play, namely the Borsuk-Ulam theorem, shedding new light on the scale-free origin's long-standing enigma. The theorem states that a single point, if embedded in just one spatial dimension higher, gives rise to two antipodal points that have matching descriptions and similar features. Here we demonstrate that, when we introduce into a system the proper fractal extra-dimension instead of a spatial one, we are able to achieve two antipodal self-similar shapes, corresponding to the distinctive scale-free's higher and lower magnifications. By showing that the elusive phenomena of fractals and power laws can be explained and analyzed in a topological framework, we make clear why the Borsuk-Ulam theorem is the most general principle underlying their pervasive occurrence in nature.

Scale-free dynamics – also called $1/f^\alpha$ behavior, pink noise, power law, self-similarity, fractal-like distribution (Newman; Slomczynski) - are an intrinsic feature of a large class of natural models, from earthquakes to brain activity (Milstein; Linkenkaer-Hansen). In particular, in many dynamical systems, the frequency spectrum displays a scale-invariant behaviour $S(f) = 1/f^\alpha$, where $S(f)$ is the power spectrum and f is the frequency. Further, α stands for an exponent, the so-called “dimension” of the fractal, which equals the negative slope of the line in a log power versus log frequency plot (Pritchard, Van de Ville) (**Figure 1A**). Such a general scheme stands both for (spatial) fractals and (temporal) power laws. For example, when a one-dimensional curve is self-similar, its fractal dimension α (also called D) is a continuous quantity ranging from 0 to infinity, characterized by the expression:

$$D = \frac{-\log N}{\log r(N)}.$$

This tells us that the fractal segment can be exactly decomposed into N overlapping segments (N stands in this case for any positive integer) (Mandelbrot). The fractal dimension gives rise to a dimension greater than the “classical” one-dimension which is generally attributed to the “normal” curves embedded in a standard Euclidean space. More importantly, the fractal dimension encourages us to have another look at the mechanism that gives rise to the ubiquitous power law distributions, both in physical and biological systems.

Several possibilities have been suggested to explain the origin of power law distributions: from combination of exponentials, to successive fractionation, from inverses of quantities to the Yule process, to multiplicative noise (Newman; Beggs & Timme). It has also been proposed that power laws are involved in random walks, phase transitions and self-organized criticality, leading to physical/biological systems of increasing complexity (Bak). Recent papers start to uncover connections between the exponent of a fractal scaling in escape paths from energy basins and the activation free energy (Perkins). The ongoing fluctuations with complex scale-free properties have been absorbed into a free energy scheme (Friston), suggesting that the critical slowing implicit in power law scaling might be mandated by any system that minimizes its energetic expenditure. It has also been demonstrated that a pink noise can be achieved by adding together a random sine wave and a proper one (Tozzi), so that a fractal system might be produced by simply choosing the appropriate oscillation to include. In such a multifaceted framework, a simple theorem from the far-flung branch of the algebraic topology, namely the Borsuk-Ulam theorem (BUT) (Borsuk 1933; Manetti) is able to elucidate the general mechanism underlying different models of scale-free behavior.

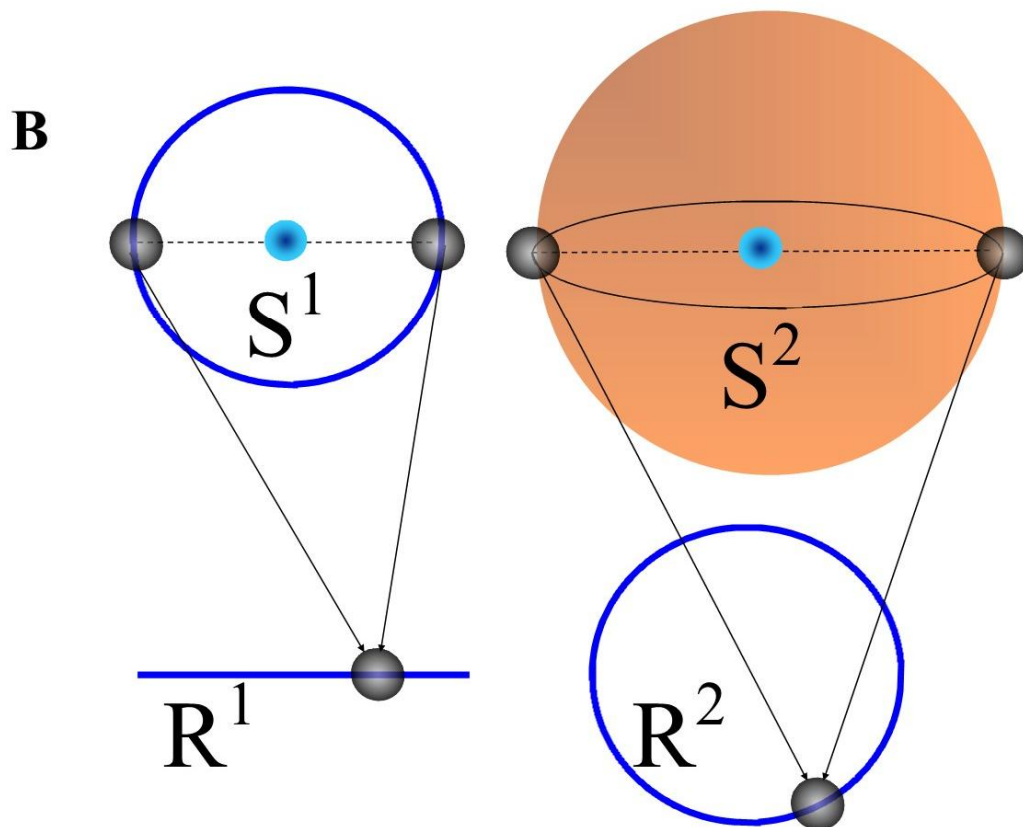
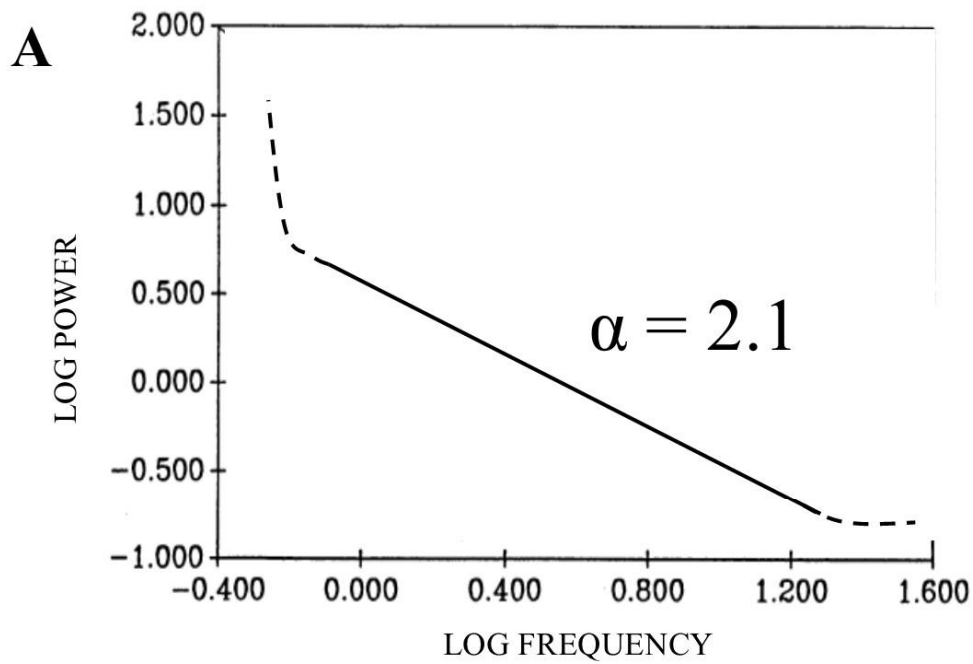


Figure 1A. Example of temporal power laws. The plot displays log power versus log frequency of an electric wave, along with the regression line (modified from Pritchard 1992). The regression line's slope (in this case, $\alpha = 2.1$) is the linear alignment of the data points reflecting the dominant power law. Note that at the slope's tails the α exponent is lost (dotted lines on the right and left of the main slope).

Figure 1B. The Borsuk-Ulam theorem for different values of S^n . Each S^n is embedded in an Euclidean space R^{n+1} . Two antipodal points (black circles) in S^n project to a single point in R^n , and vice versa. Note that the two antipodal points do

not stand just for topological points, but they can also stand either for feature vectors, or shapes, or signals, or changes in their dynamic character.

MATERIALS AND METHODS

n -spheres. The notation S^n denotes an n -sphere, which is a generalization of the circle (Weeks). An n -sphere, also called S^n , is a n -dimensional structure embedded in a $n+1$ euclidean space (Moura;Weeks). For example, a 1-sphere (S^1) is the one-dimensional circumference surrounding a 2-dimensional disk, while a 2-sphere (S^2) is the 2-dimensional surface of a 3-dimensional space (a beach ball's surface is a good illustration) (Marsaglia). A n -sphere is a n -dimensional structure embedded in a $n+1$ space. An n -sphere is formed by points which are constant distance from the origin in $(n+1)$ -dimensions (Marsaglia). For example, a 2-sphere (also called *glome* or *hypersphere*) of radius r (where r may be any positive real number) is defined as the set of points in a 3D Euclidean space at distance r from some fixed center point c (which may be any point in the 3D space) (Moura). A 2-sphere is a simply connected 2-dimensional manifold of constant, positive curvature, which is enclosed in an Euclidean 3-dimensional space called a 3-ball. A 2-sphere is thus the surface or boundary of a 3-dimensional ball, while a 3-dimensional ball is the interior of a 2-sphere. From a geometer's perspective, we have different n -spheres, starting with the perimeter of a circle (S^1) and advancing to S^3 , which is the smallest hypersphere, embedded in a 4-ball (**Figure 1**).

The Borsuk-Ulam theorem: Definition. The Borsuk-Ulam Theorem (BUT) is a finding by K. Borsuk (Borsuk 1933) about Euclidean n -spheres and antipodal points. It states that (Dodson):

Every continuous map $f: S^n \rightarrow R^n$ must identify a pair of antipodal points on S^n map to same point in R^n .

This means that diametrically opposite points (antipodes) on S^n are mapped to a single point in the n -dimensional Euclidean space R^n . Points on S^n are *antipodal*, provided they are diametrically opposite (Krantz). Examples of antipodal points are the endpoints of a line segment, or opposite points along the circumference of a circle, or poles of a sphere. A point embedded in an R^n manifold is projected to a pair of diametrically opposite points on a S^{n+1} -sphere, and vice versa. In effect, the Borsuk-Ulam theorem tells us that we can always find antipodal points on S^n (which is embedded in R^{n+1}) project to the same point on R^n (which contains S^{n-1}) (see **Figure 1B**). In other words, if a sphere is mapped continuously into a plane set, there is at least one pair of antipodal points having the same image; that is, they are mapped in the same point of the plane (Beyer; Borsuk 1958-1959). Put simply, two opposite points on a sphere, when projected on a circumference, give rise to a single point with a description that matches the description of both antipodes. This means that the projection from a higher dimension (equipped with two antipodal points) to a lower one gives rise to a single point. Conversely, we have pullback in which a point on S^{n-1} (embedded in R^n) projects back to two antipodal points on R^{n+1} (which contains S^n). As a result, this also means that the projection from a lower dimension (equipped with just one point) to a higher dimensional space, leads us back to information-carriers in the form of antipodal points that explain the origin of the single signal value predicted by the Borsuk-Ulam theorem. Note that, in the classical formulation of BUT, the function f needs to be continuous and n must be a natural number (although we will see that this is not always the case). For other definitions of BUT and its many proofs, see (Matoušek).

Description of a signal through BUT. In terms of activity, a feature vector $x \in R^n$ models the description of a signal. To elucidate the picture in the application of the BUT in signal analysis, we view the surface of a manifold as a n -sphere and the feature space for signals as finite Euclidean topological spaces (**Figure 1B**). The BUT states that for the description $f(-x)$ for a signal x , we expect to find an antipodal feature vector $f(-x)$ describing a signal on the opposite (antipodal) side of the manifold S^n . The pair of antipodal signals have matching descriptions on S^n .

Let X denote a nonempty set of points on the manifold's surface. A topological structure on X (called a topological space) is a structure given by a set of subsets τ of X , equipped with the following properties:

(Str.1) Every union of sets in τ is a set in τ .

(Str.2) Every finite intersection of sets in τ is a set in τ .

The pair (X, τ) is a topological space. Usually, X by itself is called a topological space, provided it has a topology τ on it.

Let X, Y be topological spaces. Recall that a function or map $f: X \rightarrow Y$ on a set X to a set Y is a subset $X \times Y$ so that for each $x \in X$ there is a unique $y \in Y$ such that $(x, y) \in f$ (usually written $y = f(x)$). The mapping f is defined by a rule that tells us how to find $f(x)$ (Willard).

Shapes and homotopies. A mapping $f: X \rightarrow Y$ is continuous, provided, when $A \subset Y$ is open, that the inverse $f^{-1}(A) \subset X$ is also open (Krantz). In such a view of continuous mappings from the signal topological space X on the manifold's surface to the signal feature space R^n , we consider not just one signal feature vector $x \in R^n$, but also

mappings from X to a set of signal feature vectors $f(X)$. This expanded view of signals is noteworthy, since every connected set of feature vectors $f(X)$ has a shape. It means that signal shapes can be compared.

A consideration of $f(X)$ (set of signal descriptions for a region X) instead of $f(x)$ (description of a single signal x) leads to a region-based view of signals. This region-based manifold's view arises naturally in terms of a comparison of shapes produced by different mappings from X (object space) to the feature space R^n . Continuous mappings from object spaces to feature spaces lead into homotopy theory and the study of shapes.

Let $f, g : X \rightarrow Y$ be continuous mappings from X to Y . The continuous map $H : X \times [0,1] \rightarrow Y$ is defined by:

$$H(x,0) = f(x), H(x,1) = g(x), \text{ for every } x \in X.$$

The mapping H is a *homotopy*, provided there is a continuous transformation (called a deformation) from f to g . The continuous maps f, g are called homotopic maps, provided $f(X)$ continuously deforms into $g(X)$ (denoted by $f(X) \rightarrow g(X)$). The sets of points $f(X), g(X)$ are called shapes (Manetti; Cohen).

For the mapping $H : X \times [0,1] \rightarrow R^n$, where $H(X,0)$ and $H(X,1)$ are *homotopic*, provided $f(X)$ and $g(X)$ and have the same shape. That is, $f(X)$ and $g(X)$ are homotopic, if:

$$\|f(X) - g(X)\| < \|f(X)\|, \text{ for all } x \in X.$$

Borsuk first associated the geometric notion of shape and homotopies. The early work on n -spheres and antipodal points led to the study of retraction and homotopic mappings (Borsuk 1958-59, Borsuk 1969, Borsuk 1980) and into the geometry of shapes and shapes of space (Collins). A pair of connected planar subsets in Euclidean space R^2 have equivalent shapes, provided the planer sets have the same number of holes. In terms of signals, it means that the connected graph for $f(X)$ with, for example, an e shape, can be deformed into the 9 shape. This suggests another useful application of Borsuk's view of the transformation of a shape into another, in terms of signal analysis (Schleicher; Su). Sets of signals not only will have similar descriptions, but also dynamic character and the deformation of one signal shape into another occurs when they are descriptively near (Peters). The nice thing about antipodal points is that the concept can be generalized to countless types of systems' signals (Peters 2014). It is indeed worth of note that the two antipodal points can be used not just for the description of simple topological points, but also of more complicated structures and systems, such as shapes of space (spatial patterns), shapes of time (temporal patterns), movements and trajectories (Peters 2015; Collins). The two antipodal points on a S^n -sphere are characterized by the same function, have matching descriptions and display similar features (Borsuk 1969; Borsuk 1980). The collections of signals can be viewed as surface shapes, where one shape maps to another antipodal one (Cohen). It means that different phenomena can be studied in terms of opposite points, if we only consider them embedded in just one dimension higher than the usual one. If we simply evaluate biological scale-free dynamics instead of "signals", BUT leads naturally to the possibility of a region-based, not a simple point-based, geometry of fractals. When we apply BUT and its extensions to self-similar systems, we achieve interesting results. If we regard scale-free dynamics as embedded in a dimension different from the usual one, we are allowed to study $1/f^n$ behavior in terms of opposite points on a n -sphere.

RESULTS

We proceeded as follows. At first we enclosed fractal and power law structures, equipped with antipodal self-similar points, into the abstract spaces of n -spheres. In such a way, the $1/f^n$ behavior – both in its spatial and temporal variants – can be evaluated in guise of projections on S^n . **Figure 2A** illustrates an example of "spatial" fractals in the framework of BUT. The two antipodal points A and B stand for two self-similar fractal structures, assessed at different level of observation: the point A displays the scale-free system's macrostates, while the point B displays its microstates. Although BUT has been originally described as valid just in case of n being a natural number, in this context the value of n in S^n is a fractional number: 1.3. In such a framework, the n exponent is not a natural number, as it occurs in the "classical" BUT: it is instead the scale-free dynamics' fractal dimension - which is a rational number – which stands for the n exponent. Are we allowed to modify the BUT's the exponent on an n -sphere, changing a natural number into a rational one, to describe n in a BUT fractal system equipped with two antipodal points? We here demonstrate that the answer is positive, by taking into account a Borsuk-Ulam theorem on d -spheres with Hausdorff dimension d , which is a fraction between 0 and 1.

We used the following terminology:

- 1) **Metric space:** Let X be a metric space with the metric $\mu_d(X)$ defined on it. This means that $\mu_d(X) \geq 0$ and μ_d has the usual symmetry and triangle inequality properties for all subsets of X .
- 2) **Hausdorff measure:** Let d be either 0 or a positive real number in R_0^+ . The Hausdorff measure $\mu_d(X)$ equals a real number for each number d in $X = R^d$.
- 3) **Hausdorff dimension (informal):** The threshold value of d denoted by $\dim_H(X)$ is the Hausdorff dimension of X , provided $\mu_d(X) = 0$, if $d > \dim_H(X)$, and $\mu_d(X) = \infty$, if $d < \dim_H(X)$.

Hausdorff Dimension- To arrive at the Hausdorff (fractional) dimension of a subset X in a metric space, we need to consider the Hausdorff measure of X .

Definition 1. Hausdorff measure. Let X be a subset of a metric space M and let d any real number in R_0^+ $\varepsilon \in R_0^+$ (a real number that is either positive or zero) a nonempty subset of X , $U_i, i \in \{1, \dots, n\}$ is a cover of X , i.e., X is a subset of $X \subseteq C_i$ for all i (Schleicher 2007). Here n is any positive integer. Also, let $\text{diam}(U_i) < \varepsilon$ be the diameter of the cover U_i . The d -dimensional Hausdorff measure $\mu_d(X)$ is defined by:

$$\mu_d(X) = \lim_{\varepsilon \rightarrow 0} \left[\inf_{U_i \supseteq X} \sum_{i=1}^n \left(\text{diam}(U_i) \right)^d \right].$$

The basic idea is to cover X with sets U_i with small diameters and estimate the d -measure of X as the sum of the $(\text{diam}(U_i))^d$, i.e., the sum of the U_i diameters raised to the power d .

Lemma 1. Schleicher Lemma. Let d be any real number in R_0^+ . For every bounded set X in a metric space, there is a unique value of $d := \dim_H(X)$ in $R_0^+ \cup \{\infty\}$ such that:

$$\mu_d^l(X) = 0, \text{ if } d' > d.$$

$$\mu_d^l(X) = \infty, \text{ if } d' < d.$$

Definition 2. Hausdorff dimension. The value of $d = \dim_H(X)$ in R_0^+ called the Hausdorff dimension of X . With $d = \dim_H(X)$, the Hausdorff measure $\mu_d(X)$ may be zero, positive or infinite.

Lemma 2. Schleicher Boundedness Lemma. Let d be any real number in R_0^+ and let Y be a metric space. If $X \subset Y$, then:

$$\dim_H(X) \leq \dim_H(Y).$$

Proof. Immediate from the definition of the Hausdorff dimension of a nonempty set.

Assume that X is a nonempty subset (inner sphere) of an n -sphere and having the same center as S^n with the Hausdorff measure $\mu_d(X)$ defined on it and assume that $\mu_d(X)$ satisfies the Schleicher Lemma 1 conditions. The inner sphere S^d of an n -sphere S^n can be any sub-sphere in S^n , including S^n itself. Then, the inner sphere S^d has dimension $d = \dim_H(X)$, $d \leq n$. In addition, assume that R^d is a d -dimensional space which is a subset of the n -dimensional Euclidean space R^n , $d < n$. This gives us new form of the Borsuk-Ulam Theorem (Borsuk 1933).

Theorem 1. Hausdorff-Borsuk-Ulam Theorem. Let S^d with Hausdorff dimension d be an inner sphere of an n -sphere and let $f: S^d \rightarrow R^d$ be a continuous map. There exists a pair of antipodal points on S^d that are mapped to the same point in R^d .

Proof. A direct proof of this theorem is symmetric with the proof of the Borsuk-Ulam Theorem is given by Su (1997), since we assume that S^d is an inner sphere of S^n symmetric about the center of S^n and, from the Schleicher Boundedness Lemma 2, $\dim_H(S^d) \leq \dim_H(S^n)$.

In mathematical words, we showed there that the Borsuk-Ulam theorem can be used for the description of antipodal points on d -spheres equipped with Hausdorff dimension d . Our results allow us to use the n parameter as a versatile tool not just for the description of topological manifolds, but also of biological and physical systems. It is thus suitable to make use of a rational numbers, instead of integer ones, as n exponents in S^n . The same mechanism described in Figure 2A for “spatial” fractals is valid for “temporal” power laws’ plots, when they are equipped with a slope corresponding both to the α exponent and the n -dimension. **Figure 2B** displays an example of the “temporal” variant of scale-free behavior, in the framework of the BUT: if we take into account a system with, i.e., a fractal dimension $D = 2.1$, we may regard the spatial $1/f^n$ structure (equipped with antipodal points A and B) as embedded in a sphere $S^{2.1}$.

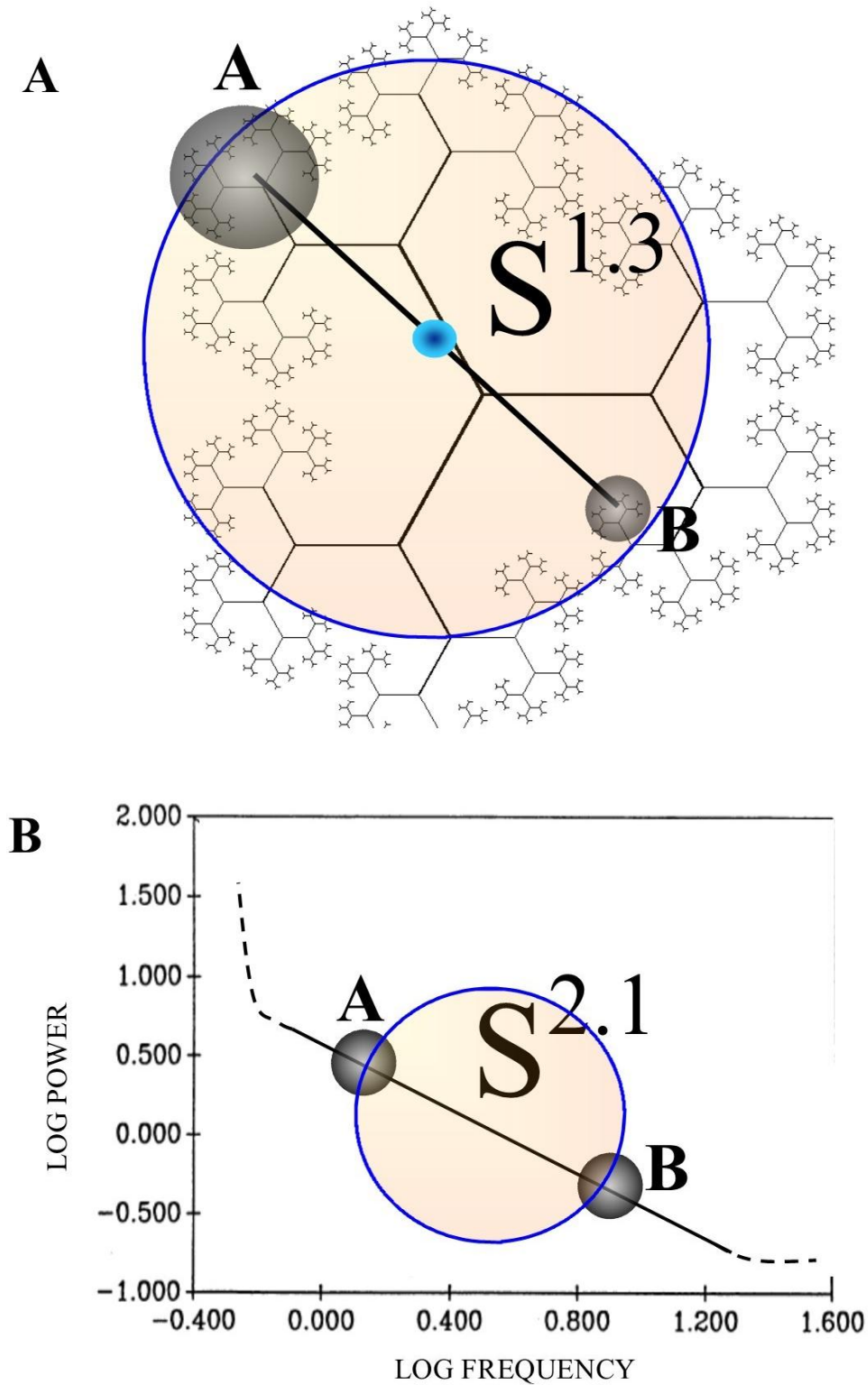


Figure 2. Antipodal points on self-similar structures.

Figure 2A. Spatial fractals embedded in a n -sphere equipped with n corresponding to a rational number. The black circles A and B depict fractals at lower and higher magnification, respectively.

Figure 2B. The figure, modified from our Figure 1A, illustrates an example of temporal power laws embedded in a n -sphere. The n -sphere, in this case, is equipped with a value of n corresponding to the fractal dimension α . Note that the Borsuk-Ulam theorem with its antipodal points is not valid at the slope's tails, where the α exponent is lost (dotted lines).

CONCLUSION

Our study elucidates how (spatial) fractals and (temporal) power laws are produced, both in physical and biological systems. The Borsuk-Ulam theorem displays two very useful general features which help us to explain a wide-range of phenomena, including fractals. First, when a single point is embedded in just one dimension higher, it gives rise to two antipodal points: it means that, by adding just a further dimension (in our case, the fractal one) to a biological or physical system, we are allowed to study it in terms of antipodal points. Second, if we evaluate scale-free dynamics instead of “signals”, a collections of fractal signals could be viewed as surface shapes (or signals) where one shape maps to another antipodal one. Although BUT has been originally described as valid just in case of n being a natural number, recent studies investigated the theorem in the framework of more general conditions. In particular, it has been shown that this extension holds for the case of rationally independent numbers (Kim). We demonstrated here that BUT holds also for n -sphere with a fractional n , and thus for scale-free systems. What does a topologic reformulation brings on the table, in the evaluation of $1/f^\alpha$ behaviors? The opportunity to treat fractals as topological structures gives us the unvaluable chance to describe them through the powerful analytical tools of homology theory and functional analysis (Matoušek; Yang; Dol’nikov). The BUT perspective allows a symmetry property located in the real space (the environment) to be translated to an abstract space and *vice-versa*, enabling us to achieve a map from one dynamical system to another. Embracing self-similarity in the framework of BUT means that scale-free’ symmetry transformations (the antipodal points) can be described as paths or trajectories on “abstract” structures (called topological configuration spacemanifolds). It takes us into the powerful realm of algebraic topology, where the abstract metric space (a projection of the physical and biological milieu’s real geometric space) is able to elucidate countless relationships of large scale structures, through correspondences from topological spaces to algebraic groups (Willard; Dodson). In conclusion, we provided a general topological mechanism which explains the elusive phenomenon of fractals and power laws, casted in a physical/biological fashion which has the potential of being operationalized.

REFERENCES

- 1) Bak, P., Tang, C., Wiesenfeld, K., 1987. Self-organized criticality: An explanation of the $1/f$ noise. *Phys. Rev. Lett.* 59(4), 381-384. PMID: 10035754.
- 2) Beggs JM, Timme N. Being critical of criticality in the brain. *Front Physiol.* 2012 Jun 7;3:163. doi: 10.3389/fphys.2012.00163. eCollection 2012.
- 3) Beyer WA, Zardecki A. The early history of the ham sandwich theorem. *American Mathematical Monthly*, 111, n. 1, 2004, 58-61
- 4) Borsuk, M. Drei s’atze “uber die n -dimensionale euklidische sph`are, *Fundamenta Mathematicae* XX (1933), 177–190.
- 5) Borsuk, M. Concerning the classification of topological spaces from the standpoint of the theory of retracts, XLVI (1958-1959), 177–190.
- 6) Borsuk, M. Fundamental retracts and extensions of fundamental sequences, 64 (1969), no. 1, 55–85.
- 7) Borsuk, M. and A. Gmurczyk, On homotopy types of 2-dimensional polyhedral , 109 (1980), no. 2, 123–142.
- 8) Cohen, M.M. A course in simple homotopy theory, Springer-Verlag, New York-Berlin, 1973, x+144 pp.,MR0362320.
- 9) Collins, G.P. The shapes of space, 291 (2004), 94–103.
- 10) Dodson, C.T.J. and P.E. Parker, A user’s guide to algebraic topology, Kluwer, Dordrecht, Netherlands, 1997, xii+405 pp. ISBN: 0-7923-4292-5,MR1430097.
- 11) Dol’nikov V. L. A generalization of the ham sandwich theorem. *Math. Notes*, 52:771–779, 1992. (refs: pp. 29, 51, 64)
- 12) Friston K, Ao P. Free energy, value, and attractors. *Comput Math Methods Med.* 2012; 2012:937860. doi: 10.1155/2012/937860.
- 13) Kim I-S. Extensions Of The Borsuk ulam Theorem. *J. Korean Math. Soc.* 34 (1997), No. 3, pp. 599–222
- 14) Krantz, S.G. A guide to topology, The Mathematical Association of America, Washington, D.C., 2009, ix + 107pp.
- 15) Linkenkaer-Hansen, K., Nikouline, V.V., Palva, J.M., Ilmoniemi, R.J. (2001). Long-range temporal correlations and scaling behavior in human brain oscillations. *Journal of Neuroscience*, 21(4), 1370-1377.
- 16) Mandelbrot B. How long is the coast of britain? Statistical self-similarity and fractional dimension. *Science.* 1967 May 5;156(3775):636-8.
- 17) Manetti, M. *Topology*, Springer, Heidelberg, 2015, xii+309 pp., DOI 10.1007/978-3-319-16958-3.
- 18) Marsaglia, G. (1972). "Choosing a Point from the Surface of a Sphere". *Annals of Mathematical Statistics* 43 (2): 645–646. doi:10.1214/aoms/1177692644
- 19) Matoušek, J. Using the Borsuk–Ulam Theorem. *Lectures on Topological Methods in Combinatorics and Geometry.* Springer-Verlag Berlin Heidelberg, 2003
- 20) Milstein, J., Mormann, F., Fried, I., Koch, C., 2009. Neuronal shot noise and Brownian $1/f^2$ behavior in the local field potential. *PLoS One* 4(2):e4338. doi: 10.1371/journal.pone.0004338.
- 21) Moura, E., Henderson, D.G. (1996). *Experiencing geometry: on plane and sphere.* Prentice Hall. ISBN 978-0-13-373770-7
- 22) Newman, M.E.J., 2005. Power laws, Pareto distributions and Zipf’s law. *Contemporary Physics* 46, 323–351.
- 23) Perkins TJ, Foxall E, Glass L, Edwards R. A scaling law for random walks on networks. *Nat Commun.* 2014; 5:5121. doi: 10.1038/ncomms6121.

- 24) Peters, J.F. *Topology of Digital Images. Visual Pattern Discovery in Proximity Spaces*, Intelligent Systems Reference Library, vol. 63, Springer, 2014, ISBN 978-3-642-53844-5.
- 25) Peters JF (2016) *Computational Proximity. Excursions in the Topology of Digital Images*. Intelligent Systems Reference Library, Springer, Berlin, *to appear*.
- 26) Pritchard, W.S. (1992). The brain in fractal time: 1/f-like power spectrum scaling of the human electroencephalogram. *International Journal of Neuroscience*, 66, 119-129.
- 27) Schleicher D, Hausdorff dimension, its properties, and its surprises, *The American Mathematical Monthly* 114 (2007), no. 6, 509–528, MR2321254.
- 28) Slomczynski W, Kwapien J, Zyczkowski K. Entropy computing via integration over fractal measures. *Chaos*. 2000; 10(1):180-188.
- 29) Su FE, Borsuk-ulam implies brouwer: A direct construction, *Amer. Math. Monthly* 104 (1997), no. 9, 855–859, MR1479992.
- 30) Tozzi, A. Information processing in the CNS: a supramolecular chemistry? *Cogn. Neurodyn.* **9**, 463-477 (2015).
- 31) Van de Ville D, Britz J, Michel CM. EEG microstate sequences in healthy humans at rest reveal scale-free dynamics. *Proc Natl Acad Sci U S A*. 2010; 107(42):18179-18184. doi: 10.1073/pnas.1007841107.
- 32) Yang C.T. On theorems of Borsuk–Ulam, Kakutani–Yamabe–Urysohn and Dynson, I. *Annals of Math.*, 60:262–282, 1954.
- 33) Weeks JR. *The shape of space*, IInd edition. Marcel Dekker, inc. New York-Basel. 2002
- 34) Willard, S. *General topology*, Dover Pub., Inc., Mineola, NY, 1970, xii +369pp, ISBN: 0-486-43479-6 54-02, MR0264581.

THE BORSUK-ULAM THEOREM ELUCIDATES CHAOTIC SYSTEMS

Nonlinear chaotic dynamics are widespread, both in physical and biological systems. This form of dynamics is frequently studied through logistic maps equipped with bifurcations, where intervals are dictated by the Feigenbaum constants. In such a multifaceted framework, a concept from the far-flung branch of topology, namely the Borsuk-Ulam theorem, comes into play. The theorem tells us that a continuous mapping from antipodal points with matching feature values on an n -sphere to the same real value can always be found. Here we demonstrate that embracing nonlinearity in the framework of the Borsuk-Ulam theorem means that bifurcation transformations (the antipodal points) can be described as paths or trajectories on abstract spheres equipped with a Feigenbaum dimension. Such an approach allows the evaluation of nonlinear systems through linear techniques. In conclusion, we provide a general topological mechanism which explains the elusive chaotic phenomena, cast in a physical/biological fashion which has the potential of being operationalized.

Open systems maintain a non-equilibrium steady-state (i.e., homeostasis or allostasis) in the face of environmental fluctuations (Friston). Such systems, widespread in physics and biology, have been described for countless phenomena, from population dynamics (Newman) to evolution (Tozzi), from diseases spread to brain function (Van de Ville). Complex, non-linear systems with non-equilibrium dynamics occur everywhere, characterized by a large number of interacting and inter-dependent components, random walks (Perkins) and circular causality (Fraiman), spontaneous self-organization and self-organized criticality (Bak) and emergent properties.

Some of these open systems are said to operate at the edge of chaos – a chaotic system displays dependence from initial conditions, positive Lyapunov exponents, and attractors – while others tend to live near a metastable state of second-phase transition - i.e., displaying infinite correlation length, countless dimensions (Afrahimovich), spontaneous avalanches and universal power laws (de Arcangelis; Beggs). Sequential, hierarchical self-organization on an increasing scale and with constitutional dynamics in non-equilibrium systems can lead to the emergence of novel features and properties at each level, organized in space as well as in time and passage beyond reversibility (Foffi). Crowding-induced changes in the

structure and dynamics of physical and biological phenomena describe a scenario of systems capable of generating well-defined functional architectures, by self-assembling from their components, thus behaving as programmed systems (Taylor). To make an example, the recent idea of “supramolecular chemistry” suggests that complex chemical entities can be reversibly constructed from molecular components bound together by labile non-covalent interactions (Lehn). The novel concept involves the storage of information at the molecular level and its retrieval, transfer and processing at the supramolecular level, via transitory processes that are self-organized, self-assembled and dynamic.

In such a multifaceted framework, a concept from the far flung branch of algebraic topology, namely the Borsuk-Ulam theory, is able to elucidate (at least some) of the dynamics underlying nonlinear systems and to shed new light on the puzzling phenomenon of the occurrence of chaos. This paper is an effort to explain some aspects of dynamic systems theory in terms of algebraic topology, and to evaluate the consequences of this strategy.

MATERIALS AND METHODS

Logistic maps and the Feigenbaum constant. A logistic map is a one-dimensional nonlinear difference equation widely used to study equations in the field of dynamic systems theory. To make an example, take into account the coupled equations (Richardson):

$$X_{(t+1)} = r_1 x_{1(t)} (1 - x_{1(t)}) + \alpha r_2 x_{2(t)} \frac{(1 - x_{2(t)})}{1 + \alpha},$$

$$X_{2(t+1)} = r_2 x_{2(t)} (1 - x_{2(t)}) + \alpha_1 r_1 x_{1(t)} \frac{(1 - x_{2(t)})}{1 + \alpha},$$

where x is a generic variable representing some observable behaviour, r is a fixed behavioral parameter (the phase parameter) and t equals time from step 0 to step n . A logistic map may be simply plotted and visualized on a one-parameter bifurcation diagram, as a function of the scaled parameter r (**Figure A**). It can be clearly observed that, at the edge of criticality, a Hopf bifurcation occurs.

In bifurcation theory, the first universal **Feigenbaum constant** is a transcendental number which expresses a ratio in a bifurcation diagram for a non-linear map (Smith). In general, every chaotic system that corresponds to a one-dimensional map with a single quadratic maximum will bifurcate at the same rate (Allgood).

The first Feigenbaum constant is the limiting ratio of each bifurcation interval to the next between every period doubling, of a one-parameter map:

$$x_{i+1} = f(x_i),$$

Where $f(x)$ is a function parameterized by the bifurcation parameter a . The constant is given by the limit (Jordan):

$$\delta = \lim_{n \rightarrow \infty} \frac{a_{n-1} - 1 - a_{n-2}}{a_n - a_{n-1}} = 4.669201609\dots$$

Where a_n are discrete values of variable a at the n th period doubling. The ratio $\frac{a_{n-1} - 1 - a_{n-2}}{a_n - a_{n-1}}$ converges to the

Feigenbaum constant. The same number arises for the following logistic maps:

$$f(x) = ax(1 - x),$$

and

$$f(x) = a - x^2.$$

n -spheres. The notation S^n denotes an n -sphere, which is a generalization of the circle (Weeks). An n -sphere, also called S^n , is a n -dimensional structure embedded in a $n+1$ Euclidean space (Moura). For example, a 2-sphere (S^2) is the 2-dimensional surface of a 3-dimensional space (a beach ball’s surface is a good illustration). An n -sphere is formed by points which are constant distance from the origin in $(n+1)$ -dimensions (Marsaglia). For example, a 2-sphere (also called *glome* or *hypersphere*) of radius r (where r may be any positive real number) is defined as the set of points in a 3D Euclidean space at distance r from some fixed center point \mathbf{c} (which may be any point in the 3D space) (Moura). A2-

sphere is a simply connected 2-dimensional manifold of constant, positive curvature, which is enclosed in an Euclidean 3-dimensional space called a 3-ball. From a geometer's perspective, we have different n-spheres, starting with the perimeter of a circle (S^1) and advancing to S^3 , which is the smallest hypersphere, embedded in a 4-ball.

The Borsuk-Ulam theorem. The Borsuk-Ulam Theorem (BUT) is a finding by K. Borsuk (Borsuk 1933) about Euclidean n-spheres and antipodal points. It states that (Dodson):

Every continuous map $f : S^n \rightarrow R^n$ must identify a pair of antipodal points on S^n map to same point in R^n .

This means that diametrically opposite points (antipodes) on S^n are mapped to a single point in n -dimensional Euclidean space R^n . Points on S^n are *antipodal*, provided they are diametrically opposite (Krantz). Examples of antipodal points are the opposite points along the circumference of a circle, or the poles of a sphere. A point embedded in an R^n manifold is projected to a pair of diametrically opposite points on a S^{n+1} -sphere, and vice versa. In effect, the Borsuk-Ulam theorem tells us that we can always find antipodal points on S^n (which is embedded in R^{n+1}) project to the same point on R^n (which contains S^{n-1}). In other words, if a sphere is mapped continuously into a plane set, there is at least one pair of antipodal points having the same image; that is, they are mapped in the same point of the plane (Beyer; Borsuk 1958-1959). Put simply, two opposite points on a sphere, when projected on a circumference, give rise to a single point with a description that matches the description of both antipodes. This means that the projection from a higher dimension (equipped with two antipodal points) to a lower one gives rise to a single point. Conversely, we have pullback in which a point on S^{n-1} (embedded in R^n) projects back to two antipodal points on R^{n+1} (which contains S^n). As a result, this also means that the projection from a lower dimension (equipped with just one point) to a higher dimensional space, leads us back to information-carriers in the form of antipodal points that explain the origin of the single signal value predicted by BUT. Note that, in the classical formulation of BUT, n must be a natural number (although we will see that this is not always the case). For other definitions of BUT and its countless proofs, see (Matoušek).

Description of a signal through BUT. In terms of activity, a feature vector $x \in R^n$ models the description of a signal. To elucidate the picture in the application of the BUT in signal analysis, we view the surface of a manifold as an n -sphere and the feature space for signals as a finite Euclidean topological space. The BUT states that for the description $f(-x)$ for a signal x , we expect to find an antipodal feature vector $f(-x)$ describing a signal on the opposite (antipodal) side of the manifold S^n . The pair of antipodal signals have matching descriptions on S^n .

Let X denote a nonempty set of points on the manifold's surface. A *topological structure* on a nonempty set X is defined by a family of sets τ on X , having the following properties:

(Str.1) Every union of sets in τ is a set in τ .

(Str.2) Every finite intersection of sets in τ is a set in τ .

The pair (X, τ) is a topological space. Usually, X by itself is also called a topological space, provided it has a topology τ on it. Let X, Y be topological spaces. Recall that a function or map $f : X \rightarrow Y$ on a set X to a set Y is a subset $X \times Y$ so that for each $x \in X$ there is a unique $y \in Y$ such that $(x, y) \in f$ (usually written $y = f(x)$). The mapping f is defined by a rule that tells us how to find $f(x)$ (Willard).

Shapes and homotopies. A mapping $f : X \rightarrow Y$ is *continuous*, provided, when $A \subset Y$ is open, then the inverse $f^{-1}(A) \subset X$ is also open (Krantz). In such a view of continuous mappings from the signal topological space X on the manifold's surface to the signal feature space R^n , we consider not just one signal feature vector $x \in R^n$, but also mappings from X to a set of signal feature vectors $f(X)$. This expanded view of signals is noteworthy, since every connected set of feature vectors $f(X)$ has a shape. It means that signal shapes can be compared.

A consideration of $f(X)$ (set of signal descriptions for a region X) instead of $f(x)$ (description of a single signal x) leads to a region-based view of signals. This region-based view of signals (and manifolds) arises naturally in terms of a comparison of shapes produced by different mappings from X (object space) to the feature space R^n . Continuous mappings from object spaces to feature spaces lead into homotopy theory and the study of shapes.

Let $f, g : X \rightarrow Y$ be continuous mappings from X to Y . The continuous map $H : X \times [0, 1] \rightarrow Y$ is defined by:

$$H(x, 0) = f(x), H(x, 1) = g(x), \text{ for every } x \in X.$$

The mapping H is a *homotopy*, provided there is a continuous transformation (called a deformation) from f to g . The continuous maps f, g are called homotopic maps, provided $f(X)$ continuously deforms into $g(X)$ (denoted by $f(X) \rightarrow g(X)$). The sets of points $f(X), g(X)$ are called shapes (Manetti; Cohen).

For the mapping $H : X \times [0, 1] \rightarrow R^n$, where $H(X, 0)$ and $H(X, 1)$ are *homotopic*, provided $f(X)$ and $g(X)$ and have the same shape. That is, $f(X)$ and $g(X)$ are homotopic, if:

$$\|f(X) - g(X)\| < \|f(X)\|, \text{ for all } x \in X.$$

K. Borsuk first associated the geometric notion of shape and homotopies during the 1950s. The early work on n -spheres and antipodal points led to the study of retraction and homotopic mappings (Borsuk 1969) and to the geometry of shapes and shapes of space (Collins). A pair of connected planar subsets in Euclidean space R^2 have equivalent shapes, provided the planer sets have the same number of holes. In terms of signals, this means that the connected graph for $f(X)$ with, for example, an e shape, can be deformed into the 9 shape. A pair of antipodal points on a S^n -sphere are characterized by the same function, have matching descriptions and display similar features (Borsuk 1980). This suggests a useful application, in terms of signal analysis, of Borsuk's view of the transformation of a shape into another (Schleicher; Su). Sets of signals not only will have similar descriptions, but also dynamic character; further, the deformation of one signal shape into another occurs when they are descriptively near (Collins). In sum, the concept of antipodal points can be generalized to countless types of systems' signals (Peters 2014). Two antipodal points can be used not just for the description of simple topological points, but also of more complicated structures and systems, such as shapes of space (spatial patterns), shapes of time (temporal patterns), movements and trajectories (Peters 2015). If the collections of signals can be viewed as surface shapes, where one shape maps to another antipodal shape (Cohen), then different phenomena can be studied in terms of opposite points, when we consider them embedded in just one dimension higher than the usual one.

RESULTS

We applied BUT and its extensions to chaotic logistic maps. The procedure we followed is shown in **figure A**. At first, we embedded nonlinear dynamics in a n -sphere, in order to be allowed to study chaotic behavior in terms of opposite topological points. However, this time the n number of the n -sphere did not stand for a spatial dimension or for a natural number as usual in Borsuk-Ulam theorem, but for the first Feigenbaum constant. Thus, our n number was a constant (not anymore a spatial dimension) and an irrational number (not anymore a natural one). Are we allowed to modify the BUT's "classical" exponent on an n -sphere, changing a natural number into an irrational one, to achieve a chaotic system equipped with two antipodal points? We here demonstrate that the answer is positive, by taking into account a Borsuk-Ulam theorem on d -spheres with the Hausdorff dimension d , which is a fraction between 0 and 1.

We used the following terminology:

- 4) **Metric space:** Let X be a metric space with the metric $\mu_d(X)$ defined on it. This means that $\mu_d(X) \geq 0$ and μ_d has the usual symmetry and triangle inequality properties for all subsets of X .
- 5) **Hausdorff measure:** Let d be either 0 or a positive real number in R_0^+ . The Hausdorff measure $\mu_d(X)$ equals a real number for each number d in $X = R^d$.
- 6) **Hausdorff dimension (informal):** The threshold value of d denoted by $\dim_H(X)$ is the Hausdorff dimension of X , provided $\mu_d(X) = 0$, if $d > \dim_H(X)$, and $\mu_d(X) = \infty$, if $d < \dim_H(X)$.

Hausdorff Dimension- To arrive at the Hausdorff (fractional) dimension of a subset X in a metric space, we need to consider the Hausdorff measure of X .

Definition 1. Hausdorff measure. Let X be a subset of a metric space M and let d any real number in R_0^+ $\varepsilon \in R_0^+$ (a real number that is either positive or zero) a nonempty subset of X , $U_i, i \in \{1, \dots, n\}$ is a cover of X , i.e., X is a subset of $X \subseteq C_i$ for all i (Schleicher 2007). Here n is any positive integer. Also, let $\text{diam}(U_i) < \varepsilon$ be the diameter of the cover U_i . The d -dimensional Hausdorff measure $\mu_d(X)$ is defined by:

$$\mu_d(X) = \lim_{\varepsilon \rightarrow 0} \left[\inf_{U_i \supseteq X} \sum_{i=1}^n \left(\text{diam}(U_i) \right)^d \right].$$

The basic idea is to cover X with sets U_i with small diameters and estimate the d -measure of X as the sum of the $(\text{diam}(U_i))^d$, i.e., the sum of the U_i diameters raised to the power d .

Lemma 1. Schleicher Lemma. Let d be any real number in R_0^+ . For every bounded set X in a metric space, there is a unique value of $d := \dim_H(X)$ in $R_0^+ \cup \{\infty\}$ such that:

$$\mu_d^l(X) = 0, \text{ if } d' > d.$$

$$\mu_d^l(X) = \infty, \text{ if } d' < d.$$

Definition 2. Hausdorff dimension. The value of $d = \dim_H(X)$ in R_0^+ called the Hausdorff dimension of X . With $d = \dim_H(X)$, the Hausdorff measure $\mu_d(X)$ may be zero, positive or infinite.

Lemma 2. Schleicher Boundedness Lemma. Let d be any real number in R_0^+ and let Y be a metric space. If $X \subset Y$, then:

$$\dim_H(X) \leq \dim_H(Y).$$

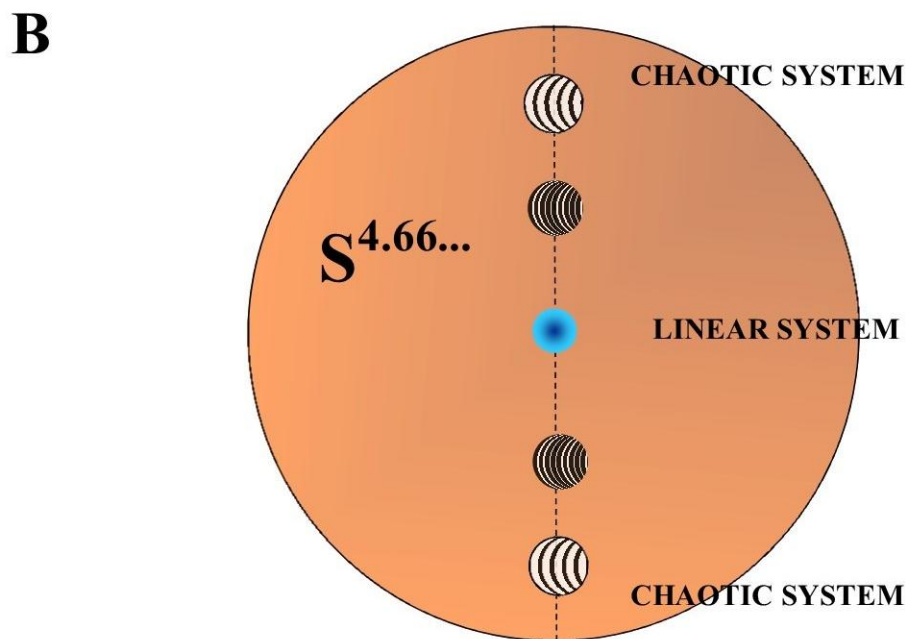
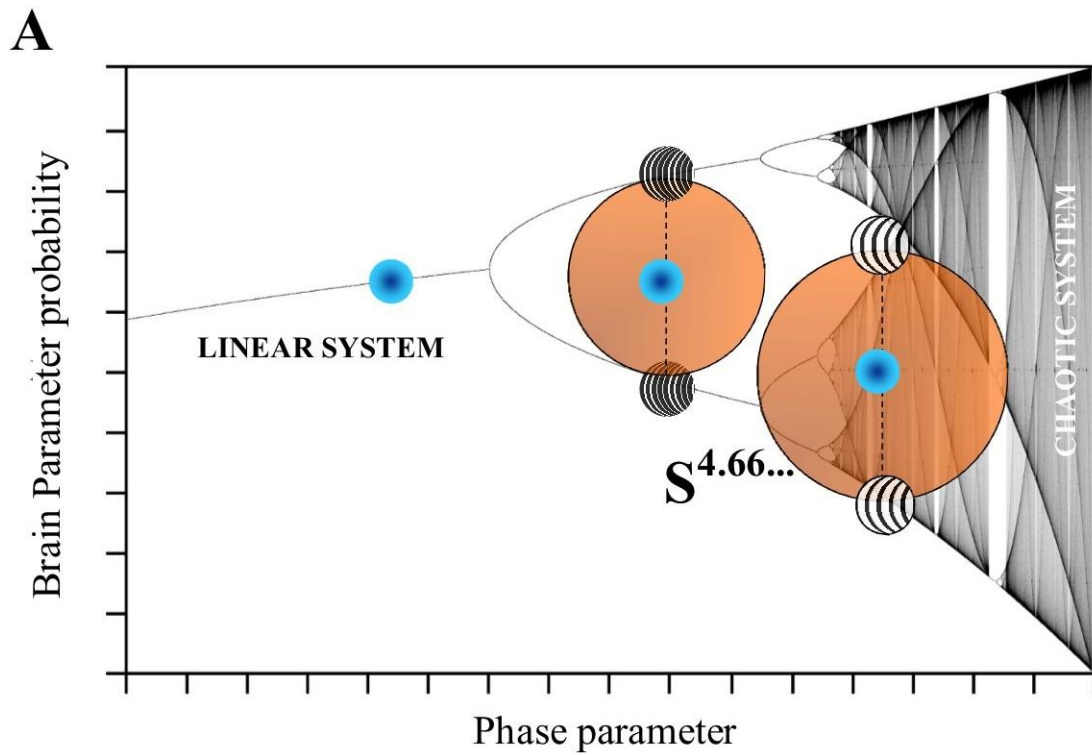
Proof. Immediate from the definition of the Hausdorff dimension of a nonempty set.

Assume that X is a nonempty subset (inner sphere) of an n -sphere and having the same center as S^n with the Hausdorff measure $\mu_d(X)$ defined on it and assume that $\mu_d(X)$ satisfies the Schleicher Lemma 1 conditions. The inner sphere S^d of an n -sphere S^n can be any sub-sphere in S^n , including S^n itself. Then, the inner sphere S^d has dimension $d = \dim_H(X)$, $d \leq n$. In addition, assume that R^d is a d -dimensional space which is a subset of the n -dimensional Euclidean space R^n , $d < n$. This gives us new form of the Borsuk-Ulam Theorem (Borsuk 1933).

Theorem 1. Hausdorff-Borsuk-Ulam Theorem. Let S^d with Hausdorff dimension d be an inner sphere of an n -sphere and let $f: S^d \rightarrow R^d$ be a continuous map. There exists a pair of antipodal points on S^d that are mapped to the same point in R^d .

Proof. A direct proof of this theorem is symmetric with the proof of the Borsuk-Ulam Theorem is given by Su (1997), since we assume that S^d is an inner sphere of S^n symmetric about the center of S^n and, from the Schleicher Boundedness Lemma 2, $\dim_H(S^d) \leq \dim_H(S^n)$.

In sum, we achieved a n -sphere with a n exponent corresponding to the Feigenbaum number. The next step was to locate the n -sphere on a logistic map, in order to embed the topological antipodal points into the bifurcation diagram of a chaotic phenomenon (**Figure A**). Once achieved two antipodal points for every bifurcation, we were allowed to map them in the concentric layers of another n -sphere (**Figure B**). We obtained a topological structure which summarizes the whole behaviour of a nonlinear, chaotic system. Note that the center of the sphere stands for a completely linear system, while, when we move along the circumference towards the sphere surface, we achieve antipodal points which represent a progressively more chaotic system. In such a vein, the knowledge of just the single central point and the first Feigenbaum constant leads to predictions about the temporal development of otherwise chaotic phenomena.



FigureA. Bifurcation diagram of a logistic map's nonlinear dynamical equation. The axis x displays the phase parameter. At the first Hopf bifurcation, the exponent n of the n -sphere corresponds to the first Feigenbaum constant. The same operation can be repeated at each of the following bifurcations: just the first and the second ones are displayed in Figure. Each sphere is equipped with two antipodal points which intersect the curves of the corresponding bifurcation and which display the same value on the axis x .

Figure B. The antipodal points described in Figure A are projected onto a single sphere, which stands for the Figure A's spheres casted in a concentric way, so that the center is the same for all of them.

CONCLUSION

In conclusion, we demonstrated a close link between topological mappings and nonlinear chaotic systems. The Borsuk-Ulam theorem is a versatile tool displaying a very useful general feature which helps us explain a wide-range of phenomena: in our case, if we evaluate nonlinear dynamics instead of “signals”, a collection of chaotic signals can be viewed as surface shapes (or sets of region signals) where one shape maps to another antipodal shape. When assessing physical and biological nonlinear dynamics as an alternative to “signals”, the BUT leads naturally to the possibility of a region-based, not a simple point-based, geometry of logistic maps. Furthermore, the BUT can be used for the description of antipodal points on n -spheres equipped with a dimension d different from a natural number. Although BUT has been originally described as valid just in case of a natural number n , recent studies have shown that this theorem is also valid in the framework of more general conditions. In particular, it has been shown that this extension holds for the case of rationally independent numbers (Kim). Here we demonstrated that the n value in S^n can be an irrational number, in this case the Feigenbaum constant. BUT is thus suitable to make use of irrational numbers, instead of integer ones, as n exponents in S^n . This suggests that the n parameter can be used as a versatile tool not just for the description of topological manifolds, but also for biological and physical chaotic systems.

What does a topologic reformulation bring to the table, in the evaluation of nonlinear chaotic systems? The opportunity to treat chaos as a topological structure gives us the invaluable chance to describe it through the powerful analytical tools of homology theory and functional analysis (Matoušek; Yang; Dol'nikov). The BUT perspective gives us a symmetry property located in the real space (the environment) to be translated to an abstract space and *vice-versa*, enabling us to achieve a map from one dynamical system to another (**Figure B**). Embracing nonlinearity in the framework of BUT means that bifurcation transformations (the antipodal points) can be described as paths or trajectories on “abstract” structures (called topological configuration space manifolds). Indeed, BUT makes it possible for us to evaluate a nonlinear system through linear techniques. It takes us into the powerful realm of algebraic topology, where the abstract metric space (a projection of the physical and biological milieu's real geometric space) is able to elucidate countless relationships of large scale structures, through correspondences from topological spaces to algebraic groups (Willard; Dodson).

REFERENCES

- 1) Afraimovich V, Tristan I, Varona P, Rabinovich M. Transient Dynamics in Complex Systems: Heteroclinic Sequences with Multidimensional Unstable Manifolds. *Discontinuity, Nonlinearity and Complexity* 2(1): 21-41, 2013.
- 2) Alligood KT, Sauer, Yorke YA. *Chaos: An Introduction to Dynamical Systems*, Textbooks in mathematical sciences, Springer, 1996.
- 3) Bak, P., Tang, C., Wiesenfeld, K., 1987. Self-organized criticality: An explanation of the $1/f$ noise. *Phys. Rev. Lett.* 59(4), 381-384. PMID: 10035754.
- 4) Beggs JM, Timme N. Being critical of criticality in the brain. *Front Physiol.* 2012 Jun 7;3:163. doi: 10.3389/fphys.2012.00163. eCollection 2012.
- 5) Beyer WA, Zardecki A. The early history of the ham sandwich theorem. *American Mathematical Monthly*, 111, n. 1, 2004, 58-61
- 6) Borsuk, M. Drei sätze über die n -dimensionale euklidische sphäre, *Fundamenta Mathematicae* XX (1933), 177–190.
- 7) Borsuk, M. Concerning the classification of topological spaces from the standpoint of the theory of retracts, XLVI (1958-1959), 177–190.
- 8) Borsuk, M. Fundamental retracts and extensions of fundamental sequences, 64 (1969), no. 1, 55–85.
- 9) Borsuk, M. and A. Gmurczyk, On homotopy types of 2-dimensional polyhedral, 109 (1980), no. 2, 123–142.
- 10) Cohen, M.M. *A course in simple homotopy theory*, Springer-Verlag, New York-Berlin, 1973, x+144 pp.,MR0362320.
- 11) Collins, G.P. The shapes of space, 291 (2004), 94–103.
- 12) de Arcangelis, L. and Herrmann, H.J. (2010) Learning as a phenomenon occurring in a critical state. *Proceedings of the National Academy of Sciences* 107, 3977-3981
- 13) Dodson, C.T.J. and P.E. Parker, *A user's guide to algebraic topology*, Kluwer, Dordrecht, Netherlands, 1997, xii+405 pp. ISBN: 0-7923-4292-5,MR1430097.
- 14) Dol'nikov V. L. A generalization of the ham sandwich theorem. *Math. Notes*, 52:771–779, 1992. (refs: pp. 29, 51, 64)
- 15) Foffi G, Pastore A, Piazza F, Temussi PA (2013) Macromolecular crowding: chemistry and physics meet biology (Ascona, Switzerland, 10-14 June 2012). *Phys Biol* 10(4):040301
- 16) Fraiman, D., & Chialvo, D.R. (2012). What kind of noise is brain noise: anomalous scaling behavior of the resting brain activity fluctuations. *Frontiers in Physiology*, 3:307. doi: 10.3389/fphys.2012.00307.

- 17) Friston K, Ao P. Free energy, value, and attractors. *Comput Math Methods Med.* 2012; 2012:937860. doi: 10.1155/2012/937860.
- 18) Jordan DW, Smith P. *Non-Linear Ordinary Differential Equations: Introduction for Scientists and Engineers* (4th Edition), Oxford University Press, 2007.
- 19) Kim I-S. Extensions Of The Borsuk ulam Theorem. *J. Korean Math. Soc.* 34 (1997), No. 3, pp. 599–222
- 20) Krantz, S.G. *A guide to topology*, The Mathematical Association of America, Washington, D.C., 2009, ix + 107pp.
- 21) Lehn JM (2007) From supramolecular chemistry towards constitutional dynamic chemistry and adaptive chemistry. *Chem Soc Rev* 36(2):151-160.
- 22) Linkenkaer-Hansen, K., Nikouline, V.V., Palva, J.M., Ilmoniemi, R.J. (2001). Long-range temporal correlations and scaling behavior in human brain oscillations. *Journal of Neuroscience*, 21(4), 1370-1377.
- 23) Manetti, M. *Topology*, Springer, Heidelberg, 2015, xii+309 pp., DOI 10.1007/978-3-319-16958-3.
- 24) Marsaglia, G. (1972). "Choosing a Point from the Surface of a Sphere". *Annals of Mathematical Statistics* 43 (2): 645–646. doi:10.1214/aoms/1177692644
- 25) Matoušek, J. Using the Borsuk–Ulam Theorem. *Lectures on Topological Methods in Combinatorics and Geometry*. Springer-Verlag Berlin Heidelberg, 2003
- 26) Moura, E., Henderson, D.G. (1996). *Experiencing geometry: on plane and sphere*. Prentice Hall. ISBN 978-0-13-373770-7
- 27) Newman, M.E.J., 2005. Power laws, Pareto distributions and Zipf's law. *Contemporary Physics* 46, 323-351.
- 28) Perkins TJ, Foxall E, Glass L, Edwards R. A scaling law for random walks on networks. *Nat Commun.* 2014; 5:5121. doi: 10.1038/ncomms6121.
- 29) Peters, J.F. *Topology of Digital Images. Visual Pattern Discovery in Proximity Spaces*, Intelligent Systems Reference Library, vol. 63, Springer, 2014, ISBN 978-3-642-53844-5.
- 30) Peters JF (2016) *Computational Proximity. Excursions in the Topology of Digital Images*. Intelligent Systems Reference Library, Springer, Berlin, *to appear*.
- 31) Richardson MJ, Dale R, Marsh KL. Complex dynamical systems in social and personality psychology. In: Reis HT, Judd CM (eds), *Handbook of Research Methods in Social and Personality Psychology*. 2nd Edition, 2014. Cambridge University Press, Cambridge. ISBN: 9781107600751
- 32) Schleicher D, Hausdorff dimension, its properties, and its surprises, *The American Mathematical Monthly* 114 (2007), no. 6, 509–528, MR2321254.
- 33) Smith R. Period doubling, information entropy, and estimates for Feigenbaum's constants. *International Journal of Bifurcation and Chaos* (2013) 23 (11): 1350190.
- 34) Su FE, Borsuk-ulam implies brouwer: A direct construction, *Amer. Math. Monthly* 104 (1997), no. 9, 855–859, MR1479992.
- 35) Taylor MB, Ehrenreich IM (2014) Genetic interactions involving five or more genes contribute to a complex trait in yeast. *PLoS Genet* 10(5):e1004324. doi: 10.1371/journal.pgen.1004324.
- 36) Tozzi A. Evolution: networks and energy count. *Nature* 11/2014; 515(7527):343.
- 37) Van de Ville D, Britz J, Michel CM. EEG microstate sequences in healthy humans at rest reveal scale-free dynamics. *Proc Natl Acad Sci U S A.* 2010; 107(42):18179-18184. doi: 10.1073/pnas.1007841107.
- 38) Yang C.T. On theorems of Borsuk–Ulam, Kakutani–Yamabe–Yujob^o and Dynson, I. *Annals of Math.*, 60:262–282, 1954.
- 39) Weeks JR. *The shape of space*, IInd edition. Marcel Dekker, inc. New York-Basel. 2002
- 40) Willard, S. *General topology*, Dover Pub., Inc., Mineola, NY, 1970, xii +369pp, ISBN: 0-486-43479-6 54-02, MR0264581.